การคัดแยก และ ดักจับ เซลล์มะเร็งผิวหนังของสุนัขชนิดมาสต์เซลล์
ในระดับเซลล์เดี่ยวด้วยระบบของไหลจุลภาค

นายเดชธชัย เกตุพันธุ์

วิทยานิพนธ์นี้เป็นส่วนหนึ่งของการศึกษาตามหลักสูตรปริญญาวิทยาศาสตรดุษฎีบัณฑิต
สาขาวิชาชีวศาสตร์ทางสัตวแพทย์ ภาควิชากายวิภาคศาสตร์
คณะสัตวแพทยศาสตร์ จุฬาลงกรณ์มหาวิทยาลัย
ปีการศึกษา 2560

MICROFLUIDICS-BASED SINGLE CELL ISOLATION AND TRAPPING OF CANINE CUTANEOUS MAST CELL TUMOR CELLS

Mr. Dettachai Ketpun

A Dissertation Submitted in Partial Fulfillment of the Requirements
for the Degree of Doctor of Philosophy Program in Veterinary Biosciences
Department of Veterinary Anatomy
Faculty of Veterinary Science
Chulalongkorn University
Academic Year 2017

Thesis Title	MICROFLUIDICS-BASED SINGLE CELL ISOLATION AND TRAPPING OF CANINE CUTANEOUS MAST CELL TUMOR CELLS
By	Mr. Dettachai Ketpun
Field of Study	Veterinary Biosciences
Thesis Advisor	Professor Achariya Sailasuta, D.V.M., Ph.D.
Thesis Co-Advisor	Prapruddee Piyaviriyakul, D.V.M., M.Sc., Ph.D.
	Assistant Professor Alongkorn Pimpin, B.Eng., M.Sc., Ph.D.

Accepted by the Faculty of Veterinary Science, Chulalongkorn University in Partial Fulfillment of the Requirements for the Doctoral Degree

.....Dean of the Faculty of Veterinary Science

(Professor Roongroje Thanawongnuwech, D.V.M., M.Sc., Ph.D.)

THESIS COMMITTEE

.....Chairman

(Assistant Professor Sirakarnt Dhitavat, D.V.M., Ph.D.)

.....Thesis Advisor

(Professor Achariya Sailasuta, D.V.M., Ph.D.)

.....Thesis Co-Advisor

(Prapruddee Piyaviriyakul, D.V.M., M.Sc., Ph.D.)

.....Thesis Co-Advisor

(Assistant Professor Alongkorn Pimpin, B.Eng., M.Sc., Ph.D.)

.....Examiner

(Assistant Professor Werayut Srituravanich, B.Eng., M.Sc., Ph.D.)

.....Examiner

(Associate Professor Theerayuth Kaewamatawong, D.V.M., Ph.D.)

.....External Examiner

(Wutthinan Jeamsaksiri, B.Eng., M.Sc., Ph.D.)

เดชธชัย เกตุพันธุ์ : การคัดแยก และ ดักจับ เซลล์มะเร็งผิวหนังของสุนัขชนิดมาสต์เซลล์ในระดับเซลล์เดี่ยวด้วยระบบของไหลจุลภาค (MICROFLUIDICS-BASED SINGLE CELL ISOLATION AND TRAPPING OF CANINE CUTANEOUS MAST CELL TUMOR CELLS) อ.ที่ปรึกษาวิทยานิพนธ์หลัก: ศ. สพ.ญ. ดร.อัจฉริยา ไศละสูต, อ.ที่ปรึกษาวิทยานิพนธ์ร่วม: ดร.ประพฤติดี ปิยะวิริยะกุล, ผศ. ดร.อลงกรณ์ พิมพ์พิณ, 110 หน้า.

งานวิจัยนี้มีวัตถุประสงค์เพื่อพัฒนาระบบของไหลจุลภาค สำหรับทำการแยกเซลล์มะเร็งผิวหนังของสุนัขชนิดมาสต์เซลล์ในระดับเซลล์เดี่ยวโดยทำการคัดแยกตามขนาดของเซลล์มะเร็งผิวหนังที่แบ่งออกเป็นสี่กลุ่มคือ กลุ่มมะเร็งผิวหนังของสุนัขชนิดมาสต์เซลล์ที่มีขนาด 5-9 ไมโครเมตรเป็นกลุ่มที่หนึ่ง ขนาด 10-14 ไมโครเมตรเป็นกลุ่มที่สอง ขนาด 15-20 ไมโครเมตรเป็นกลุ่มที่สาม และขนาด 20 ไมโครเมตรขึ้นไปเป็นกลุ่มที่สี่ รวมทั้งพัฒนาระบบของไหลจุลภาคที่สามารถดักจับเซลล์เดี่ยวของมะเร็งผิวหนังของสุนัขชนิดมาสต์เซลล์ด้วยชุดหลุมดักจับรูปสามเหลี่ยม และจัดเก็บเซลล์ที่ถูกดักจับไว้ในหลุมดักจับในอัตราส่วน 1 เซลล์ต่อ 1 หลุม ผลการศึกษาชี้ให้เห็นถึงความสำเร็จในการพัฒนาระบบของไหลจุลภาคดังกล่าว โดยอุปกรณ์ของระบบของไหลจุลภาคทั้งหมดได้ถูกประกอบขึ้นมาด้วยวิธีการ soft-lithography ทำให้ได้อุปกรณ์ระบบของไหลจุลภาคสองชิ้นได้แก่ ระบบของไหลจุลภาครูปก้นหอยประกอบด้วยขดของท่อโค้งรูปสี่เหลี่ยมผืนผ้ามีความกว้าง 500 และสูง 130 ไมครอนที่มีจำนวนขดเท่ากับ 5 ขด และมีท่อทางออกหลักแบบรูปกรวยยาว 720 ไมครอนที่แยกออกเป็นท่อทางออกย่อยแบบไม่สมมาตรจำนวน 10 ท่อ สำหรับใช้แยกเซลล์ตามขนาดที่อัตราการไหล 1 มิลลิลิตรต่อนาที และระบบของไหลจุลภาคที่ประกอบด้วยชุดของหลุมดักจับรูปสามเหลี่ยมด้านเท่าที่มีความสูง 40 และลึก 15 ไมครอนและมีช่องการไหลหลักสูง 160 ไมโครเมตร กว้าง 5 และยาว 27 มิลลิเมตร สำหรับใช้ดักจับเซลล์มะเร็งเดี่ยวภายใต้รูปแบบการไหลแบบมีการหยุดพักเป็นช่วงๆ ที่อัตราการไหล 0.01 มิลลิลิตรต่อชั่วเป็นเวลา 30 วินาทีและหยุดพัก 3 นาที ผลการศึกษาชี้ให้เห็นว่าอุปกรณ์ในส่วนการคัดแยกเซลล์ตามขนาด สามารถแยกเซลล์มะเร็งในกลุ่มที่สามและสี่ซึ่งเป็นกลุ่มเป้าหมายออกจากเซลล์ในกลุ่มที่หนึ่งและสองได้ อย่างไรก็ตามสิ่งที่ต้องได้รับการแก้ไขสำหรับอุปกรณ์ในการคัดแยกคือ การลดผลของความเค้นเฉือนและผลของความเค้นในการยืดตัวของของไหล ซึ่งแสดงให้เห็นได้ด้วยแบบจำลองทางคอมพิวเตอร์ ในท่อโค้งจุลภาคต่อความอยู่รอดของเซลล์ เพราะจากการตรวจสอบความอยู่รอดของเซลล์ด้วยวิธีการนับจำนวนเซลล์ การย้อมสี trypan blue และ TMRM การตรวจสอบรูปร่างของเซลล์ด้วยกล้องจุลทรรศน์แบบใช้แสงและกล้องจุลทรรศน์อิเล็กตรอนแบบส่องกราด และการตรวจสารพันธุกรรมที่รั่วไหลจากของเหลวเหนือตะกอนเซลล์พบว่า จำนวนของเซลล์หลังการคัดขนาดมีจำนวนลดลงค่อนข้างมาก รูปร่างของเซลล์มีการยืดยาวขึ้นหรือมีการฉีกขาดของเซลล์ส่งผลให้ค่าสารพันธุกรรมที่รั่วไหลมีค่าสูงขึ้นกว่ากลุ่มควบคุม 2.4 เท่าและมีอัตราการรอดของเซลล์มะเร็งที่แยกได้อยู่ที่ร้อยละ 40 ในส่วนของการดักจับเซลล์พบว่าอุปกรณ์ของไหลจุลภาคที่พัฒนาขึ้นมีความสามารถในการดักจับเซลล์มะเร็งไว้ได้ โดยชุดของหลุมดักจับมีประสิทธิภาพในการดักจับเซลล์มะเร็งที่ในรูปเซลล์เดี่ยวอยู่ที่ร้อยละ 35 และดักจับเซลล์เดี่ยวพร้อมๆกันหลายๆเซลล์ต่อหนึ่งหลุมดักจับที่ร้อยละ 15 ดังนั้นในการศึกษาครั้งนี้จึงแสดงให้เห็นถึงความสำเร็จเป็นครั้งแรกในทางสัตวแพทย์ ที่มีการพัฒนาอุปกรณ์ระบบของไหลจุลภาคที่มีความสามารถในการคัดแยกเซลล์มะเร็งผิวหนังสุนัขชนิดมาสต์เซลล์ตามขนาดได้ และสามารถดักจับเซลล์มะเร็งแบบเซลล์เดี่ยวไว้ในหลุมดักจับได้ และในอนาคตมีแนวโน้มที่จะสามารถพัฒนาอุปกรณ์ทั้งสองส่วนเพิ่มเติมเพื่อให้เกิดประสิทธิภาพในการทำงานสูงสุด รวมทั้งสามารถทำการรวมอุปกรณ์ทั้งสองส่วนเข้าด้วยกันเพื่อให้เป็นอุปกรณ์ระบบของไหลจุลภาคสำเร็จรูปที่สามารถคัดแยก ดักจับ และเพาะเลี้ยงเซลล์เดี่ยวทุกชนิดบนอุปกรณ์ชิ้นเดียวได้ ซึ่งจะเป็นประโยชน์อย่างมากสำหรับการศึกษาทางด้านวิศวกรรมชีวเวชต่อไป

ภาควิชา กายวิภาคศาสตร์	ลายมือชื่อนิสิต ----------
สาขาวิชา ชีวศาสตร์ทางสัตวแพทย์	ลายมือชื่อ อ.ที่ปรึกษาหลัก ----------
ปีการศึกษา 2560	ลายมือชื่อ อ.ที่ปรึกษาร่วม ----------
	ลายมือชื่อ อ.ที่ปรึกษาร่วม ----------

5575408731 : MAJOR VETERINARY BIOSCIENCES
KEYWORDS: CANINE CUTANEOUS MAST CELL TUMORS / ENTRAPMENT / EXTENSIONAL FLUID STRESS / FLUID SHEAR STRESS / MICROFLUIDIC / SINGLE CELL / SORTING

DETTACHAI KETPUN: MICROFLUIDICS-BASED SINGLE CELL ISOLATION AND TRAPPING OF CANINE CUTANEOUS MAST CELL TUMOR CELLS. ADVISOR: PROF. ACHARIYA SAILASUTA, D.V.M., Ph.D., CO-ADVISOR: PRAPRUDDEE PIYAVIRIYAKUL, D.V.M., M.Sc., Ph.D., ASST. PROF. ALONGKORN PIMPIN, B.Eng., M.Sc., Ph.D., 110 pp.

In this research, the primary objective was to develop a microfluidic platform utilized for the size-based single cell sorting of canine cutaneous mast cell tumor (MCT) cells which were categorized into 4 groups; I, II, III and IV, upon their individual sizes ranged from 5-9, 10-14, 15-19, and equal to or over than 20 mm respectively. And the secondary aim was to establish the microfluidic-based entrapping microdevice which had a capacity to ensnare single MCT cells into its triangular microwell array at the ratio of one cell per one microwell. The study consequence consistently indicated the accomplishment of device developments. All microfluidic devices were designed and fabricated under the standard soft-lithography. Finally, two microfluidic devices were constructed; the Archimedian spiral microchannel (ASM) and the triangular microwell array. The configuration of ASM consisted of 5-turned, 500mm-wide x 130mm-high, rectangular spiral microchannel with 720mm-long conical exit microchannel separated into 10 asymmetric exit slots. Meanwhile, the entrapment microdevice were composed of the array of 40mm-high x 15mm-deep triangular microwell with 160mm-high main flow channel. The study result indicated that, at the flow rate 1 ml. min^{-1}, the spiral microchannel had a capability to separate single MCT cells in group III and IV, which were the targeted cells, out of the MCT cells group I and II, based upon their sizes. However, the detrimental effects of fluid shear stress and extensional stress in the spiral microchannel, exhibited by the computational simulations, were required an amendment. Because, under hemocytometry quantification, trypan blue and TMRM staining, light-microscopy and SEM morphological assessments and leaky DNA assays, they suggested that the amount of sorted MCT cells was significantly reduced and the cell vitality was only 40 percent. Meanwhile, the morphological assays also confirmed cell elongation and/or wreckage causing the 2.4-fold increment of leaky DNA. For single MCT cell entrapment, the study consequence exhibited that, under pulsatile flow (0. 01 ml. h^{-1} inflow rate for 30 sec and 3min pausing interval), the trapping microdevice had an ability to stochastically entrap MCT cells in its triangular microwell array. And the efficacy of the microdevice for single and multiple MCT cell entrapment was 35% and 15% respectively. In the epilogue, this study is the first report on the attainments in microfrabication engaged in veterinary field for size-based single MCT cell sorting and entrapment. In addition, there are a tendency to merge these two microdevice components together to form a complete microfluidic-based single cell sorting, trapping and culturing on a chip which is essentially benefit to biomedical engineering researches in the future.

Department:	Veterinary Anatomy	Student's Signature	----------
Field of Study:	Veterinary Biosciences	Advisor's Signature	----------
Academic Year:	2017	Co-Advisor's Signature	----------
		Co-Advisor's Signature	----------

ACKNOWLEDGEMENTS

Firstly, I would like to thank my study programmme at the Unit of Biochemistry, Department of Veterinary Physiology, Faculty of Veterinary Science, Chulalongkorn University for furnishing me with the great opportunity for developing myself in the field of Veterinary Bioscience. Secondly, I would like to send my gratitude to my thesis principal advisor, Prof. Dr. Achariya Sailasuta, who encourages me since I studied the master degree in Veterinary Pathobiology until nowadays, for everything both on the stage and at the back stage. I also appreciate my thesis co-advisor, Dr. Papruddee Piyawiriyakul of the Unit of Biochemistry, Department of Veterinary Physiology, Faculty of Veterinary Science, and Assist. Prof. Dr. Alongkorn Pimpin from Department of Mechanical Engineering, Faculty of engineering, Chulalongkorn University, for all helpful recommendation and excellent troubleshooting in my laboratory processes. Additionally, I acknowledge Assist. Prof. Dr. Werayut Srituravanich from Department of Mechanical Engineering, Faculty of Engineering, Chulalongkorn University for his approval on my financial support for studying aboard in the University of British Columbia, Okanagan Campus, British Columbia, Canada, including his benevolence in my dissertation defense.

Thanks for Assoc. Prof. Dr. Theerayuth Kaewamatawong for advocating my thesis defense as well as Assoc. Prof. Dr. Anudep Rungsipipat for his very big suggestions in my dissertation, I will never omit. The other I have to thank for is Assist. Prof. Sirakarnt Dhitavat, the chairperson of the study programme, who has officially supported me along my Ph.D. study, in addition with her patience on me. Endlessly, I would like to acknowledge Dr. Wuttinan Jeamsaksiri, my greatest external examination, from Thai Microelectronic Center (TMEC), Ministry of Science and Technology for his treasury collaborations along the study as well as Mr. Witsaroot Sripumkhai, Mr. Charndet Hruanun, Mr. Jakrapong Supadech, Mr. Jirawat Jantawong and Dr. Win Bunjongpru, all from TMEC for their greatest associations. Specially, I again acknowledge Dr. Kowit Pattanapanyasat and Dr. Nuttawat Onlamoon from Faculty of Medicine, Siriraj Hospital, Mahidol University for their great collaborations in Flow cytometry size-based quantification. So many times, I would like to thank Mr. Anusorn Kaneungthong, Dr. Siriluk Meesuwan and Dr. Sudchaya Bhanpattanakul for your helpful associations especially when I was in UBCO. In addition, Mr. Thammawit Suwannaphan, Mr. Attawut Thanormsridetchai and Mr. Tewan Tongmanee, from BioMEM laboratory, Department of Mechanical Engineering, Faculty of Engineering, Chulalongkorn University, for their excellently preliminary works in microfluidics, especially in CFD simulation and microdevice designs.

Furthermore, I would like to be thankful the research grants from the National Research Council of Thailand (NRCT 2015 and 2017-2019), the Special Task Force for Activating Research (STAR) of Chulalongkorn University, Health Cluster Through Micro-Nano Research group (GSTAR 56-005-21-002), and the Companion Animal Cancer Research Unit, CAC-RU, Chulalongkorn University (GRU-002-31-002).

Ultimately and endlessly, I would like to acknowledge my father and my mother for your all backup bringing me about the victory in this study as well as with the special thanks to my wife, son, daughter and grandchild for your encouraging and patience along my study.

CONTENTS

Page

Page

Page

Page

Page

LIST OF TABLES

LIST OF FIGURES

LIST OF ABBREVIATIONS

%	Percent
1X	One-fold
10X	Ten-fold
4X	Four-fold
400 X	Four hundred-fold
a_p	Particulate diameter
ASM	Archimedean spiral microchannel
BSA	Bovine Serum Albumin
CD117	Cluster of Different 117
CFD	Computational fluid dynamic
DAB	Diaminoenzidine Tetrahydrochloride
DLD	Deterministic lateral displacement
DNA	Deoxyribonucleic Acid
EFS	Extensional fluid stress
EMB	Eosin-methylene blue
FACS	Fluorescence-activated cell sorting
FCS	Fetal calf serum
FSC-A	Forward scattering light
FSS	Fluid shear stress
HPF	High Power Field
ICF	Immunocytofluorescence
Hct	Hematocrit

H&E	Hematoxylin and eosin
hr	Hour
HMW	High molecular weight
LTC_4	Leukotriene C_4
LTD_4	Leukotriene D_4
M	Molar
MCT	Canine Cutaneous Mast Cell Tumors
MCT-CIC	MCT-cancer initiating cells
min	Minute
ml	Milliliters
mm	Millimeters
^oC	Celsius degree
OD	Optical density
PCV	Pack cell volume
PFF	Pinched flow fractionation
PDMS	Polydimethylsiloxane
qPCR	Quantitative polymerase chain reaction
rpm	Round per minute
SEM	Scanning electron microscopy
SCA	Single cell analysis
s	Second
TMRM	Tetramethylrhodamine-methyl ester
μg	Micrograms
μl	Microliters

μm	Micrometers
τ_w	Wall shear stress
ω	Confinement ratio

CHAPTER I
INTRODUCTION

1.1 Importance and Rationale

In the prologue, neoplastic diseases (tumors and cancers) have the long-lasting history since the first evidence of cancers has been reportedly recognized in the bone fossil of Egyptian ancient, as the presumptive osteosarcoma (Strayer and Rubin, 2012).

In the recent decade, neoplasms are incurably deleterious, formidable non-communicable diseases. A neoplasm presumably arises when a singly normal cell in a given tissue has dynamically accumulated irreversible genetic impairments and instability of such key genes. And these preposterous genes usually incurs a perversity of cell cycle, growth, proliferation, differentiation, survival as well as senescence because they have lost their regulatory functions (Abaci et al., 2014; Hanahan and Weinberg, 2000; Kumar, 2013; Strayer and Rubin, 2014).

Since the molecular lesions of those anomalous key genes are driving the disordered cell to 1) circumvent the genomic repairing mechanisms, 2) resist to any forms of programmed cell death, and 3) autonomously proliferate indefinitely; therefore, they beget an atypically cellular outgrowth and a neoplastic formation (Hanahan and Weinberg, 2011). Although, the causative agents for genomic instability and cell transformation have been detracted (Kumar, 2013; Strayer and Rubin, 2014). Nevertheless, the progressive development of the diseases is likely governed by multiplex factors which handle a balance of cellular proliferation versus differentiation, including various mutations of proliferation-regulatory genes, epigenetic dysfunctions and alterations, and abnormally proliferative signaling-pathways (Kumar, 2013). Therefore, a comprehension in the abnormal functionalities of these elementary factors is indispensable.

In the recent decade, cancers are the secondarily leading incommunicable diseases which result in the death of Asian, European and North American people (Longo, 2010). Although, the total incidence of almost cancers and the death tolls

seem to be reduced worldwide according to early effective diagnoses, preventions and advanced target therapies. However, some typical cancers such as hepatic and pancreatic cancers have increased their incidences so far in almost cancerous population (Longo, 2010; Siegel et al., 2017). In veterinary medicine, this propensity in other mammalian metazoans is also remarkably resemblance to humans (Butler et al., 2013; Merlo et al., 2008; Reif, 2007).

Naturally, neoplasms are composed of at least two mixed-parenchymal-cell subpopulations; the terminally-differentiated (mature) and undifferentiated (immature or blast-like) cells which sometimes referred as cancer initiating cells (CICs).

In the first category, the neoplastic cells are generally monomorphic, well-differentiated, copious and unaggressive. Their morphology usually resembles to their normal cells of origin. Principally, they have charge of being the major constituent of neoplastic bulks.

On the other hand, the hallmarks of the second subpopulation are generally pleomorphic, anaplastic, rare and aggressive. The neoplastic cells in this class are inferred to be responsible for a disease propagation as well as a replenishment of mature neoplastic cells by asymmetrical cell divisions. Moreover, they are supposed to possess the self-renewal capacity and stemness (Reya et al., 2001; Ward and Dirks, 2007). Morphologically, the cells are generally thought to be larger than 15 μm; meanwhile, the sizes of their elementary progenies are variegated from 7-15 μm depending on cell types. Since, the morphology, biological behavior and function of CICs are disparate from their mature counterparts. Thus, irrefutably, any outright comprehension in the elaborate biology of CICs will expedite oncology connoisseurs to establish a *bona fide* mode of treatment for disease annihilation.

However, the major hindrance which hampers the study achievement in CIC biology is that of cellular heterogeneity. Because either normal cells or in particular cancerous cells commonly alter their pathophysiologic properties over the time. Cellular heterogeneity is contemplated to be influenced by both genetic and non-genetic (epigenetic) elements (Marusyk et al., 2012), microenvironment, cell-to-cell

communication and cell-to-non-cellular component interaction (Visvader and Lindeman, 2012).

To cope with this obstacle, single cell analysis are hitherto recommended throughout the world as a solution pack for resolving this dilemma. Therefore, an analysis of live cancer initiating cells at the single cell level is so imperative for demolishing the impact of cell heterogeneity. Moreover, the analysis must furnish a statistically meaningful information of any CIC changes. In addition, the analytic performance must be 1) high-throughput, 2) highly-sensitive (Lecault et al., 2012; Wheeler et al., 2003; Yin and Marshall, 2012), and 3) not be harmful to targeted cells.

Unfortunately, any in-hand conventional laboratory methods we have to date, are however not precisely suitable for single cell study because they naturally measure an average response from all cell populations in a given cell cluster. Moreover, they do not have any ability to demarcate live targeted cells from their mixed populations. Thus, one can mislead the consequence of change in which its signal from a deviant cell is very low but most salient.

As previously described, CICs play a critical role in oncogenesis within a given cancer. Hence, the isolation of single CICs from their counterparts is the first essential step which brings about a further study in a diversity of CIC biology. Since the dimension of CICs often differs from their mature counterparts, especially the size so that the usage of this distinguished biological property is so beneficial for isolating CICs from the others. In addition, any size-based cell isolation eases researchers to primly handle and manage targeted cells as well.

Even though, there are some research gears which can currently serve cell biologists for single cell analysis, particularly size-based cell separations, such as fluorescence activated cell sorting (FACS or flow cytometry), magnetic activated cell sorting (MAC), laser microdissection (LMD) and dielectrophoresis (DEP) (Gross et al., 2015; Tanaka et al., 2012). However, almost are label-dependent and require prolong and intricate sample preparation, well-trained personnel to operate and a large space occupation for instrumentation. Moreover, they are usually harmful to the cells

because of their labeling processes (Tanaka et al., 2012). Flow cytometry itself causes a noxious effect to sorted individual cells as well, owing to the high fluid shear stress (FSS) in its sheet-flow system (Cheng et al., 2016).

Therefore, a critical hitch for size-based cell isolation to date is the scantiness of trusty methods which are label-free (passive), sensitive and easily reproducible. Moreover, the technique performance should be high-throughput and convenient to operate without a need for well-trained workforces. Significantly, the method must not be detrimental to the viability of sorted cells.

One of the innovative methods which is recently appealed to overcome this problem is microfluidics. It is an integrative science and engineering technology employed for precisely manipulating behaviors of small amounts of fluid flowing in a typically-designed downscale microchannel (Mu et al., 2013; Ouellette, 2003). This technology does indeed augment researchers to accurately control not only hemodynamic properties of fluid flow but also spatiotemporal particulate movements in the fluid, as seen in an inertial focusing of microspheres in a spiral microchannel (Kuntaegowdanahalli et al., 2009). In addition, it is a label-free, especially antibody-independent, technique which is not dreadful to targeted cells.

Because of the cornerstones of microfluidics including small specimen volume utilization, low cost fabrication, label-free cell preparation, short reaction time, high-throughput (Chen et al., 2013) and microenvironment mimicry to *in vivo* milieu; hence, there are many microfluidic platforms recently devised worldwide for singly cell-based assays particularly for single cell entrapment and culture as well. Moreover, with an advantage in optical transparency of the polydimethylsiloxane (PDMS) generally used for fabricating microfluidic replicas, a real-time monitoring for phenotypic and functional alterations of target cells is easily performed (Wu et al., 2011).

Canine cutaneous mast cell tumor (MCT) is the skin-form mast cell sarcoma frequently occurring in canids. Its incidence is approximately 7-21%. With the aggressively variated biological behavior of MCT cells, almost patients thus usually suffer from either cancer invasion or paraneoplastic syndrome due to degranulation of

actively biological mediators, such as histamine, serotonin and heparin. Habitually, paraneoplastic syndrome can result in a fatal effect to MCT patients, including gastrointestinal perforation and acute cardiac failure caused by histaminic vasodilation (London and Thamm, 2013; Thamm and Vail, 2007). Therefore, almost MCT patients in general require a rigorous treatment to pause disease progression.

Taken together, MCT is a prevalently lethal skin neoplasm in dogs and requires an aggressively therapeutic strategy. Theoretically, MCT itself should contain cancer initiating cells (MCT-CICs) which their property is fit into the CIC criteria. Therefore, a comprehension in MCT-CIC biology is so essential because it will determine an optimally therapeutic protocols which can eradicate the disease. However, cell heterogeneity is still the key obstacle that masks our insight.

To circumvent this difficulty, it is indispensable to study live MCT-CICs at the single cell level. And the first step is to isolate them out of neighboring cells based on the difference on sizes. As well as, MCT-CIC culture is essentially recommended because it will provide a perpetual information on biology alteration of MCT-CICs.

Since microfluidics has recently emerged to promise us a single cell analysis so far. Hence, an invention of microfluidic chips, which are able; to isolate live, single MCT cells depending on their sizes and trap a number of the individually isolated cells, will enhance our capability; to separate the real MCT-CICs from their counterparts and further cultivate them for monitoring their real-time biologic changes.

Ultimately, any study information of those isolated MCT-CICs at the single cell level will take us into the comprehension in MCT pathogenesis and lead us to establish the most effective therapy for MCT in the upcoming days.

1.2 Research questions and Hypothesis

By the way of introduction, it tacitly indicates the significance role of single cell analysis on oncologic study. Because the key hindrance is cellular heterogeneity caused by the dynamic alteration in neoplastic cell biology.

Moreover, in the recent decade, we have no traditional methodology which can optimally serve us to perform a single cell analysis by without a harmful effect to studied cells. And MCT is still a problematically cutaneous cancer in canids.

Taken together, hence, this study has ultimately been setup to answer our preliminary questions inquest under the hypothesis as following;

- Research questions,

    1. Can we apply a label-free, microfluidic-size-based system to isolate MCT cells, and entrap them?

    2. After isolation, are the microfluidic-separated MCT cells still alive?

    3. Could we determine some key-biological properties of individually trapped MCT cells after passively inertial microfluidic entrapment?

- Research hypothesis:

    1. Under passive inertia microfluidic platforms, we can use a label-free Archimedean Spiral Microchannel (ASM) to separate single MCT cells depending on their individual sizes. And we can use a microwell array to capture single MCT cells without antibody intervention.

    2. After passively hydrodynamic-inertial cell sorting with ASM, all isolated MCT cells are viable.

    3. We can evaluate self-renewal and cell vitality of single MCT cells entrapped in microwell array.

1.3 Objectives of the study

Upon the aforementioned research questions and hypothesis; therefore, the objectives of this study have been setup under the following conditions;

- Objectives of the study

    1. To develop two label-free, unlethal microfluidic platforms; an ASM for size-based single MCT cell isolation and a microwell array for single MCT cell capturing.

    2. To investigate the self-renewal and the vitality of single MCT cells entrapped in the microwell array.

CHAPTER II
LITERATURE REVIEW

2.1 Canine cutaneous mast cell tumor (MCT)

Canine cutaneous mast cell tumor (MCT) is a common skin neoplasm of canids. The disease is proposed to arise from an uncontrollable proliferation of an aberrantly dwelling mast cell in the skin. The incidence of MCT has been reported up to 20% of all canine cutaneous neoplasms (London and Thamm, 2013; Thamm and Vail, 2007) and the disease is usually observed in dogs aging over than 8-year-old. In addition, there is no gender predilection. Although, the breed predilection is still arguable; however, Boxer, Bull dog, Pug, Labrador retriever, and Golden retriever have been accounted for the most susceptible breeds for MCT.

Pathologically, MCT usually presents as a singly pinkish-solitary, well-circumscribed, erythematous firm nodule by with or without skin and/or subcutis ulcerations. The preferential sites are in general 50% on the trunks and perineal regions, 40% on the limbs, and 10% on the heads and necks. However, there are approximately 10 to 15% of MCT dogs presenting multiple tumors particularly in Golden retrievers. And it is not necessarily associated with the poor prognosis.

Basically, MCT which are at the muco-cutaneous junctions such as buccal cavities and inguinal areas, are generally more aggressive. MCT metastasis is barely observed in canine species. Its metastatic rate is perhaps lower than 3% in almost MCT populations (Dobson and Scase, 2007). The growth rates of MCT are almost always low in benign (low-grade) and rapidly high in malignant (high-grade) MCT. In the most cases of the last category, they frequently come along with poor prognosis (London and Seguin, 2003).

Morphologically, well-differentiated MCT cells from the low-grade are varied from 10 to 20 μm in diameter. Their nuclei are hypochromatic and often round to slightly oval, with a degree of aggregated chromatin and single nucleoli. The cytoplasm usually contain metachromatic granules and clearly refractive vacuoles. Anaplastic

MCT cells from the high-grade are approximately 12 to 35 μm in diameter. They are commonly binucleated. Their cytoplasm are composed of fewer metachromatic granules; however, the granules may be absent in such anaplastic MCT cells (Duncan and Prasse, 1979).

The clinical signs of MCT in general are resulted from degranulation which is the liberation of various vasoactive amines contained in the membrane-bound cytoplasmic granules. Intriguingly, a mechanical manipulation during physical examination may induce degranulation leading to severe erythema and wheal formation (Darrier's sign). Anyhow, the most seriously paraneoplastic syndrome of MCT is gastrointestinal ulceration and perforation caused by histamine (London and Seguin, 2003; London and Thamm, 2013; Thamm and Vail, 2007) and cardiac failure.

2.2 Cellular and intratumor heterogeneity

One of the major challenges in cellular biology is how individual cells processing either intrinsic or extrinsic signals and responding to stimulus cues. Anyhow, some cell-to-cell variegation, usually regarded as cellular heterogeneity, always exist among cell subpopulations (Zhang et al., 2016). This divergence always results in the ensemble biology of all cell populations and it might not represent the exact behavior of any individual cell (Altschuler and Wu, 2010).

Cellular heterogeneity is an omnipresent biology feature in all viable cells (from bacteria to mammals). It could be observed anytime and in either normal stem cells which have cultivated in the best conditions (Tang, 2012) or normal mature cells in which they live in the same environment (Friedman, 2013). Thence, in a given tissue, there is inhomogeneous intermixing between pluripotent stem cells and partially committed cells which have disparate biological properties (Tang, 2012). By this, any cell is not identical. As in normal mast cells, cellular heterogeneity also occurs. Normal mast cells from a divergence of anatomical locations principally always differs from one another in their morphological, histological, biochemical and functional characteristics (Huntley, 1992). This might suggest each individual mast cells might

variably respond to diversely spatiotemporal stimuli (de Mora et al., 2006; Hill and Martin, 1998). Histologically, the heterogeneity of mast cells might assort normal mast cells into two subpopulations; connective tissue mast cells (CNT-MCs) and mucosal mast cells (MCS-MCs), depending on their cytoplasmic granule contents investigated by both cytochemistry and immunohistochemistry. For example, MCS-MCs usually stain blue with alcian blue; meanwhile, CNT-MCs are tangible red with safranin (Hill and Martin, 1998). Moreover, MCS-MCs in the alimentary tracts predominantly produce more prostaglandin D_2 (PGD_2) than leukotriene C_4 (LTC_4) which is contrary to those found in the pulmonary tracts. This would also imply the physiological heterogeneity of mast cells (Prussin and Metcalfe, 2006). In addition, C2 mast cell line synthesizes prostanoids series D_2 and E_2 depending on stimuli (de Mora et al., 2006). Therefore, undoubtedly, cellular heterogeneity should take place in case of MCT as well.

At the genetic viewpoint, all neoplasms presumably arise from a singly transformed cell through a Darwinian-like clonal evolution (Marusyk and Polyak, 2010; Zellmer and Zhang, 2014); therefore, all neoplastic cells are contemplated to be homogenous (Kent et al., 2011). However, there have been a plethora of evidence substantially unveiled the existence of cancer heterogeneity in various steps of cancer development. In fact, cancers always consist of divergently cellular subpopulations in which one subset is different from one another in their morphology, phenotype and functionality (Sengupta and Cancelas, 2010), as well as behavior. Thus, all neoplasms are not identical even in a given cancer (Kosovsky, 2012).

The intratumor heterogeneity has long-lasting been traced. Approximately 150 years ago, Rudolf Virchow, the father of modern cellular pathology, observed the pleomorphic cancer cells in his investigated specimens. Later, since 1970s, many investigators have also identified the distinct neoplastic cell subpopulations based on their morphology, size, antigenic determinant, biochemistry, phenotype, cell-to-cell-interaction or even behavior and functionality (Michor and Polyak, 2010; Visvader and Lindeman, 2012), intermixing with their major well-differentiated subpopulations (Almendro et al., 2013; Magee et al., 2012).

Basically, the heterogeneity in cancerous cells is overtly observed by a diversity of experimental methods, in particular histopathology and immunohistochemistry. For example, a histopathological section could demonstrate the persistence of immature and well-differentiated cancerous cells which are distinguished from each other in morphology, molecular characteristic, biological functionality and aggressiveness (Zhang et al., 2016). Epistemologically, the heterogeneity of neoplastic cells is presumably driven by the integration of both stochastically genetic and non-genetic (epigenetic) element alterations and instabilities (Magee et al., 2012; Marusyk et al., 2012), including other various factors, for example cancer microenvironment, cell-to-cell communication and cell-to-non-cellular component interaction (Zhang et al., 2016).

Unfortunately, our traditional laboratory methods recently used could not eradicate the impact of intra-tumoric heterogeneity because they as usual measure an average response from all cell populations including targeted cancer cells in a given cancer resulting in misleading interpretations. Furthermore, the heterogeneity of cancer cells would gradually make the boundary line between targeted cancer cells and the rest becomes blurry (Shipitsin and Polyak, 2008). Thus, the interpretations in various experimental models should be performed with the caveats. Because the characteristics of most abundant cancer cells might not be the surrogates in biological properties of the targeted cancer cells but are for the mixed populations instead (Marusyk et al., 2012).

2.3 Single cell analysis

Single cell analysis (SCA) is a research technology used for interrogating altered cell biology of each individual cell in many aspects (e.g., proteomic, transcriptomic, genomic and metabolomics) in that the average measurements of changes from all cell subpopulations with traditional methods could not do. Fundamentally, methodology of SCA can be merely defied into invasive and non-invasive SCA respectively. Invasive SCA or chemical SCA is a toolbox exploiting a variety of

chemicals such as antibodies and fluorochromes to quantify intracellularly targeted components. Meanwhile, non-invasive SCA (biological SCA) is utilized for measuring the biological responses of each intact cell after being stimulated. It can further be classified into time and non-time dependent noninvasive SCA (Fritzsch et al., 2012).

Because single cells are the basic unit of a living organism; thence, a comprehension on the biological variability of the cell becomes a key requirement for biomedical researches. However, our in-hand traditional cell assays under the cell heterogeneity regime for study cell division, differentiation, gene expression and stimulus response are immensely operated on total cell population instead of the single cells.

Since the awareness in cellular heterogeneity provides valuable insights and caveats in systemic, stem cell and neoplastic biology including tissue engineering. And the usage of single cell analysis also benefits for gene expression mapping and sorting complex samples. In addition, the utilization of study methodologies at the single-cell resolution would potentially be suitable for investigating dynamic proteomics and tracking cell populations of stem cell and cancer cells (He et al., 2015).

To resolve the above dilemma, the analysis of individual cancer cells is thence indispensable for eliminating the effect of cell-to-cell variability. And any dynamic, biological process must be easily monitored on individual living cells (Friedman, 2013). Furthermore, the methods must provide a statistically meaningful data, a high-throughput and highly sensitive means for single cell analysis (Lecault et al., 2012; Yin and Marshall, 2012).

2.4 Conventional versus microfluidic single cell analysis

Cell separation and identification are the essence processes in all biological studies including single cell analysis (Pinho et al., 2013; Russom et al., 2009). In the last decade, various contemporary study techniques have been employed for single cell analysis so far, for instance flow cytometry and laser-based microdissection (He et al., 2015). Anyhow, the advantages and disadvantages of those traditional methods are

long processing time, well-trained personnel requirement and intricate sample preparation (Tanaka et al., 2012) label-independent which increase the lethal impact on targeted cells. In the last decade, Flow cytometry is the most mature technique used for single-cell analysis. Fluorescence-activated cell sorting can sort single cells which has been tagged by specific fluorescent markers, such as antibodies. Although, flow cytometry can isolate labelled-single cells; however, it cannot analyze individual cells in their natural environment at the real time (He et al., 2015). Fortunately, these hassles have been overcome since a state-of-the art methodology called microfluidics have been devised (Friedman, 2013).

Microfluidics is an innovatively integrative science and engineering technology employed for precisely manipulating behaviors of fluid flowing in a downscale microchannel (Mu et al., 2013; Ouellette, 2003; Sackmann et al., 2014), enables an attractive means for handling micro-particles including cells suspending in fluid media. It also provides a microenvironment mimicry in which natural cells have resided. Moreover, the other goal of microfluidics is to fundamentally implement and integrate various fluid regulation components such as pneumatic pumps and valves, membrane filters and analytic mixers, to a variety of advanced analytical cell isolation and evaluation methods including electrophoresis, chromatography, cytometry and electrochemical detection methods, on individual microdevice for a complete on-chip analysis (Fiorini and Chiu, 2005). Since microfluidics has widely been introduced into the fields of biomedical engineering. There is a plethora of evidence exhibiting the successfulness in the applications of this technology for a variety of cell researches, such as cell sorting and separation, cell entrapment, on chip cell culture, DNA sequencing, PCR, proteomic (Fiorini and Chiu, 2005), cytometry and enrichment of rare cells in particular circulating tumor cells at the single cell (Mu et al., 2013; Zhou and Papautsky, 2013).

However, many phenomena in passive microfluidics are still obscured and required more attentions to verify their underlying factors before this technology can absolutely be utilized especially in biomedical researches within a couple of upcoming years. Luckily, much more endeavors to accomplish the aims are underway.

2.5 Microfluidic platforms for single cell sorting and entrapment

Since microfluidics has promised biomedical and bioengineering researchers to ease their single cell analysis. Various integrated methods for cell manipulation based on microfluidic lab-on-a-chip platforms referred as microfluidic chips, are currently devised. On microfluidic platforms, single cell sorting, single cell entrapment, mRNA purification and quantitative polymerase chain reaction (qPCR) can be concurrently operated on the chips. Moreover, the on-chip single-cell genomics, epigenomics, transcriptomics and proteomics can finally answer various enduring questions in biological and biomedical sciences effectively (He et al., 2015).

Upon the advantages of microfluidics, various microfluidic regimes have been applied in many diverge fields of cell biology so far. For example, Cheng and his coworkers had developed a high-speed, label-free microfluidic platform which was capable to isolate single $CD4^+$ T lymphocytes in HIV-positive whole blood based on the differential shear flow across the cells (Cheng et al., 2007). Moreover, there was the invention of microfluidic platform which could dynamically monitor the heterogeneous insulin-secretome signatures (secretion fingerprint) from individual pancreatic Langerhans' β-cells (Castiello et al., 2016).

Fundamentally, cell separation is the first key step in cell biology study. In the recent decade, there are diverse contemporary methods are being used in single cell separation in addition with entrapment. Of these, almost are fluorescent activated cell sorting (FACS) or flow cytometry (FCM) at 33%, laser microdissection (17%), manual single cell harvesting (17%) and stochastic cell dilution (15%). However, microfluidic-based single cell analysis has been used approximately only 12% out of overall single cell analysis technology so far (Gross et al., 2015). Essentially, the key parameters for a design of microfluidic-based cell separations are as of the following; 1) highly segregating resolution, 2) high purification yield, 3) high throughput, 4) multidisciplinary utilization across different cell species and 5) executive robustness. Fortunately, almost microfluidic cell separation regimes devised to date are coverage all requirements because most of the microchannel geometries are properly scaled down to the cell size giving rise the better cell manipulation (Warkiani et al., 2016). Cell viability is also

the additionally crucial parameter which cannot be neglected when performing microfluidic single cell sorting. Because, Cellular response to mechanical for example, hydrodynamic stress will result in cell differentiation and decreased cell viability. Therefore, all microfluidic cell sorting must furnish a gentle means of cell extraction and handling when performing on naturally live cells (Gross et al., 2015). Nevertheless, the other key challenges in cell sorting not only in all traditional methods but microfluidics are the discrimination of sorted cells in their sizes, densities, shapes, surface protein molecules (Mohamed, 2012), albeit these could be utilized for cell sorting, they are however bringing about a resolution interference of microdevice as well.

For microfluidics, there are two microfluidic isolating paradigms; the active and the passive platforms, are being utilized in single cell sorting. Basically, the active process in such magnetophoresis, dielectrophoresis and acoustophoresis, requires the external force fields applied to sort and trap the targeted cells. Meanwhile, the passive regime always use a geometry of microfluidic microchannel and the inherited hydrodynamic property of fluid to manipulate the cells almost based on cell sizes. Even though, active processes are more sensitive and precisely controllable; however, they have not been favorable because of their low-throughput performances, external force fields and multiplex auxiliary systems required causing a complicated device fabrication, and immuno-labeling technique. Nevertheless, the residential time of separated cells in the microchannel is usually prolonged so as to increasingly accumulate more stresses. For instance, some active processes such as electrophorhesis and dielectrophoresis require the external power for its batch operation (Kuntaegowdanahalli et al., 2009). Thence, there is a probability in which trapped cells can be injured through membrane electroporation by unsealing and/or membranal protein denature (almost movable charged proteins). These have been caused by Joule heating or alteration in intramembrane current. Generally, the threshold potential for electrical membrane break-down is ranged from -450 to -500 mV (Chen, 2006). Furthermore, an exposure of continuous low-voltage DC electrical field (> 1ms) can result in a change in molecular structures of cytoplasmic organelles

(Lee, 2005). In addition, almost techniques are low throughput which is not suitable for a bulky cell separation.

Since the passive microfluidic sorting is principally not dependent on the external force fields. Therefore, this method should not be deleterious to the targeted cells. Nevertheless, there are several passive microfluidic models have been nowadays introduced worldwide for single cell sorting, for instance spiral microchannel, pinched flow fractionation (PFF), centrifugal and gravitational sedimentation, hydrodynamic chromatography (HDC), deterministic lateral displacement (DLD), and contraction-to-expansion inertial focusing and porous membrane filtration (Kuntaegowdanahalli et al., 2009; Martel and Toner, 2012). However, the most disadvantages particularly in PFF and DLD are the cell obstruction (Kuntaegowdanahalli et al., 2009) causing a depletion of targeted microparticles in the rage of 1 nm to 100 μm (Park and Jung, 2009), and the need of intricate 3D fabrication in porous membrane percolation (Kuntaegowdanahalli et al., 2009).

Although, there are some limitations of passive microfluidic cell separation. However, the usage of internal hydraulic properties of fluid in a passive process is currently more attractive and could enable for a high-throughput cell separation (over than 0.5 ml. min^{-1}). Moreover, without any applications of external forces, the method is to economize the fabrication cost because of its assembly simplicity, and increased device portability. Critically, based upon the basis of passive microfluidic, this method should not be hurtful for the cells of interest and is cost-effective as well. Notwithstanding, the accomplishment on the goals is dependent on an optimal design of microchannel geometry and a proper control of intrinsic hydrodynamic components inside the channel (Zhang et al., 2014). For examples, Yamada and colleagues had successfully fabricated a rectangular microchannel with a series of side narrow (30μm-wide) and broad (50 μm-wide) microchannel for adjusting the specific flow resistances, to passively separate hepatocytes from their non-parenchymal cells (Yamada et al., 2007).

Of those, the spiral microchannel seems to be the most effective method for size-based single cell sorting. Therefore, there are many geometrical configurations of spiral microchannel have been used so far. For example, a trapezoidal spiral microchannel, a gradually varied width spiral microchannel with a pillar-array microfilter (Geng et al., 2013) and a double spiral microchannel. However, the Archimedean spiral microchannel is most favorite geometry used (Di Carlo et al., 2007; Kuntaegowdanahalli et al., 2009; Tanaka et al., 2012). For instance, Kuntaegowdanahalli and colleagues have achievably employed a spiral microchannel to passively separate SH-SY5Y neuroblastoma cell sized at 15μm from 7μm C6 rat Glioma cells (Kuntaegowdanahalli et al., 2009). Nevertheless, Hur and his team has also used a similar configuration of spiral microchannel to spanwise sort human WBCs from RBCs. The other intrigued successfulness is the separation of bacteria contaminating in the diluted human blood by Wu's research team (Salieb-Beugelaar et al., 2010) as well as the sorting of human platelets from other blood components (Tanaka et al., 2012). Thence, almost studies have emphasized in the applications of various geometries of curved microchannel to focus the cells.

Fundamentally, the inertial cell focusing in spiral microchannel is governed by the secondary flow fields including Dean Vortices. Anyhow, the studies of the underlying physical mechanisms for an optimal modulation of inertial focusing and their dreadful factors cells such as fluid shear stress (FSS) and extensional flow Stress (EFS) on cell viability are paid the less attention (Zhou and Papautsky, 2013).

In single cell trapping, basically, the hydrodynamic cell entrapment with microfluidic chips usually utilizes the passively structural control to allow a single cell to be ensnared by minimizing the trap size to fit with its average cell size. However, the disadvantage of this paradigm is the need for specific designing and its inflexibility (Gross et al., 2015). In one study, Chen and his colleagues have used a 1024-microchamber microfluidic device to form the neoplastic microsphere from the single cell under a hydrodynamic capturing scheme. They have reported that their 70% of microchambers could entrap single cancer cells (Chen et al., 2016).

2.6 Physiologic and pathophysiologic effects of fluid shear stresses on cell biology

Physiologically, in fact, hydrodynamic shear stress can exert on the cells to determine their morphology and internal physiology. It also plays a critical role in physiologic adaptation of cells such as cell elongation (Akenhead and Shin, 2015) by spatial reorganizing subcellular cytoskeleton (Galbraith et al., 1998) in particular increased stress fiber formation (Cucina et al., 1995), a decrement of cell proliferation, lowering angiogenic gene expression, and increased cortical actin formation in endothelial cells, as seen in a microfluidic vascular model (Abaci et al., 2014). In addition, the shear stress always contributes to stimulate vascular endothelial cells to differentiate into a blood-brain barrier (Cucullo et al., 2011).

In pathology viewpoint, fluid shear stress can incite endothelial remodeling and membrane fluidity through shear stress receptors such as cell-to-cell or cell-to-matrix adhesion molecules, ion channels, tyrosine kinase receptors and caveolae resulting in development of diseases such as atherosclerosis (Butler et al., 1999; Resnick et al., 2003). The effect of fluid shear stress on morphological and pathological changes of cells is commonly dependent on the exposure magnitude and duration. One study has shown that kidney cells would start cytoplasmic enzyme leakage caused by plasma membrane disintegration without any morphological change when they experienced the FSS at the 12 N. m^{-2}. And they have initiated morphology alteration at the FSS of 26 N. m^{-2}. In addition, the morphological change was increased when time went by under fixed fluid shear stress (12 N. m^{-2}). Nevertheless, high wall shear stress also impacts on the branching of cerebral aneurysm by increasing aneurysm initiation sites (Geers et al., 2017).

Fundamentally, cell wreckage under fluid shear stress such as extensional shear stress has long been interested, in particular in the rheological study of the erythrocytes susceptible to hemolysis under an immediate change of fluid shears in such medical devices, for example prosthetic cardiac valves, cardiopulmonary bypass and renal dialyzer (Down et al., 2011). Basically, cell lysis is frequently relevant to membrane integrity. Naturally, the major composition of cell membrane is phospholipid bilayer which is prone to rupture by excessive membrane tension but

not a compression. When the membrane surface tension is increased, it would tear off as notified in the micropipette aspiration and the osmotic (Braasch, 1969.; Kretzmer and Schugerl, 1991). Nevertheless, human leukocytes exhibits an attenuation of the pseudopodium retraction under fluid shear resulted from an abolishment of β1-integrin attachment to the endothelium (Marschel and Schmid-Schönbein, 2002).

CHAPTER III

MATERIALS AND METHODS

Section I: MCT cell preparation

3.1 Patient selection

Dogs with a variety of cutaneous masses were selected at the Veterinary Oncology Unit, Small Animal Teaching Hospital, Faculty of Veterinary Science, Chulalongkorn University, during 2015 to early 2016. All clients were notified in research participations. Fine needle aspiration (FNA) with Giemsa staining was performed to rule out MCT patient from others, case by case. In a case which its cytology was vague or resemblance to other canine round cell tumors, it was underwent CD117-immunocytofluorescence to ratify the existence of MCT cells.

Finally, six MCT patients (regardless of histopathological grades, WHO clinical staging and TNM criteria) were accepted to take part in this study. Their complete histories of physical examinations, therapeutic protocols and individual client consents were reviewed. Later, each MCT dog was performed an excisional operation to remove the MCT mass by licensed veterinarians. Half of each mass was submitted to Department of Pathology, Faculty of Veterinary Science, Chulalongkorn University for MCT confirmation with Giemsa staining and histopathology. The remaining half of each mass was then sent to our laboratory for CD117-immunocytofluoresence and single MCT-cell isolation using trypsinization.

3.2 CD117-immunocytofluorescence screening

To clarify an existence of MCT cells, 25 μl of FNA neoplastic cells were smeared on a clean silane-coated glass slide (Sigma-Aldrich, USA). The cells were preserved in 4°C acetone for a minute and incubated by 1ml fetal calf serum (FCS) for 30 min at room temperature for nonspecific protein blockage.

Later on, PE-conjugated mouse monoclonal anti-human CD117 (KIT) antibodies (Clone Y.B5.B8, Becton and Dickinson, USA) were incubated on the cells at the dilution of 1:100 at the room temperature in a dark chamber for 30 minutes. The nuclei were then counterstained by 4', 6-diamidino-2-phenylindole (DAPI, Invitrogen, USA) and they were visualized under fluorescent microscopy with the 575 nm light source for PE activation (Ketpun et al., 2013).

3.3 Single MCT cell isolation

To reduce the bias on cell vulnerability and viability, freshly single MCT cells of each case were noninvasively isolated and harvested from the cutaneous MCT mass removed by the operative intervention. Stepwise, one gram of the lean MCT tissue was chopped into tiny pieces (approximately 2 x 2 x 2 mm^3). Each diminutive specimen was further collected in a 2ml centrifuge tube and was trypsinized (200 μl of 0.025% Trypsin-0.01% EDTA) in 500 μl PBS at 38°C for 20 min. The reaction was then terminated by 1 ml of 2% FCS. An undigested tissue remnant was filtered out via a 30μm cell strainer. The cell flow-through of each tube was pooled together into 15ml centrifuge tube and was centrifuged at 3000 rpm for 5 minutes to collect single MCT cells. Finally, the cells were washed by PBS and centrifuged at 3000 rpm for 5 minutes at 4°C, twice. Ultimately, eosin-methylene blue (EMB) staining was done to evaluate MCT cell morphology and to affirm the existence of single MCT cells in the suspension.

Section II: Biomedical engineering assessment of cell vitality

3.4 Hemocytometry cell enumeration

Stepwise, a glass hemocytometer and coverslip were rinsed and cleaned by absolute alcohol (Sigma Aldrich, USA) before use. The coverslip was moistened with PBS and affixed to the hemocytometer. The cell suspension was then gently swirled by a vortex to evenly distribute single MCT cells. Further, 100 μl of the cell suspension was micropipetted and infused into a counting chamber of the hemocytometer. The total cells in 16 counting grids of each 1mm corner-square were tallied using light-microscopy with the 10X objective (Weiss and Tvedten, 2012). Ultimately, the total concentration of single MCT cells was reckoned by the equation in Appendix A. In addition, the microstructure of counting grids and the counting rule were illustrated in the appendix as well.

3.5 *in vivo* Vital dye bioassays

The cell vitality was simultaneously evaluated using two-tier vital dye systems; trypan blue (TB) and tetramethylrhodamine-methyl ester-perchlorate (TMRM). Basically, trypan blue is utilized to investigate cell permeability. It is gradually be permeated through the cell membranes of nonviable cells. In the meantime, TMRM is used to evaluate mitochondrial functionality. It always positively stains within the oxidative mitochondria of viable cells.

Stepwise, 500 μl of 0.4% Trypan blue (Hyclone™, GE Healthcare Life Sciences, USA) were admixed into 200 μl of PBS and 1 ml of 10 μM cationic-probe TMRM (Thermo Fisher Scientific, USA) was diluted in 500 μl PBS.

For microfluidic size-based cell sorting, 300μl sorted MCT cell suspension was aliquoted into a new 2ml collection tube. The cells were then incubated by prepared trypan blue as described above for 5 minutes in the dark chamber. After incubation, they were twice washed by PBS and centrifuged at 3000 rpm for 10 minutes. Cell permeability was evaluated using hemocytometry numbering for distinguishing live

MCT cells from the dead. To examine the functioning mitochondria of sorted MCT cells, 200 μl of MCT cells was incubated by TMRM admixture at 25°C for 30 minutes in the dark chamber. Excessive dyes were washed out from the suspension by PBS twice. After flushing, the cells were counterstained by DAPI (1:100) for 10 min. The fluorescent signals of TMRM were acquired under the fluorescent microscopy with TRIT-C filter at λ_{910}. Vital MCT cells would uptake TMRM into their oxidative mitochondria of which the florescent signals were detected as the red dots in the mitochondria (Romanelli et al., 2013).

3.6 Plain light-microscopy for cell morphology assay

In turn, 35 μl of MCT cell suspension was pipetted onto a clean glass slide and stabilized by a cover slip. To identify cell normalcy, deformation, degeneration and necrosis, the configurations including nuclei figures and cytoplasmic contents of individual MCT cells were evaluated under the plain light-microscopy at the high power magnification (40X) within the five different areas.

The interpretative criteria were as of the following;

I. Intact or well-differentiated or undegenerated MCT cells, their morphology was usually round to slightly pair-shaped in such circumstances. The cell membranes were normally integrative. The cells always contained round or oval nuclei with the numerous refractive cytoplasmic granules.

II. Deformed MCT cells, the deformability was defined as an ability of MCT cells could easily elongate or change their morphology under such induction factors including mechanical shear stresses. Principally, deformed MCT cells were usually elongated with oval to ellipsoidal nuclei. However, their plasmalemmas were still continuously integrated. The deformation degree were determined by the cell deformation index (CDI) in which it is the ratio of the alterative width to the

length of deformed MCT cells. Generally, the CDI value of ideally normal cells is equal to one. The principles of calculation for CDI was adapted from the measurement of shape index (SI) of bovine aortic endothelial cells (BAEC) deformed by the hydrodynamic shear stress (Nerem, 1991).

III. Degenerative MCT cells, the cells which underwent degenerative changes were identified based on their pathophysiological morphology. Severely elongated cells with slight membrane discontinuity and/or deformity such as blebbing were a landmark for MCT degeneration. Nonetheless, degenerative MCT cells were often swelling with or even without cloudy cytoplasm. Most of the cytoplasmic granules were often swollen as well.

IV. Necrotic MCT cells, in this category, the MCT cells undergoing necrosis had abnormal configurations such as severely distorted shape or even cell wreckage. The rigorous disintegration of plasmamembrane was also a crucially necrotic hallmark. Moreover, the abrasion and/or the dispersion of cytoplasmic contents were the predominant feature of necrosis as well. In addition, nuclear dislocation or sloughing was a harshly degenerative or necrotic figure for MCT cells.

3.7 Scanning electron microscopy (SEM) for morphology bioassay

Briefly, single MCT cells were washed twice in Hank's balanced salt solution (HBSS) and resuspended in 1 ml HBSS. They were further fixed in 1.2 % glutaraldehyde with 0.1 M sodium cacodylate (CAC) buffer (pH 7.3) for 1 hour and washed twice in 0.16 M CAC buffer (pH 7.3). They were post-fixed in 1% osmium tetroxide (OsO_4) in 0.1 M CAC buffer (pH 7.3) for 1 hour. The cells were serially dehydrated by graded ethanol

(25%, 50%, 75%, 95% and 100% for 10 min of each), by a series of three mixtures of ethanol-iso-amyl acetate at the ratio of 3:1, 1:1 and 1:3, and by pure iso-amyl acetate.

Several drops of cell suspension were transferred onto 10 mm aluminum membrane dishes and were left to settle for 2 min. Finally, the cells were dried in CO_2 in a critical point dryer, the specimen dishes were attached to aluminum stubs by carbon-propanol glue and coated with gold in a sputtering device (Burkhardt, 1979). The MCT cells were examined with a scanning electron microscope (JEOL JSM-6610LV, Tokyo, Japan) at the acceleration voltage of 15 kV. The criteria for evaluation; normalization, deformation, degeneration and necrosis, were in the same ways described in the plain light-microscopy above.

3.8 Spectrophotometry bioassay of leaky DNA

The disintegration of cell membrane, cell rupture or the increment of membrane permeability always result in a leakage of DNA from cells. Fundamentally, leaky DNA can be quantified by the standard spectrophotometry. Briefly, sorted MCT cell suspension from each outlet was centrifuged at 2000 rpm for 5 minutes. The supernatant was further diluted by DI water at the dilution ratio of 1: 100. The optical density (OD_{260}) of DNA was measured by a spectrophotometer at the wavelength of 260 nm (A_{260}). DNA concentration was calculated back by the following equation; dsDNA concentration = 50 μg/ml × OD_{260} × dilution factor.

3.9 Computational emulations of fluid shear stress and extensional flow stress in the size-based sorting system

Two mainly hydrodynamic inertia components; the fluid shear stress (FSS) and the extensional flow stress (EFS) were systematically simulated using the modeling software, COMSOL Multiphysics® version 6.3 (COMSOL, USA) under the finite element method.

The setup parameters of the fluid were composed of the following; the fluid medium was supposed to be Newtonian incompressible fluid with a batch of

physicochemical properties of density at 1000 kg. m^{-3} and dynamic viscosity at 1.003 x 10^{-3} kg. m^{-1}. s^{-1} at 20°C.

In the simulation, two key domains; the feeding conduit and the spiral loop were modelized with 5 x 10^6 controlling meshwork. The simulation was grid-independent. Appendix B summarizes the input parameters of the cell delivery domain used in the simulation. In addition, the simulation was based upon the non-slipped boundary condition and the preferential flow rate for the emulation was 1 ml. min^{-1}. The flow profile was presumably uniformed.

The formation of FSS and EFS were expressed in term of the locations and the color spectrums of their magnitudes. This information was finally utilized to predict their lethal effects on sorted MCT cell vitality.

Section III: Microfluidic-device designs and fabrications

3.10 Theoretical microfluidic designs

3.10.1 Geometrical design of curvilinear microfluidic microchannel (Archimedean spiral microchannel)

Passive inertial focusing, in general, uses the intrinsic hydrodynamic effect of one or more fluid sheaths around micro-particles including cells to orderly align them into two-dimensional widespread focusing band or three-dimensional single focusing streamline (Wang et al., 2015). Hydrodynamically, there are at least two dominant inertia forces; viscous drag force and inertial lift force, dictate the migration of neutrally buoyant micro-particles under the Poiseuille flow field in a strength rectangle microchannel (Kuntaegowdanahalli et al., 2009; Martel and Toner, 2012; Zhou and Papautsky, 2013).

Principally, the viscous drag force induced by fluid shear gradient entrains and moves suspended micro-particles parallel to the central axis flow. Meanwhile, underneath the limited channel Reynolds number, the nonlinear inertial lift force (F_L) is predominant and causes the lateral migrations of micro-

particles across the streamlines directed to the inner sidewall (Xiang et al., 2015; Zhou and Papautsky, 2013). After that, when particulates have got close to the inner wall, they are then influenced by the wall repulsion forces to push them away to the opposite directions (Di Carlo et al., 2007; Martel and Toner, 2012). Finally, the counterbalance of these two forces cause suspended micro-particles to stabilize at the certain positions around the microchannel (Appendix C). This phenomenon was firstly observed by Serge' and Silberberg in 1961 (Martel and Toner, 2014).

Later, in 2007, Di Carlo and his colleagues have demonstrated an inertial focusing of differently-sized micro-particles at their specific locations in a curvilinear rectangular microchannel. Nevertheless, the consequences have suggested that the amplitudes of focusing are depending on the channel Reynolds' numbers (Re_C) and micro-particle sizes (a_p) (Di Carlo et al., 2007). Although, inertia-microfluidic sorting is quite simply regulated on the basis of physical properties of the fluid flow. However, a tightly cell focusing by inertial microfluidics, from time to time, may require a sophisticated external control system and a complex device design and fabrication which can delicately balance a fluid sheath flow and micro-particle immigration across the axis streamlines (Wang et al., 2015).

When fluid has turned in a curved microchannel, there are two counter-rotating secondary flows called Dean Vortices, originate at the top and the bottom halves of the microchannel cross-sections (Hou et al., 2013). In accordance with the centrifugal effect of the Dean Vortices, two additional counter-rotating components referred as Dean Drag Forces (F_D) have been awakened (Tanaka et al., 2012). They further exert on micro-particles pushing them across the main flow streamlines to the inner sidewall of the microchannel in the opposite directions. The magnitude of the forces is governed by these parameters; $F_D = 3\pi\mu U_{Dean} a_p$ or $5.4 \times 10^{-4} \pi\mu De^{1.63} a_p$; where, μ, U_{Dean}, a_p and De are viscosity of fluid media, diameter of each micro-particle, and the Dean Number respectively. Intriguingly, an excessive increment of the

Dean number owing to increased flowrate and U_{avg} causes a focusing breakdown (Martel and Toner, 2012). When the micro-particles have moved closer to the inner wall of the microchannel, the wall then counteracts them with the inertial repulsion forces; Inertial Lift Force (F_L), resulting in the backward migration of the micro-particles to the microchannel centre. This force is equated by the following parameters; $F_L = \rho G^2 C_L a_p^4$; where ρ, G and C_L are fluid density, shear rate and lift coefficient (Kuntaegowdanahalli et al., 2009; Martel and Toner, 2014; Zhou and Papautsky, 2013).

At a certain lateral displacement from the inner wall, a micro-particle is paused because of the equipoising between F_D and F_L. And, the position also relies on the micro-particle diameter. Therefore, undoubtedly, micro-particles which are equal in the diameter, will continually be immobilizing at the same equilibrium position causing the micro-particles entrain into a single focusing stream, as seen (Appendix C). Since, the stream focusing has been handled by two counterbalanced forces and micro-particle diameters; therefore, the larger micro-particle will reach its stabilized location more closely than the smaller one (Di Carlo et al., 2007; Kuntaegowdanahalli et al., 2009; Nivedita and Papautsky, 2013; Tanaka et al., 2012). However, if the Dean Drag Forces are predominant over the inertial wall lift forces, the cell particulates will defocus into multiple-streams (Geng et al., 2013).

Additionally, the amplitude of focusing in a rectangular microchannel is also determined by the confinement ratio (ω) between the diameter of micro-particles (a_p) and the microchannel height (H) expressed by $\omega = a_p/H$ (Martel and Toner, 2014). However, the previous studies have suggested that a streamline focusing occurs when the a_p/ H value is equal or greater than 0.07 (Hasni et al., 2011; Kuntaegowdanahalli et al., 2009). By the way of abovementioned introduction, the principles of inertia-microfluidic sorting would probably be suitable for size-based MCT cell separations.

3.10.2 Geometrical design of triangular microwell array

The microfluidic device with an array of triangular microwell is designed based on the studied parameters previously described by Park and colleagues in 2010. The configuration the device is composed of two key components; the array of 40μm-high x 15μm-deep equilateral triangular microwell positing on the base and the 160μm-high, main flow microchannel covering the microwell array.

Theoretically, there are at least two key inertial microcirculations governing a single microparticle trapping; the lamina flow in the main flow microchannel and the microwell recirculation summarized in Appendix D. The achievement of trapping thus depends on the nature and the handling of these two microcirculations. Iteratively, to ensure the steadily laminar flow of the microcirculation; hence, the fluid media must flow as slowly as possible.

Based on the 3D computerized simulation, the triangular microwell generates the strongest recirculation inside which causes the particle is effectively trapped when compared to other microwell configurations, for example the circular, the rhomboidal or the square (Appendix E). Moreover, the triangular microwell has the less possibility to trap multiple microparticles (Appendix F) because the the top of triangular microwell is the only possible area to allow the particulates flowing closer. Antithetically, the particles can easily reach all boundaries of the circular or the square microwell because they can travel within the nearly equal distances.

3.11 Microfabrication

All microfluidic devices were fabricated using the standard photo-resist-soft lithography as previously described elsewhere. Briefly, the silicon mold was constructed by transferring the tracery of the designed microchannel onto a 6-inch silicon wafer by exposing it through the photoresist mask (MX5050 dry film, Microchem, USA) with UV. The wafer was chemically etched. Further, the admixture of liquid

elastomer; polymethysiloxane (PDMS), and the curing agent at the ratio of 10:1 (Sigma-Aldrich, USA), was poured on the mold and was degassed in a vacuum. The replica was cured at 60°C for 4 hours and was allowed to cooling down. The PDMS replica was then peeled off and bounded on a glass slide by oxygen plasma. The inlets and outlets of the device were drilled using a metal punch and bound to silicone-tubes which glued by liquid PDMS (Wang et al., 2015). The schematic diagram of the technique is demonstrated in Appendix G.

Section IV: Experimental setup

Noticeably, to obtain the statistically meaningful study results, all experiment sub-procedures were repeatedly performed at least three-times. All numerical parameters were statistically reckoned in term of mean ± SD.

3.12 Procedure establishment and device instrumentation

For size-based MCT cell sorting, the microdevice was equipped to the cell-feeding and the buffer systems. Both were empowered by the 2-port automatic syringe pump (F100, Chymex, USA). The sorted MCT cells were obtained from their calculatedly responsible outlets. Data acquisitions were performed by the digital camera (Moticam 2000, Motic, Hongkong, China) with the standard software (Motic image plus 2.0, Motic, Hongkong, China).

In single MCT cell entrapment, the trapping microchip was connected to the cell delivery system through its inlet. The 2-port automated syringe pump (F100, Chymex, USA) was connected to the microchip via the outlet. The pump reversely empowered the microdevice at the assigned flow rates and flow types. The entrapment was observed by light-microscopy. The instrumentation diagrams of both study processes is illustrated in Appendix H.

Before sorting, the total concentration of trypsinized single MCT cells from each preparation was enumerated by hemocytometry for determining the dilution of

MCT cell suspension used in each round of experiments. Finally, the initial concentration of the neoplastic cells was fixed at 40,000 cells/μl.

Section V: Device efficacy assessments

3.13 FACS relatively size-based analysis

To ensure the accuracy of the sorting microchip, 300 μl of calibrating microbeads sized 5, 10, 15 and 20 μm respectively, were sorted by a flow cytometer. The forward scattering light (FSC-A) of each microsphere was measured. Basically, the FSC-A is relatively proportionated to the size of microsphere. The microspheres which got into the same FSC-A range were electronically gated. Further, the dot plot of each group was drawn by BD™ FACS-suite software (Becton and Dickinson, USA). The FSC-A range in each group was calculated by the software and was used as the size-based reference for comparative FACS-size quantification of sorted MCT cells.

Before undergoing single MCT cell sorting, the cells were divided into four groups based on the sizes as 1) group I (5-9 μm), 2) group II (10-14 μm), 3) group III (15-19 μm) and 4) group IV (≥ 20 μm). These ranges were harmony to those established by the reference microspheres. Furthermore, the maximal, minimal and average confinement ratio (ω) of each group were also calculated to anticipate the theoretically inertial focusing of each cell group. Following ASM sorting, the sizes of sorted MCT cells from each outlet were then measured by Flow cytometry under the same aforementioned protocol. The FSC-A of the cells were quantified and then compared to the reference. Ultimately, the sorted cells of each outlet were grouped based on their FSC-A. The data acquisition was plotted in term of the cell size against the number of cells.

3.14 Light microscopy appraisal for the triangular microwell array capability

The capacity of the microwell array to entrap single MCT cells was appraised by light-microscopy. A standard, 1mm^2 grid array was underlay the microdevice for

partitioning the whole area of the microwell array into the subareas (Appendix I). Finally, the total amount of the microwell was calculated by multiplying the total number of subareas with the amount of microwell in a subarea.

After the passively inertial entrapment, the amounts of microwell occupied by single and multiple MCT cells were enumerated subsector-by-subsector. Ultimately, the efficacy of the microdevice was presented in term of the percentage of single cell occupying.

Section VI: OCT4-immunocytofluorescence

3.15 Intranuclear OCT-4 immunocytofluorescence in entrapped MCT cells

For the self-renewal assay, the expression of embryonic transcription factor; OCT4, was testified by immunocytoflorescence (ICF). Stepwise, to assure the functionality of the antibodies, freshly trypsinized MCT cells were smeared on a silane-coated glass slide. Their cell membranes were pierced by the membrane-piercing solution (CU-Vet MPS®, see the formulaic components in Appendix J) developed in our microfluidic laboratory. Further, the cells were added by FCS at the ambient temperature for 5 min. to block non-specific proteins. The cells were washed by PBS and then incubated by PE-conjugated mouse anti-human OCT4 monoclonal antibodies (1:200) at 37°C for 1 hr. in the dark chamber. The cells were washed by PBS and their nuclei were counterstained by DAPI (1:100) at 37°C for 5 min. in the dark chamber. The fluorescent signaling was then detected by florescent microscopy with 575 nm light source.

In the secondary step, to examine the self-renewal in suspending MCT cells, a 500μl fresh MCT cell suspension was aliquoted and centrifuged at 3000 rpm, 4°C for 5 min. the cells were incubated by CU-Vet MPS® for 15 min. and were washed twice. Next, the cells were centrifuged at 3000 rpm, 4°C for 5 min. and resuspended by 200μl FCS. The cells were centrifuged and were admixed by 1μl OCT4 antibodies in 100μl PBS in the dark chamber. Their nuclei were thereafter counterstained by DAPI.

Henceforward, data acquisition was performed by micropipetting 35μl tangible MCT cells onto a sialane-coated glass slide mounted by a cover slip. The fluorescent signal was detected by fluorescent microscopy.

For the last step, to detect the self-renewal in trapped MCT cells, the fluid media in the cell-ensnaring microdevice was drained out. Henceforth, the CU-Vet MPS® was slowly infused into the microdevices and the cells were incubated by the solution at the ambient temperature for 30 min. Further, the cells were gradually washed by PBS twice and incubated by FCS at the room temperature for 30 min. They were next washed and incubated by the PE-conjugated mouse monoclonal anti-human OCT4 antibodies (Clone 40/Oct-3, Becton and Dickinson, USA) at the dilution of 1:100 at 37°C for 2 h. and DAPI for 10 min., in the dark chamber. Ultimately, the fluorescent signal was detected by fluorescent microscopy with the 575 nm light source for PE activation.

CHAPTER IV

RESULTS

4.1 Histopathological and CD117-immunocytofluoresent ratifications for MCT diagnosis

According to histopathology performed by the Department of Veterinary Pathology, the consequences had confirmed that all skin masses used in this study were MCT. Irrespective of grading, the histopathologic sections exhibited that the MCT cells were moderately pleomorphic. Their conformations were varying from round, oval to pyramidal and, from time to time, anaplastic. The sizes of well-differentiated MCT were averagely ranged from 10-15 μm with round hyperchromatic single nuclei; meanwhile, the anaplastic MCT cells were approximately 20-35 μm with indent or vacuolated single to multiple nuclei. Their cytoplasm were basophilic containing fine metachromatic granules in both cases; however, glistening cytoplasmic vacuoles were predominant in undifferentiated MCT. The arrangement of neoplastic cells was frequently sheet-like with a variation degree of fibrovascular connective tissue intervening (Figure 4.1).

Nonetheless, CD117-ICF also indicated that almost cells were MCT cells which positively interacted with CD117 antibodies detected by the red fluorescent signals both in the cytoplasm and on the plasma membranes (Figure 4.2). The nuclei were stained blue by DAPI. Notably, some cells were negative to CD117-ICF indicating the intermixing of various cell subpopulations, albeit almost cells were positive. And these negative cells were speculated to be non-MCT cells.

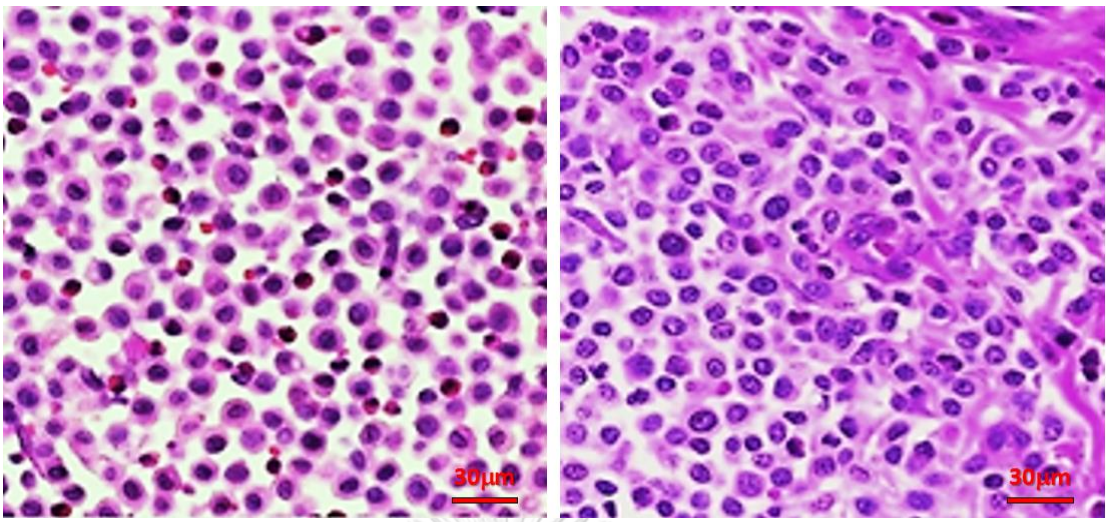

Figure 4. 1: The figure panel displays the histopathologic sections (H&E) of MCT masses exploited in this study. The configurations of almost MCT cells were variegated from round to polyhedral. Basophilic cytoplasm with fine metachromatic granules were the remarkable appearances of almost neoplastic cells.

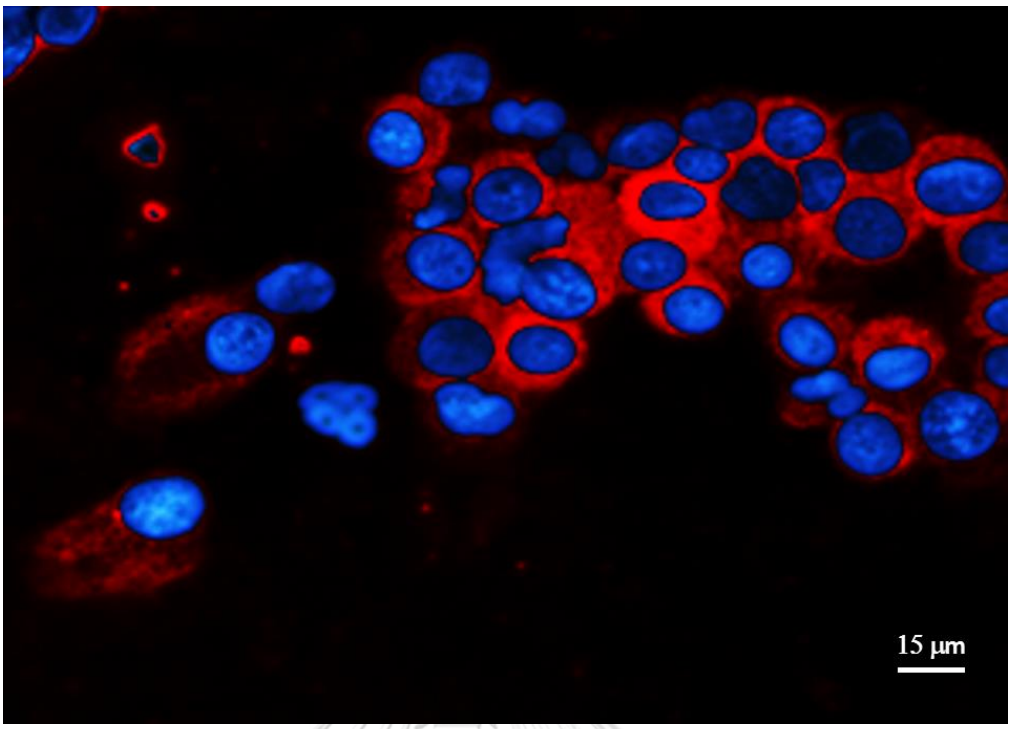

Figure 4. 2: This figure exhibits the positive CD117-ICF immunoreactivity in MCT cells. Notably, the red fluorescent signals both in the cytoplasm and on the plasma membranes were specifically emitted only in MCT cells. Meanwhile, the non-MCT cells were negative with CD117-ICF (Ketpun et al., 2013).

4.2 The architectures of the microfluidic devices and fabrications

In this study, the microfabrication of the devices had been accomplished under the standard photoresist-soft-lithography previously described in size-based polystyrene microsphere separations (Ketpun et al., 2015). And the replicas were constructed using polydimethylsiloxane (PDMS).

4.2.1 The microfluidic device for size-based cell sorting

The geometrical configuration of the Archimedean spiral microchannel (ASM) was composed of five-turned curvilinear rectangle microchannel with the constant interspace between two contagious loops at 500 μm.

At the cross-section, the dimension of rectangular microchannel was 500 μm in width and 130 μm in height. The curvature radii of the innermost loop (1st loop) and the outermost loop (5th loop) were 5.5 and 9.5 mm respectively.

The feeding slots consisted of two inlets of which the first one was used for delivering the cell suspension and the latter was for the control buffer. The exit slot was composed of a single 720μm-long conical microchannel asymmetrically expanded into ten individual slots. Each expansive slot then continually connected to its individually harvesting outlet where sorted cells were collected (Figure 4.3).

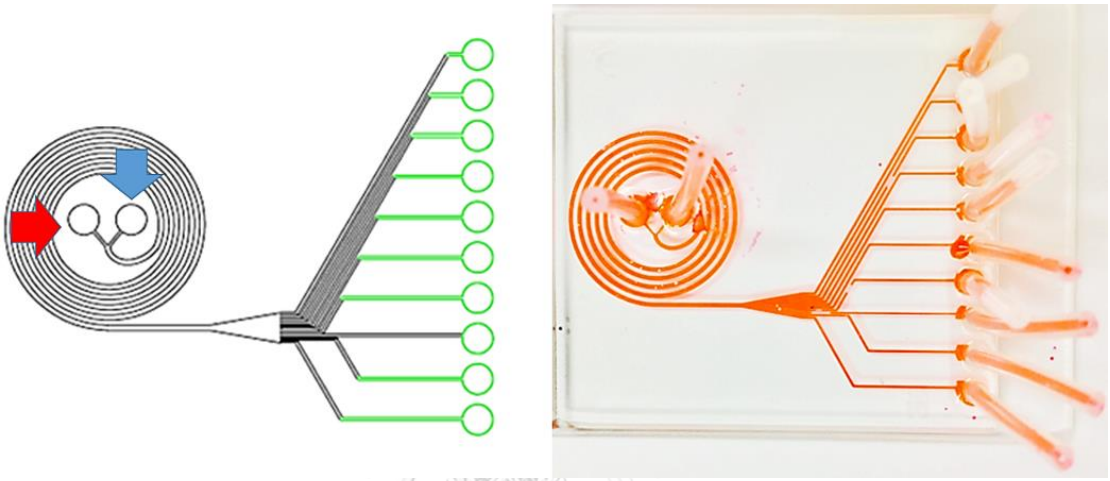

Figure 4. 3: This figure illustrates the semblance of the fabricated microfluidic device used in this study. The microdevice consisted of two feeding inlets connecting to the ASM. The first inlet was for delivery cell suspension (blue arrow) and the last one was for feeding the PBS control buffer (red arrow). The exit slot was conical asymmetrically expanding into 10 exit-slots which each individually connected to its responsible harvesting port.

4.2.2 The microdevice for single MCT cell capturing

The entrapment microdevice was two-layered PDMS composite microchip which consisted of 1) the ground layer and 2) the upper layer of the main flow microchannel. In approximation, an average amount of total microwell in the array was 9,310. They were lining in the matrix of 63 x 143. The dimensional parameters of each microwell were 40 μm in longitudinal axis and 15 μm in depth. The microwell array was encompassed by the main flow microchannel of the upper layer. The dimension of the microchannel was 27mm long, 5mm wide and 160μm high. The length of cell-entry microchannel was 15 mm connecting to the inlet port; meanwhile, the exit microchannel was 10mm long linking to the outlet port (Figure 4.4 & 4.5).

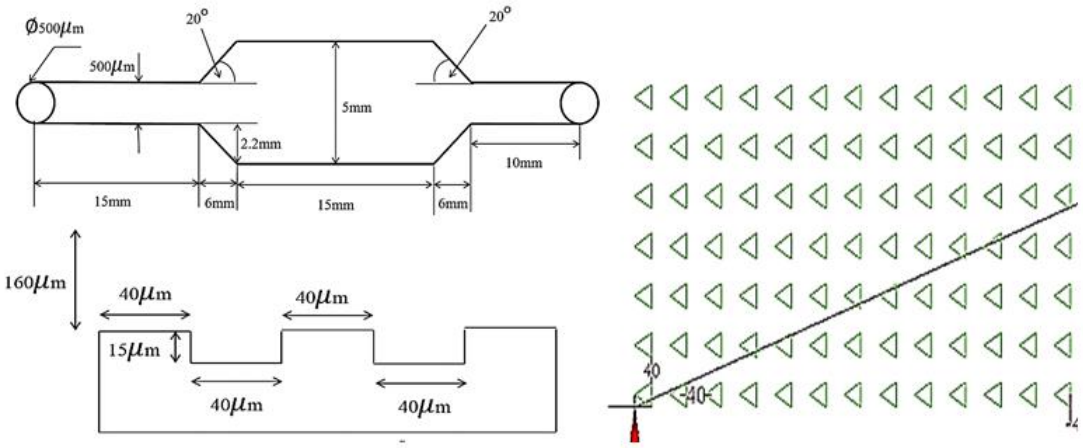

Figure 4. 4: The schematic diagram depicts the designed blueprint of entrapping microdevice engaged in this study. The dimensional scales of individual portions are also shown.

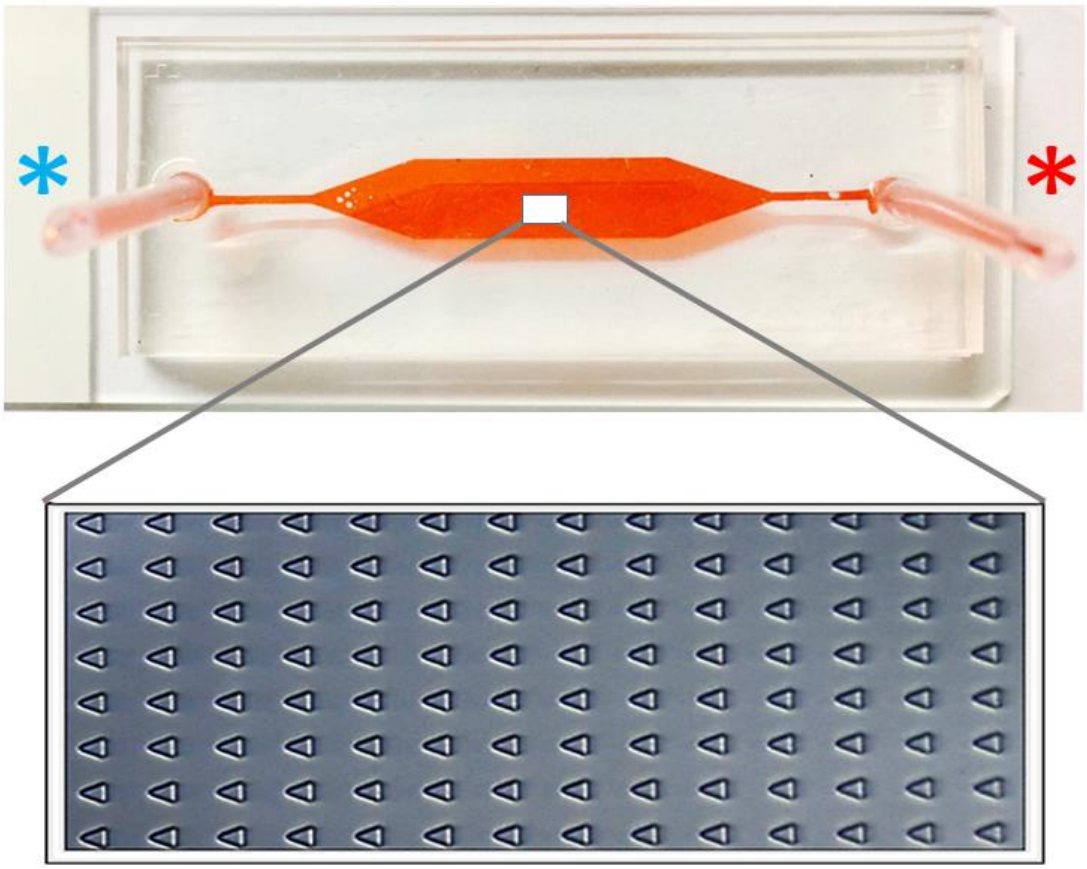

Figure 4. 5: This picture exhibits the external configuration and internal orientation of triangular-microwell array in the device. Noteworthy, there are a feeding inlet connecting to the main cell-entry microchannel (blue asterisk) and one outlet port (red asterisk) for media drainage.

4.3 Microfluidic size-based cell sorting of single MCT cells

4.3.1 Focusing prediction of naturally buoyant MCT cells in the suspension

Prior to the size-based cell sorting, the confinement proportion (ω) of MCT cell diameter (a_p) to the microchannel height (H_c) from each group was calculated for assuring the occurrence of cell focusing. Upon the focusing theory, the average a_p/H_c of each MCT group had to be equal to or greater than 0.07. The calculation indicated that the confinement ratios were 0.039-0.069, and 0.077-0.108 in MCT group I (5-9 μm) and II (10-14 μm) consecutively. At the meantime, the ratio intervals of the group III (15-19 μm) and IV (20-30 μm) were 0.115-0.146, and 0.154- 0.231 respectively (Figure 4.6).

Based on the average confinement ratio of each group, MCT cells in the group I (5-9 μm) were predictively unfocused and distributed throughout the microchannel in virtue of the lowest a_p/H_c (< 0.07). On the other hand, cells in the other groups (II, III and IV) were prophesied to focusing into their respective streams.

Since the hydrodynamic inertia focusing is the function of Dean's Drag Forces generated in the Dean Vortices; therefore, to ensure the generation of Dean Vortices at the upper and lower boundaries of the curvilinear rectangle microchannel, a computerized simulation was performed. The vector analysis suggested the procreation of supposed Dean Vortices in the fabricated ASM. There were the alterations of velocity profile taking place at the top and the bottom across the cross-section of curved microchannel (Figure 4.7).

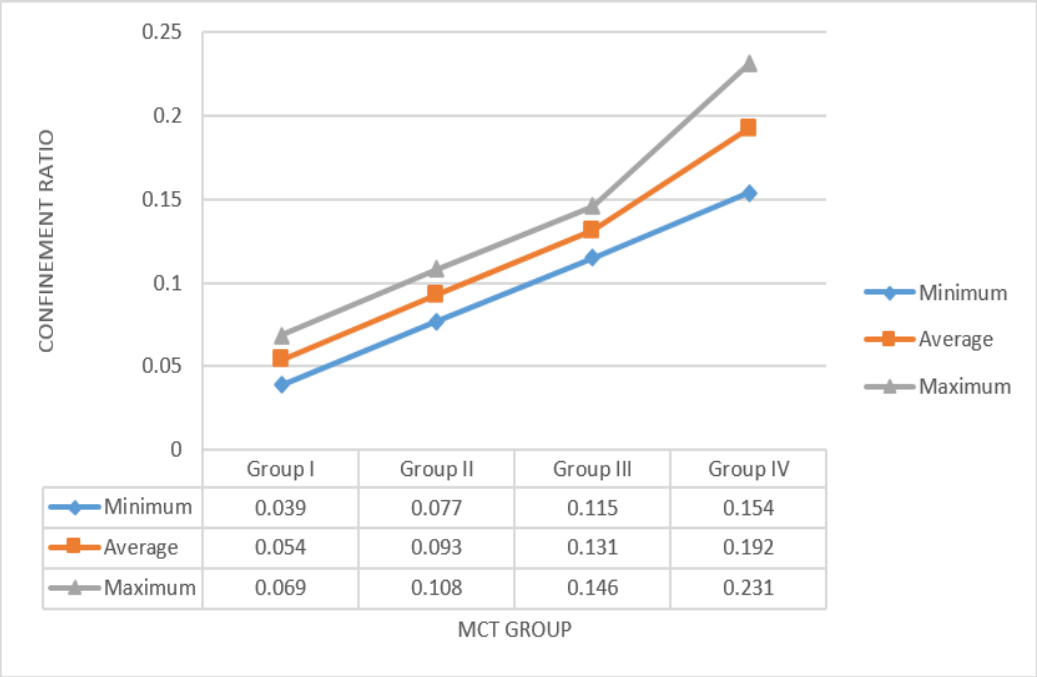

Figure 4. 6: The line graph shows the minimal, maximal and average confinement ratio (ω) of MCT diameter (a_p) to the microchannel height (H_c) utilized for predicting cell focusing in ASM. Notably, the ratio must theoretically be equal to, or over than 0.07 (Kuntaegowdanahalli et al., 2009).

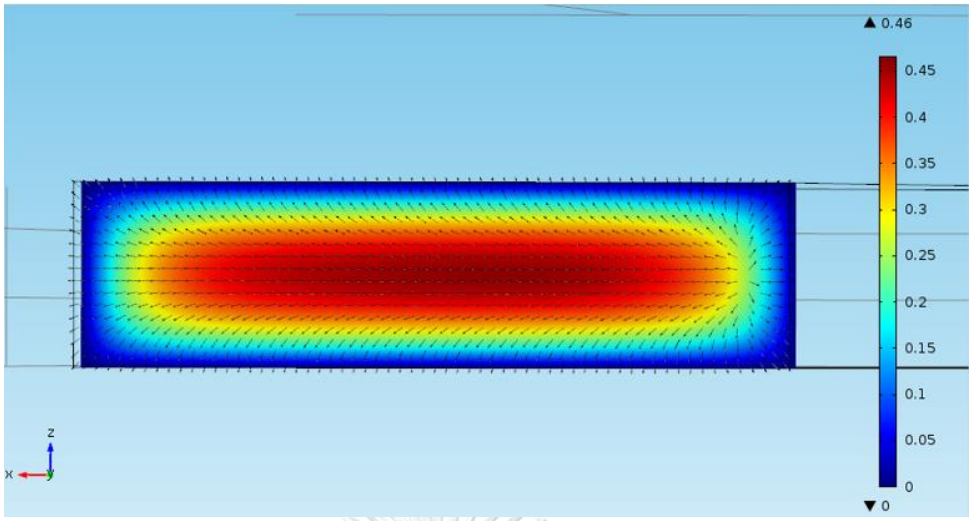

Figure 4. 7: The computational simulation presents the formation of two Dean Vortices at the top and the bottom halves of the curvilinear microchannel based upon the vector analysis of fluid velocity (COMSOL Multiphysics® version 6.3, COMSOL, USA).

4.3.2 Naturally buoyant MCT cell focusing in ASM and the device resolution

Although, the throughput of ASM device was admirably high (at 1 ml. min^{-1} in this study) and the system was appropriate for high-volume size-based cell separation. In our previous study, the result distinctly exhibited that 10 and 15μm polystyrene microparticles in suspension were completely focused into their responsible streamlines (3D focusing) depending on their individual sizes (Figure 4.8).

In contrary to polystyrene-microbead focusing, it was however noticeable that each MCT group did not sharply focus into its single streamline (2D focusing) under light-microscopy investigation. This suggested that there was an opportunity in which two appositive focusing streamlines were swaying and bouncing to each other. This would result in a deviation of exiting-trajectory of each focusing streamline which impacted on the efficiency (resolution) of the device.

To verify the resolution of our fabricated ASM, the mixture of four differently-sized calibrating polystyrene microbeads (5, 10, 15 and 20 μm) was utilized and they were electronically gated depending on their individual forward scattering lights (FSC-A). The referral range of FSC-A from each subset was then measured (Figure 4.9).

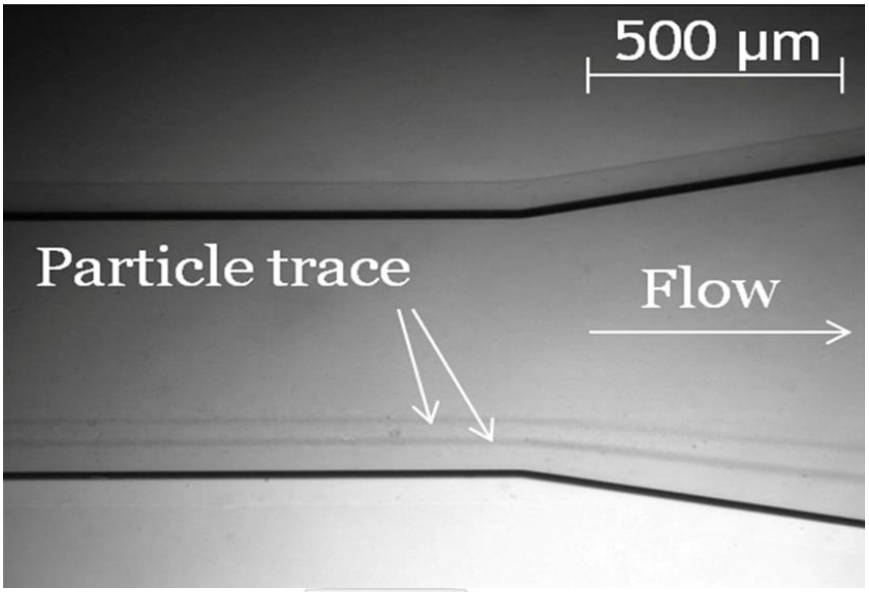

Figure 4. 8: The exploited micrograph exhibits two distinguishingly separated 3D-focusing traces of 10 and 15μm polystyrene microspheres within the predesigned ASM in the former study (Thanormsridetchai et al., 2014).

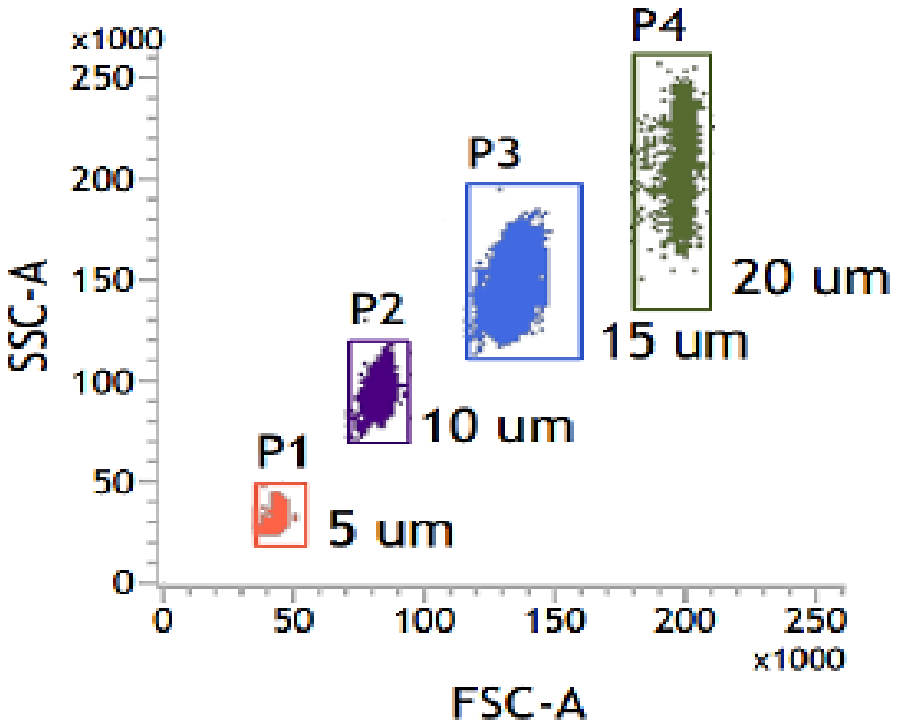

Figure 4. 9: The FACS-dot plot depicts the referral ranges of FSC-A which are reflecting the size of polystyrene microspheres in each group.

Henceforth, FACS size-based quantification of sorted MCT cells obtained from each outlet was performed. The forward scattering light (FSC-A) of them were admeasured and compared to the references. The cells which got into the same FSC-A ranges, were electronically grouped together and were numbered. The quantification result substantially indicated that the FSC-A values of individual MCT cells of group I, II, III and IV were less than 32.5-50, 70-90, 120-150 and greater than 165 respectively. Sorted MCT cells which their FSC-A less than 32.5 were supposed to be acellular components.

Consistently to the MCT sorting result, the MCT cells in group I were unfocused and suffused throughout the exit tract. Antithetically, the MCT cells in group IV were completely focused into a single streamline nearby the inner wall. Because they were almost harvested from the outlet-port II. Intriguingly, the cells in group III focused into a single streamline appositive to the streamline of MCT cell group IV. However, the cells were defocused when they had reached the tip of second outlet wall. Thus, there were some MCT cells in group III deviating their trajectory to the center of the microchannel and then flowing through the third outlets. And they contaminated with the MCT cells group II which had been focusing and flowing to the outlet III.

This might yield some focusing cells in group II had defocused and were in part askew to the outlet IV. Therefore, the study result suggested that our single MCT had not sharply entrained into their individual focusing streams based on their typical sizes. And each focusing stream was closely overriding to one another. In agreement with other consequences in this study, however, they suggested that our ASM system was potently capable to differentiate naturally multiple-sized single MCT cells form one another. Even though, the resolution still requires any improvement. The resolution of the microdevice could be summarized in Figure 4.10.

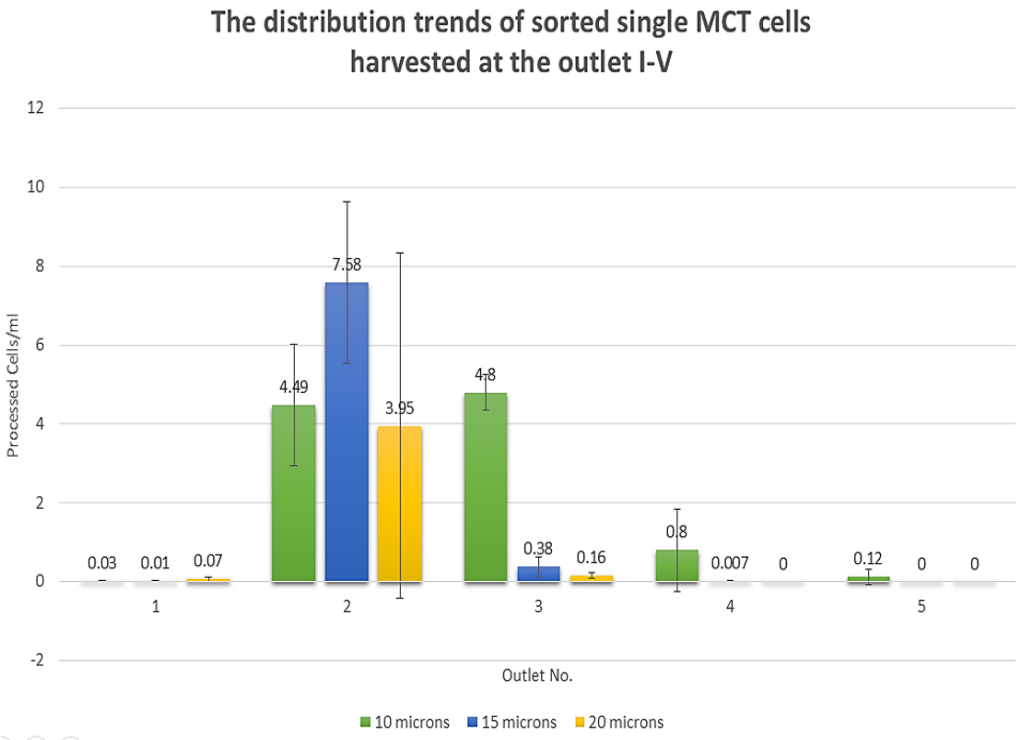

Figure 4. 10: The histogram illustrates FACS size-based quantification of sorted single MCT cells in each outlet. Notably, the cells in group III and IV (the targeted cells) were mainly harvested at the outlet II; meanwhile, the sorted MCT cells in group II predominantly exited at the outlet III and II, respectively. The existence of MCT group II would mean there were defocusing of MCT group II in the exit slot.

4.4 Systematically bioengineering appraisal of MCT cell vitality after ASM Sorting

The rheological study of cell vitality indicated that hemocytometry enumeration had confirmed the loss of MCT cells in the system. Distinctly, the concentration of sorted MCT cells was lower than foreseen. Approximately sixty percent of the cells were lost or necrotized in the system including in the cell delivery portion and in the spiral microchannel. However, the remaining cells, which had been sorted out to the outlet port II, III and IV, were not almost healthy. Many were vulnerable, deformed, aggregated or dead after sorting based on light microscopy, scanning electron microscopy, vital dye staining and leakage DNA content assay. The following sections below will be describing the consequences of vitality verifications in this study.

4.4.1 Light-microscopy

4.4.1.1 Hemocytometry enumeration of MCT cells in ASM sorting system,

Hemocytometry enumeration confirmed the loss of MCT cells in the system. The result unveiled that the concentration of sorted MCT cells was sharply decreased compared to the foreseen. Approximately twenty percent of MCT cells were lost in the cell transit system. And forty percent of the cells were lost in ASM sorting system. The mean loss in the both systems was around sixty percent totally (Figure 4.11). The conformational changes and cell aggregation of sorted MCT cells were exhibited in Figure 4.12. Notably, most sorted MCT cells were breaking down suspected to be influenced under hydrodynamic shear stresses in the sorting system.

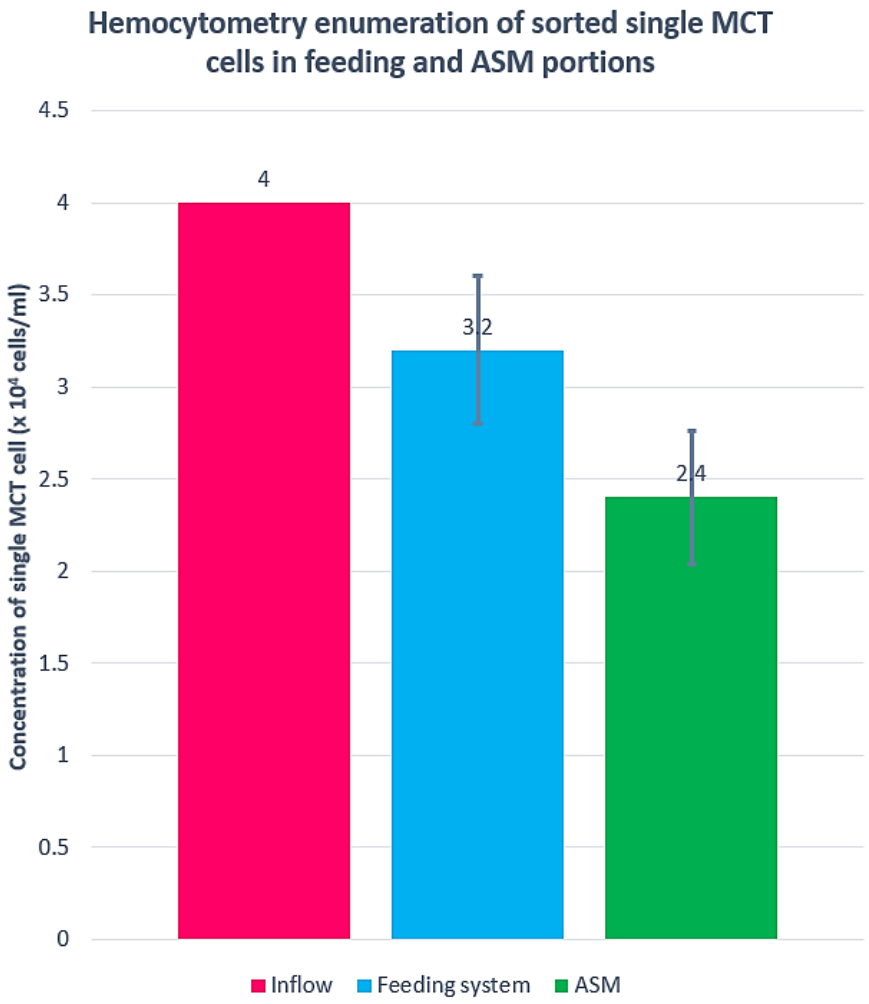

Figure 4. 11: The histogram exhibits the reduction of MCT concentration after ASM sorting compared to the inflow concentration (pink bar). The result suggested that approximately sixty percent of sorted cells were lost in both transit and ASM systems, totally.

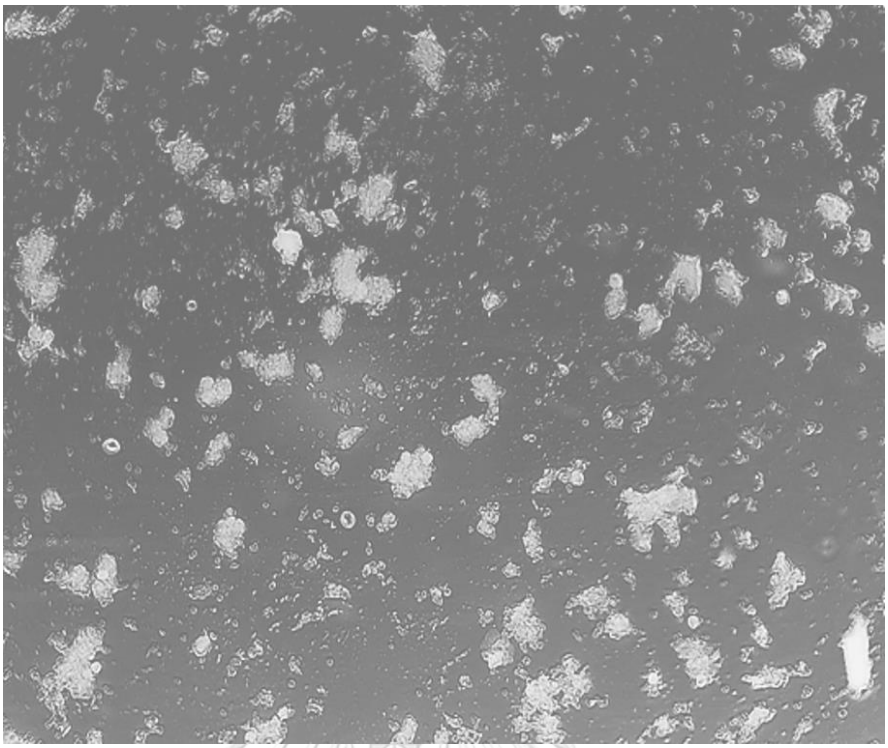

Figure 4. 12: The micrograph exhibits the attrition in MCT after ASM sorting. Severe cell wreckage and aggregation were greatly observed in the smear. They suggested that approximately sixty percent of sorted cells were lost in both transit and ASM systems, totally.

4.4.1.2 Normal morphology of trypsinized MCT cells,

Under light microscopy, the cells shaped round to oval; meanwhile, a few caudate MCT cells were infrequently observed in such circumstances. The sizes of individuals were usually variegated from 6-8 to over than 15 μm (Duncan and Prasse, 1979; Sailasuta et al., 2014) at which the largest cells (≥ 15 μm) were supposed to be neoplastic initiating cells in this study. The cytoplasm is usually fulfilled with variably-sized refractive granules which contain various chemomediators which plays in various physiologic functions (Figure 4.13). In addition, EMB staining also ratified that singly intact MCT cells were round to oval mononuclear cells with basophilic, radiopaque, granular and/or clearly-glistening vacuolated cytoplasm (Figure 4.14).

Basically, these cytoplasmic granules contain various preformed water-soluble chemomediators, such as sulfated glycosaminoglycan, proteoglycan heparin and chondroitin sulfate-E (de Mora et al., 2006; Hill and Martin, 1998; Sailasuta et al., 2014; Theoharides et al., 2012). The nuclei were large, eccentric to concentric and round to oval mononuclei with the prominent single nucleoli. Anyhow, binuclei or even polynuclei were observed in some specimens as well. The nucleus-to-cytoplasm (N/C) ratio variated from 1:1 to 2:1. And, the higher ration was almost seen in the larger cells.

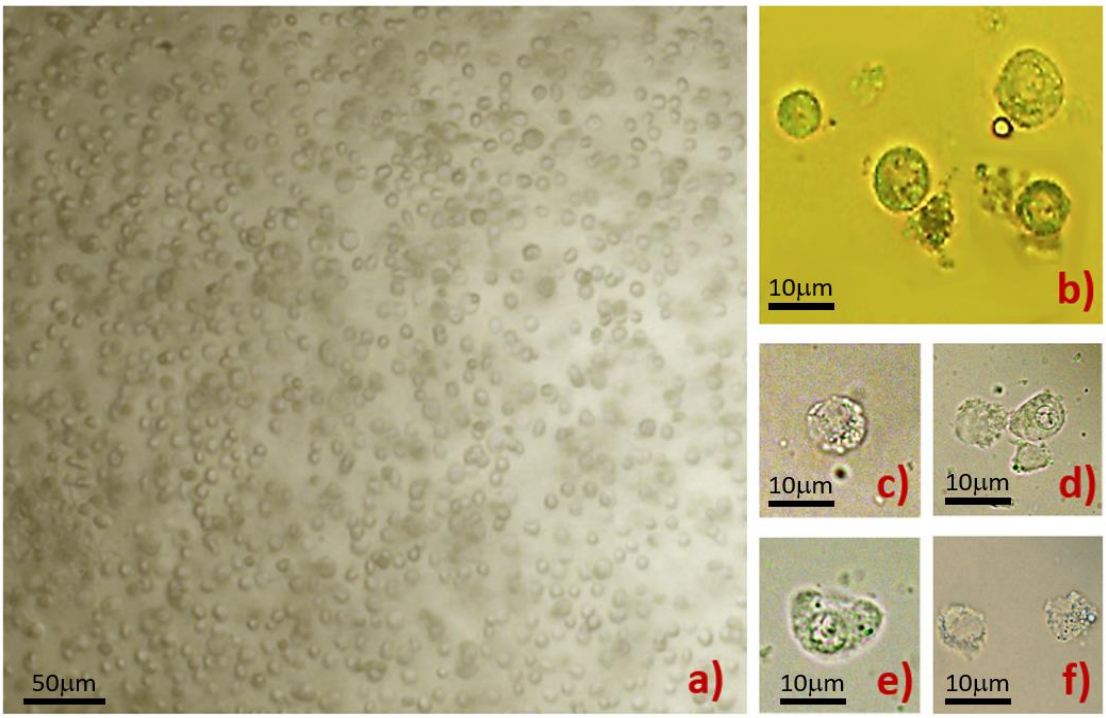

Figure 4. 13: The plain micrograph illustrates the morphology of viably trypsinized MCT cells in the bright-field microscopy. In general, the MCT cells are round (a, b and c) or oval (d) in shape. However, in such circumstances, they were caudate cells (e). Their nuclei are usually round with scarcely coarse chromatin and prominently single nucleoli. The cytoplasm is usually fulfilled with variably-sized refractive granules which contain various physiological chemomediators.

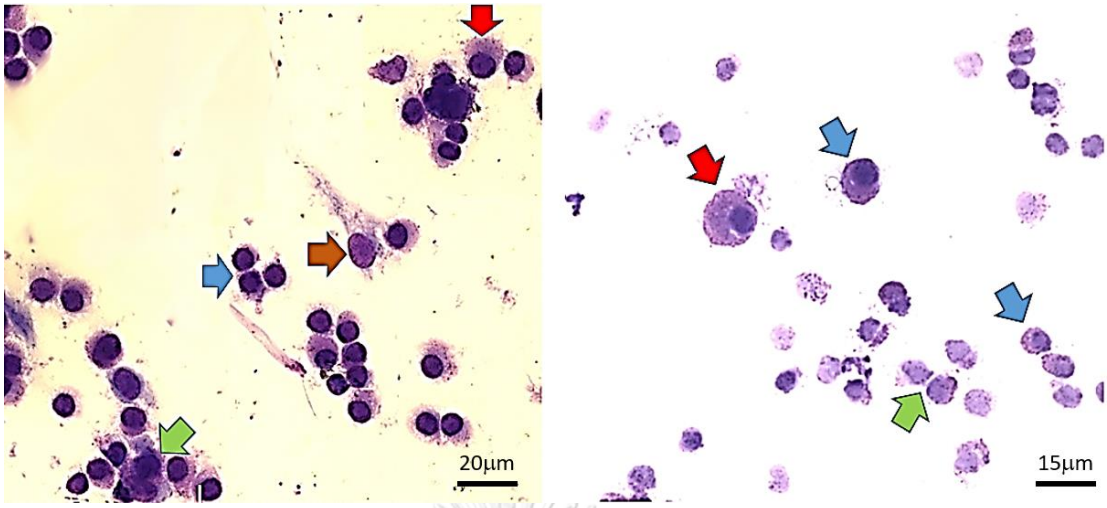

Figure 4. 14: The EMB staining reveals trypsinized MCT cell configurations in this study. Almost neoplastic cells were in general round to slightly oval. Their cytoplasm was finely basophilic containing fine-metachromatic granules. Noteworthy, there were at least two MCT subpopulations defied in EMB staining. The first was large MCT cells (red arrows) and the last was small MCT cells as indicated by blue arrows. The other cell types such as mesenchymal cells (yellow arrow) and macrophages (green arrows) were also observed.

4.4.1.3 Evaluation of morphological deformity of sorted MCT cells,

As predicted, after inertial cell sorting with the fabricated Archimedean Spiral Microchannel, the study result substantially indicated cell deformation, degeneration and necrosis of sorted cells in the system. Cell deformation was characterized by the elongation of cells in which their CDI indices were increased when compared to normal MCT cells. The average CDI indices of deformed cells were in between 1.6-4.5. Nevertheless, the nuclei of these cells were also elongated in such circumstances. Finally, pseudopodium formation might be observed in some degenerated cells.

For cell degeneration, not only cell elongation but also cytoplasmic devastation of the cells were observed. Their cytoplasmic volume and content were remarkably reduced, and/or spilled causing increased N/C ratio. The integrity of cell membranes seemed to be normal; however, it could not be easily clarified under light-microscopy. The CDI index of necrotic MCT cells was varied from 0 (unmeasured) to 1 (cytoskeletal recoiled) as seen in Figure 4.15c and d.

Moreover, cell degeneration could be readily defined into several instances. In benign degeneration, cell membrane blebbing was remarkably observed. However, in the progressive state, the enlargement of cytoplasmic granules was a predominant configuration in association with or without pyknotic and/or dislocated nuclei. Moreover, many degenerated cells were cloudy swelling indicating increased membrane permeability (Figure 4.15d). For malignant degeneration or necrosis, the laceration of cell membrane was the dominant features in which all most cells lost their membrane integrity. Nuclear luxation commonly was seen (Figure 4.15d and e).

4.4.1.4 Trypan blue vitality assay of sorted MCT cells,

Almost deformed cells were stained negative for trypan Blue. However, some of them were also slightly positive in their membrane-bounded cytoplasmic granules, predicted to be in the progression of irreversibly degenerative change or necrosis. Undoubtedly, cells which underwent necrosis were positively stained blue (Figure 4.16).

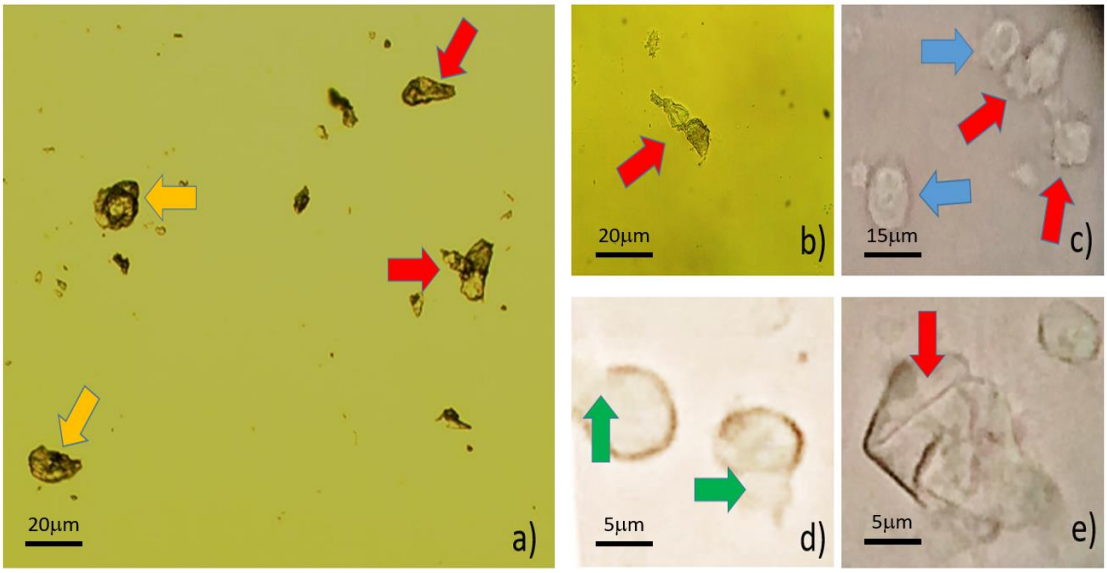

Figure 4. 15: The figure panel illustrates morphological deformation (yellow arrow), degeneration (green arrow) and necrosis (red arrow) of MCT cells after ASM sorting. The normal MCT cells (blue arrow) were also observed but in the low number when compared to those degenerated or necrotic. In Figure 4.15d, severe membrane disintegrations were seen in case of malignant degeneration. Figure 4.15e indicates the cell debris owing to the cell rupture.

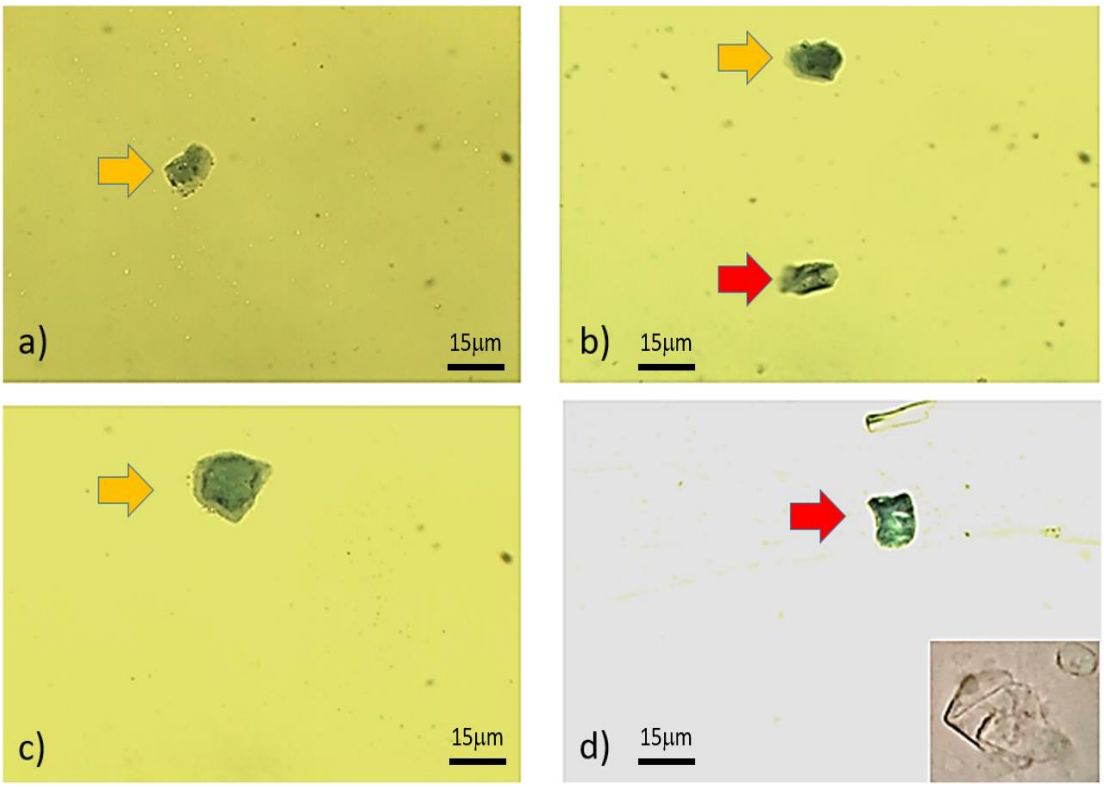

Figure 4. 16: This figure panel shows the trypan blue vitality assay of single MCT cells after ASM sorting. It is remarkably that MCT cells were undergoing cell necrosis, although there was the cell deemed to be normal based on its morphology. But its N/C ratio was decreased. Almost sorted MCT cells were positively stained by trypan blue. This indicates the necrosis of them (yellow arrows). Furthermore, cell debris were also identified especially in Figure 12d, as seen in the plain light-microscopy assay (the right lower inset).

4.4.2 Scanning electron microscopy

4.4.2.1 Morphological evaluation of necrotic MCT cells after ASM sorting,

Scanning electron microscopy also patently unveiled MCT cell deformation, degeneration and death. As in the light-microscopy, deformed cells under SEM were elongated or aberrantly disoriented with normal or slightly disintegrated cell membranes. Anyhow, their nuclei in general were *in situ* normal. Cell degeneration and necrosis characterized by severe membrane interruption, loss of surface proteins, nuclear sloughing, membrane blebbing, and cell wreckage (Figure 4.17).

4.4.3 TMRM fluoroscopy for cell vitality assay

The lipophilic cations, TMRM dye, had been utilized to doubly ensure sorted-MCT cell vitality. Its fluorescent signals were positively detected throughout the cytoplasm of viably trypsinized, single MCT cells indicating that almost mitochondria of the cells were actively functioning. Their membrane potentials ($\Delta\Psi_m$) were maintained and normalized by proton transfers between the matrix and the intermembrane spaces under an association of succinate and ADP (Baracca et al., 2003; Joshi and Bakowska, 2011; Scaduto Jr and Grotyohann, 1999). The active mitochondria would extrapolate to the viability of single MCT cells.

Moreover, the staining system could picturize the conformation of sorted MCT cells. As seen in the viable MCT cells, the contour of neoplastic cells was obviously round to oval with the normal configuration of nuclei stained blue by DAPI (Figure 4.18). Notwithstanding, deformed and degenerated MCT cells including cell debris also stained positive with TMRM at the membrane rims. However, the intensity of fluorescent signals sharply dimmed or reduced (Figure 4.19 and 4.20) and the decay rate of the signals was

proportional to the membrane potential (Baracca et al., 2003). Thence, the unstained spaces between the nuclear border and the membrane rim suggested inactively degenerated mitochondria.

For necrotized cells, there were two kinds of cell debris clearly identified under TMRM fluoroscopy. The first was the membrane-bounded cytoplasmic debris with karyorrhetic or karyolytic nuclei, referred as the ghost cells. And the last consisted of the nuclei remnants with scanty or without cytoplasm (Figure 4.19). Hence, the results were harmonious to those seen in the light microscopy and SEM.

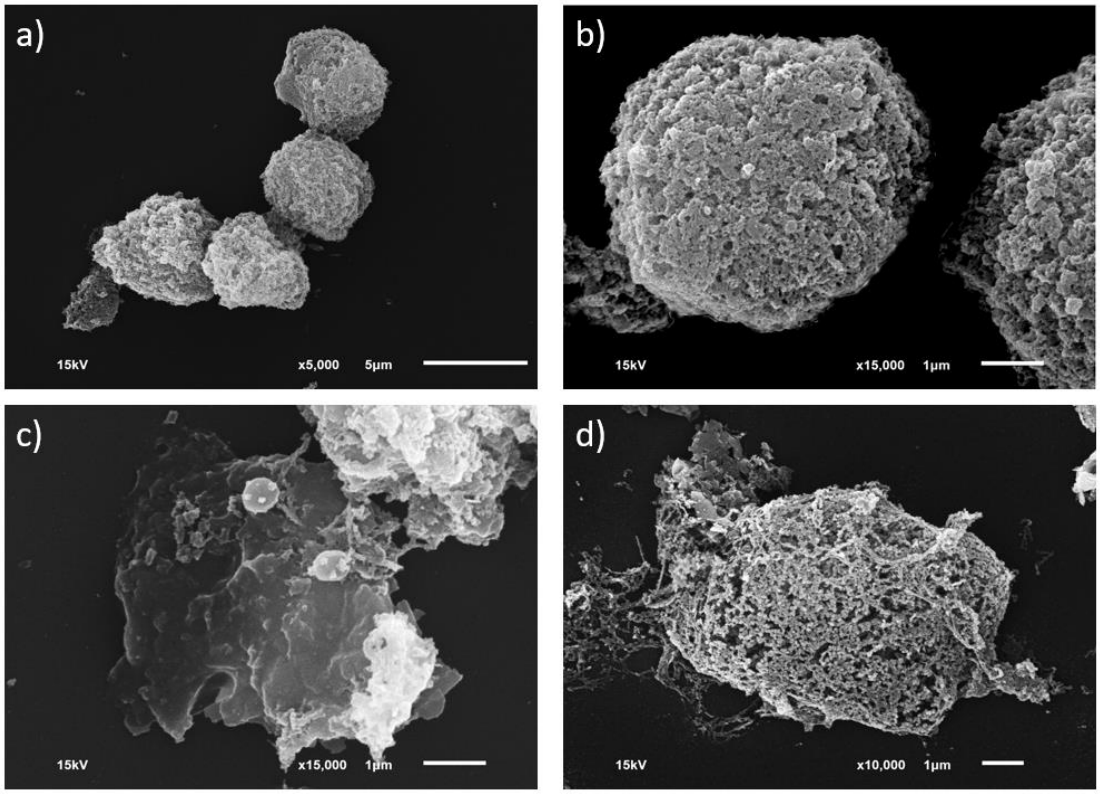

Figure 4. 17: The panel of SEM micrograph (JEOL JSM-6610LV, Tokyo, Japan) exhibits the morphology of well-differentiated viable MCT cells (Figure 4.17a and b) versus necrotic cells after ASM sorting (c & d). Notably, necrotized MCT cells had diminished surface proteins (Figure 4.17c) and/or perforated cell membrane (Figure 4.17d).

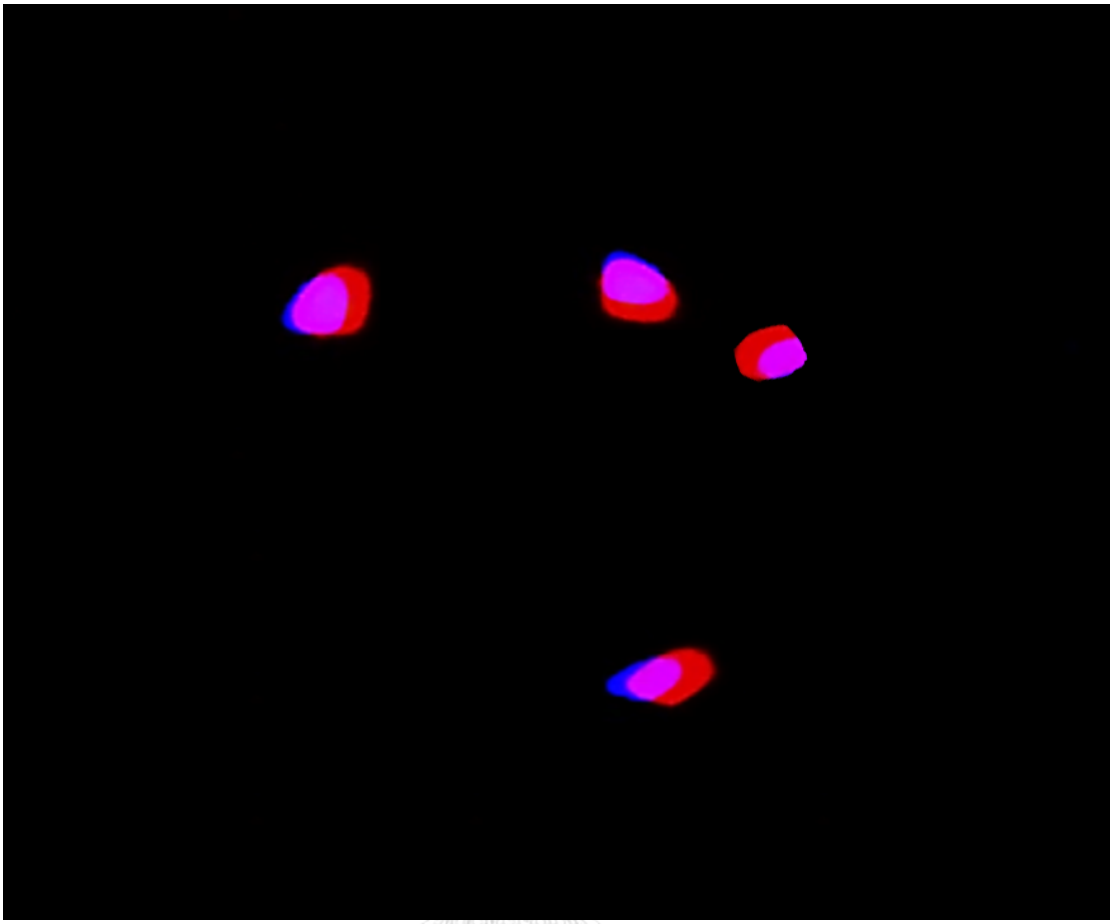

Figure 4. 18: This figure illustrates the positivity of TMRM fluoroscopy in four viably trypsinized single MCT cells. It indicates that the oxidative mitochondria could maintain their membrane potentials ($\Delta\Psi_m$) by proton pumping in the electron transport chain (Baracca et al., 2003; Joshi and Bakowska, 2011; Scaduto Jr and Grotyohann, 1999) in which the process always takes place in the vital cells.

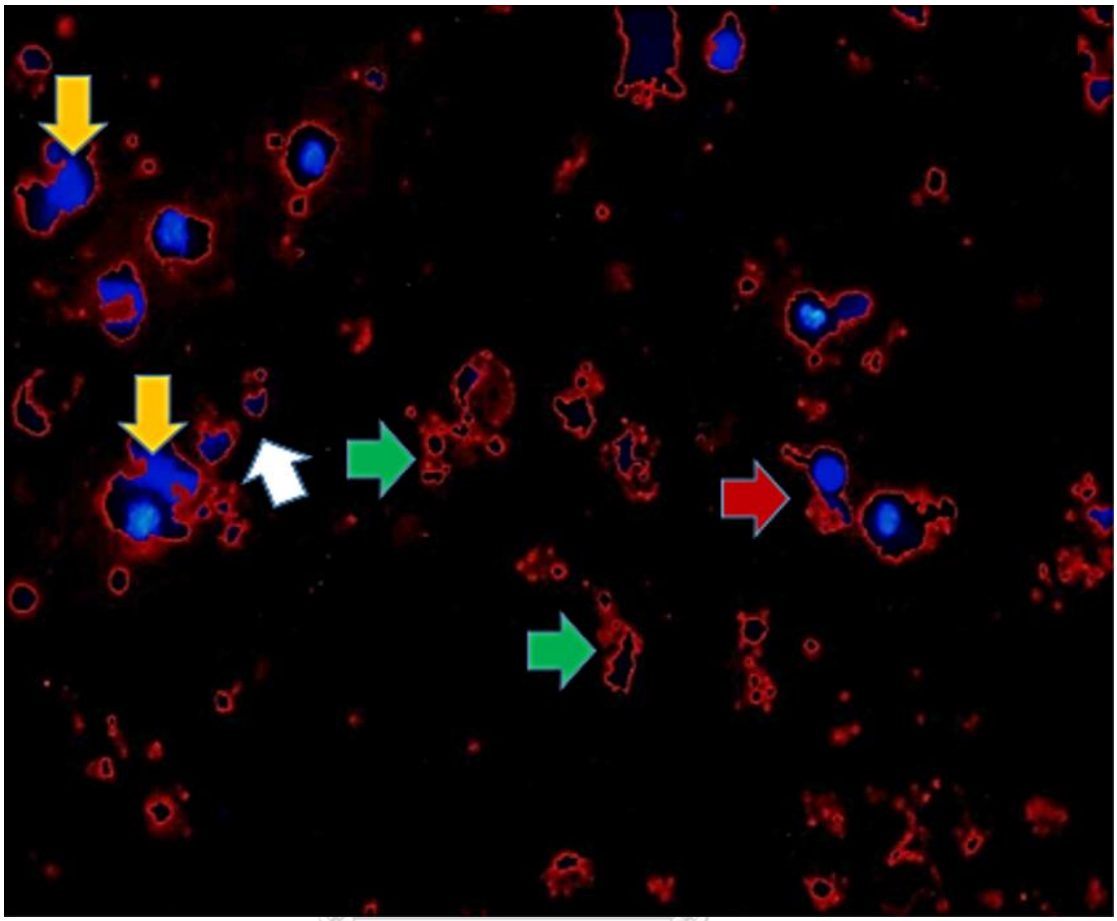

Figure 4. 19: This figure illustrates TMRM fluoroscopy of degenerated and necrotic sorted single MCT cells. Remarkably, some neoplastic cells were composed of only cytoplasm (green arrow) indicating nuclear sloughing (white arrow) or cytoplasmic wreckage; meanwhile, the other had reduced N/C ration with aberrantly deformed nuclei and/or abnormal cell morphology (yellow and red arrows). The intensity of TMRM signal was also declined in those cells when compared to normal MCT cells in Figure 4.18.

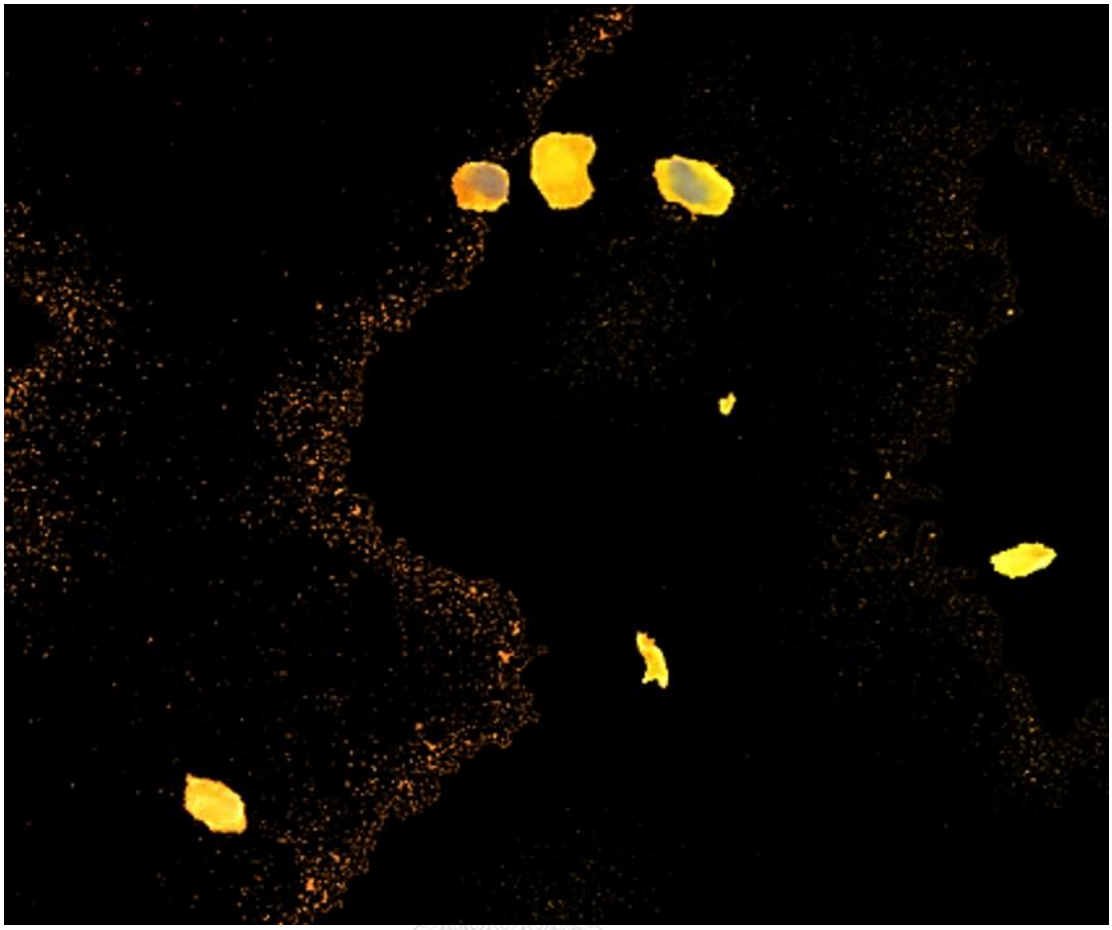

Figure 4. 20: The intensity of TMRM signal was declined in sorted single MCT cells when compared to normal MCT cells in Figure 4.18 after cultivating with RPMI-1640 for 4 hours. This would indicate the cells underwent the ongoing necrosis because of MCT cell vulnerability after sorting (Joshi and Bakowska, 2011).

4.4.4 Spectrophotometry

4.4.4.1 Spectrophotometric quantification of leaky DNA,

The investigation of leaky DNA content clearly implied cell membrane disintegration and/or cell rupture after sorting. The average concentration of DNA leakage in ASM-sorted MCT cells was 2.4 fold accrued when compared to the control (12,470 ± 2080.41 and 5,200 ± 928.72 μg/ml, respectively), based on standard spectrophotometry (Figure 4.21). However, the concentration was not sharply soared as predicted because many membrane-less debris still had ghost nuclei without nuclear wreckage (Figure 4.19, white arrow) in order that DNA contents did not leak out in this case.

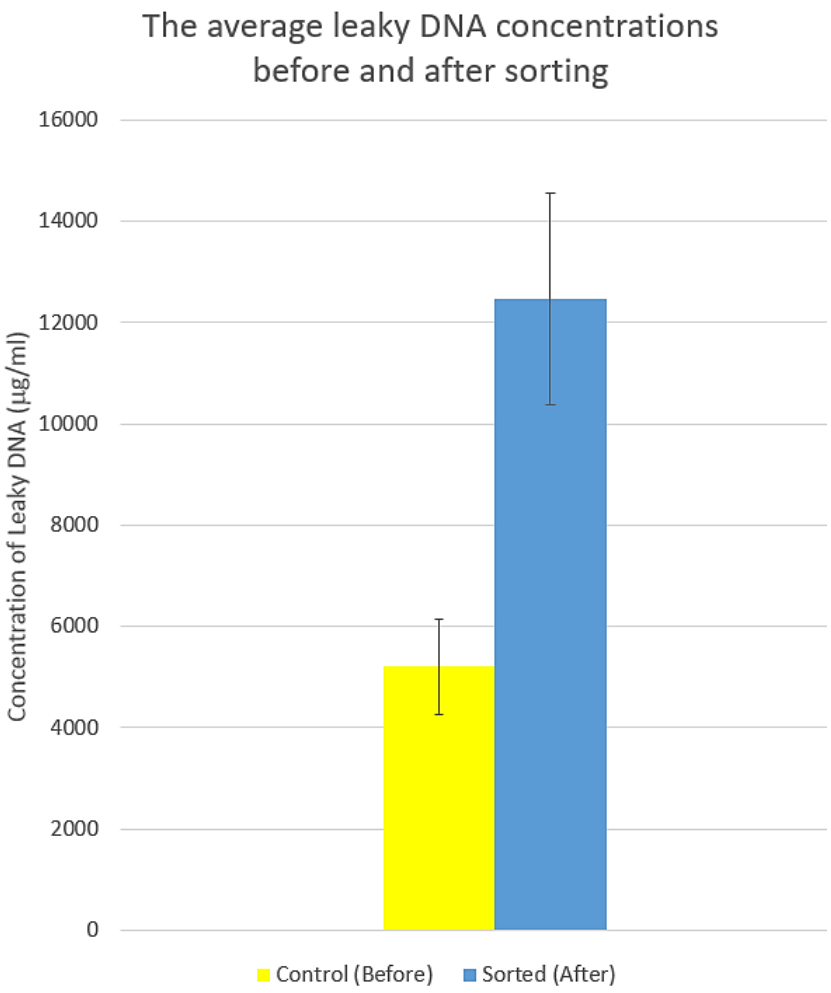

Figure 4. 21: The histogram illustrates the concentration of leaky DNA measured by standard spectrophotometry in the control and the sorted MCT supernatant. The average concentration of leakage DNA was approximately 2.4 fold sored in sorted MCT cells indicating membrane disintegration.

4.4.5 Computerized fluid dynamic simulation of fluid shear stress and extensional fluid stress

4.4.5.1 CFD emulation and approximation of FSS and EFS and their impacts on MCT vitality in feeding conduit,

To the best of our knowledge, there are at least two hydrodynamic components; fluid shear stress (FSS) and extensional flow stress (EFS), have currently been reported to majorly govern the vitality of sorted cells. Therefore, to address the failure in cell vitality after passively inertial cell sorting in fabricated ASM, the CFD assessment was integrated for validating this restriction.

Subsequently, the net fluid shear stress and extensional fluid stress in the delivery system were further computationally reckoned (Figure 4.22 and Figure 4.23). The consequence exhibited the gaining of FSS and EFS in the square manner as of increased flow velocity in the feeding system.

However, in the first moiety of the delivery system, the simulation unveiled the intraluminal velocity profile of fluid flowing in 3ml syringe barrel at the flow rate 1 ml. min^{-1}, was homogeneously distributed (Figure 4.22c). This implied that the velocities of the flows at the boundaries around and at the central axis of flow in the barrel were totally equal. Thus, there was no wall fluid shear stress (τ_w) generated in the syringe barrel.

Intuitively, the velocities sharply increased when the fluid had flown through the syringe luer tip and the cell transit conduit (female needle hub, IV catheter, silicone tube and metal connector, consecutively). The increment of velocity was inured from immediately reduced cross-sections of the transit conduits upon Bernoulli's principles. Therefore, the FSS was maximal at the surfaces of peripheral

wall of the feeding conduit because of the velocity gradient between the central axis and the wall surface.

The CFD simulation also revealed that the wall shear stress soared suddenly at the interfaces between the hubs of syringe lure tip and the barrels because of tremendously altered diameter of the junction between syringe barrel and needle hub (Figure 4.21c, d and e). In addition to FSS, the extensional flow stress was significantly abrupt as well. Therefore, the combinatorial effect of FSS and EFS would forthwith induce cells to deform or progressively degenerated or necrotized. Fundamentally, EFS befalls when a transection instantaneously alters from the wider to the narrower (Aguado et al., 2012).

In our case, the EFS invoked when the fluids had been flown through the conical hubs of syringe lure tip causing the abrupt changes of the linear velocity profiles of the flow in particular at the central axis of the flow (Figure 4.23).

4.4.5.2 CFD simulation and estimation of FSS and EFS in ASM,

In the second moiety of sorting system, the computational simulation unveiled a generation of FSS around the wall and EFS at the lesser curvature of the microchannel, consecutively. The maximum amplitude of FSS in ASM was approximately 20 Pa (Figure 4.24); meanwhile, the EFS was 40 Pa (Figure 4.25).

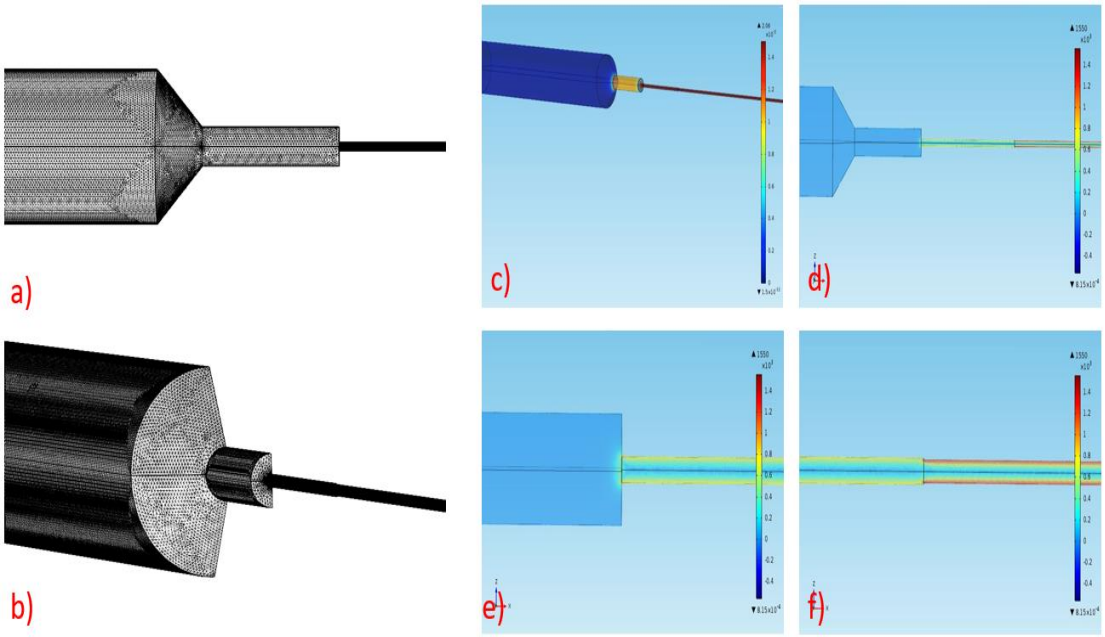

Figure 4. 22: This figure shows the CFD (COMSOL Multiphysics® version 6.3, COMSOL, USA) of fluid shear stress at the various portions of the feeding system (see the legend in 4.4.5.1).

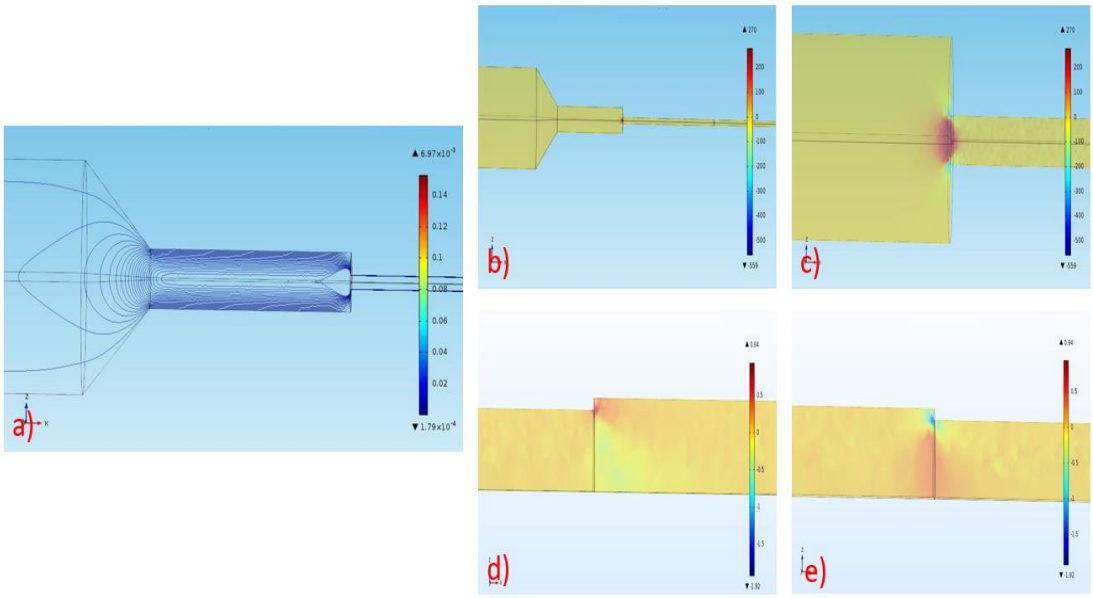

Figure 4. 23: This CFD (COMSOL Multiphysics® version 6.3, COMSOL, USA) depicts the generation of extensional fluid stress in various portion of the feeding system (see the full details in 4.4.5.1).

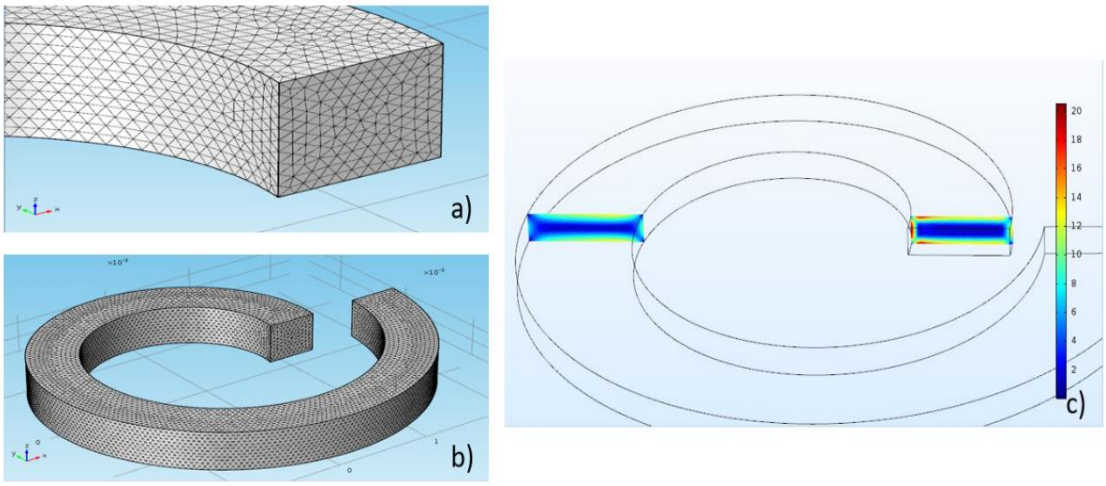

Figure 4. 24: The computerized simulation (COMSOL Multiphysics® version 6.3, COMSOL, USA) exhibits the generation of FSS and its magnitude in ASM (for the description, see in 4.4.5.2).

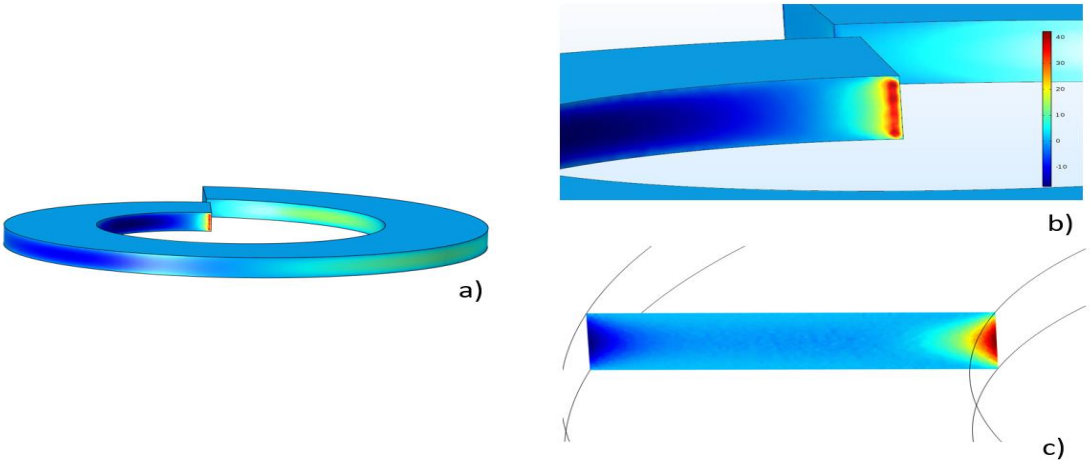

Figure 4. 25: This simulation depicts EFS (COMSOL Multiphysics® version 6.3, COMSOL, USA) generation and its magnitude in ASM sorting system (see 4.4.5.2 for full explanation).

4.5 Inertial entrapment of single MCT cells in triangular microwell array

Under the pulsatile flow at the inflow rate of 0.1 ml. min^{-1} for 30 sec. with the paused time 3 min, averagely, 4,949 out of 9,310 microwell (53.16%) occupying MCT cells. Of these, 3,614 microwell (38.82%) entrapped single MCT cells; meanwhile, 1,335 microwell (14.34%) were multiple MCT cell occupation. The ratio of single cell to multiple cell occupation was 2.71:1. Of the totally occupied microwell, the percentage of either single cell or multiple cell entrapments to all occupancy was 73.03 and 26.98 respectively. Table 4.1 summarizes the overall performance of the entrapment microdevice and the trapping characteristic is illustrated in Figure 4.26 and 4.27 at the various objective powers (4X, 10X and 40X).

	Microdevice I	Microdevice II	Microdevice III	Average ± SD
Total microwell	9,309	9,313	9,308	9,310 ± 2.65
Occupied microwell	4,951	4,962	4,934	4,949 ± 14.11
Single occupancy	3,605	3,602	3,635	3,614 ± 18.25
Multiple occupancy	1,346	1,360	1,299	1,335 ± 31.95

Table 4. 1: This table recapitulates the overall performance of the trapping microdevice. It is noteworthy that over fifty percent of microwell were occupied by single MCT cells. Of these, almost (38.82%) were single cell entrapment; meanwhile, the others were possessed multiple MCT cells under pulsatile flowing profile.

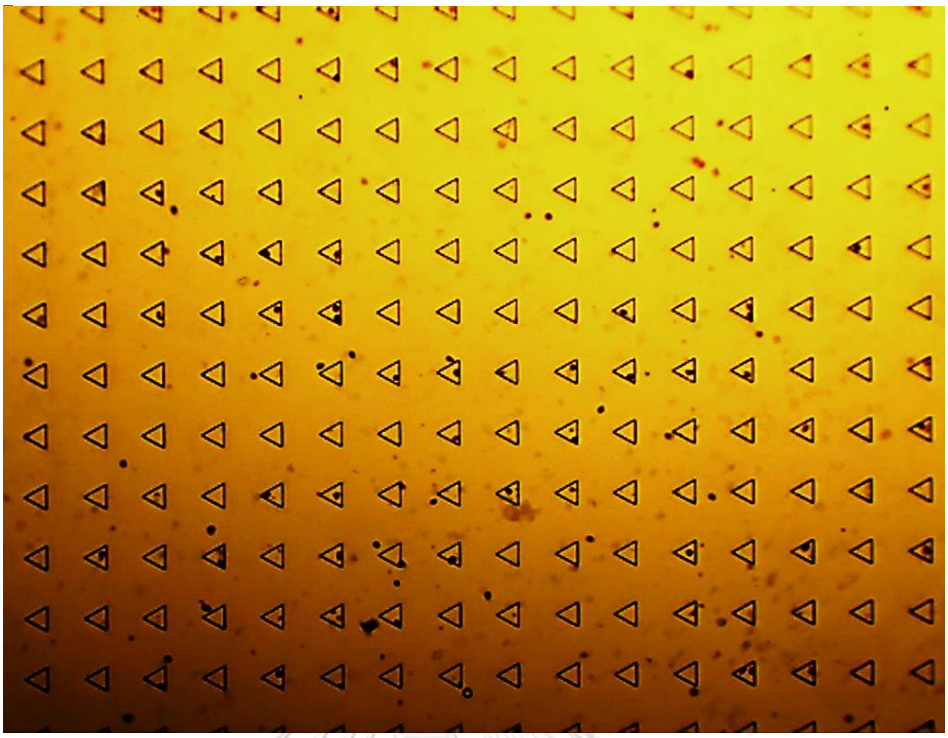

Figure 4. 26: At the scanning magnification power (4X), the exploit micrograph revealed the internal structure of the entrapment microdevice. Notably, it had a capability to entrapping single MCT cells in their microwell array (approximately 53.16%) and almost were single entrapments.

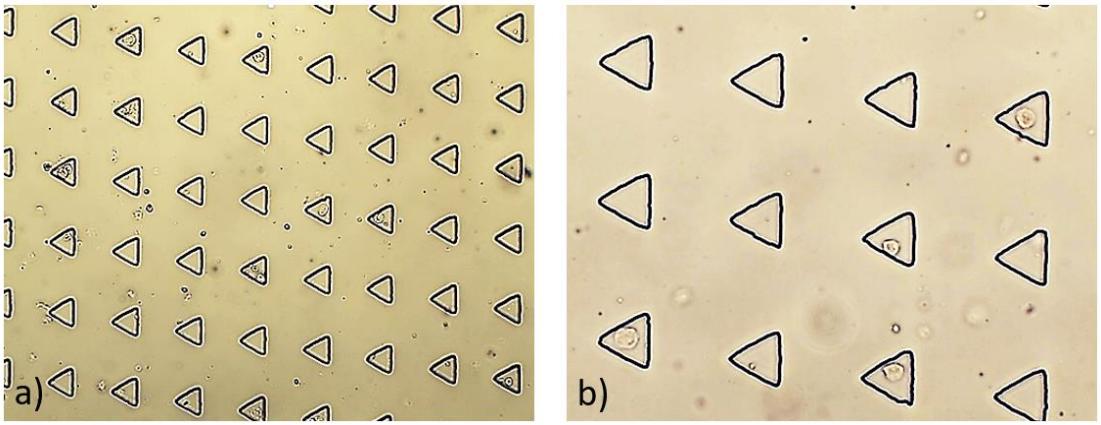

Figure 4. 27: The figure panel manifests the entrapment of single MCT cells in the triangular microwell at the low-magnification power (10X) on the left figure (a) and at the high-power magnification (40X) on the right figure (b).

4.6 Additional parameters influencing on passively hydrodynamic entrapment of single MCT cells in triangular microwell array

4.6.1 Effect of dilutions of singly trypsinized MCT cells on microdevice performance

Based upon hemocytometry enumeration, the initial concentrations of freshly single MCT cells after trypsinization were 1.28 $x10^5$ and 3.65 x 10^5 cells/ml respectively. And the mean concentration was at 2.465 $x10^5$ cells/ml.

Obviously, under the 10 fold and 100 fold dilutions, the efficiency of microdevice was geometrically exponentially reduced to 31.3% and 8.3% consecutively but the opportunities of single MCT cell ensnaring were increased in both cases particularly in 100 fold dilution.

4.6.2 Impact of inflow rate microdevice capacity

The effect of inflow rate also impacted to the device capacity. When the inflow rate was accrued from 0.01 to 0.03 ml. hr^{-1}, the capture percentage was proportionately 16.72 fold increased. However, when the fluid influx rate was increased from 0.03 to 0.05 ml. hr^{-1}, the probability of cell entrapment was bluntly accrued (0.04 fold). Moreover, the incidence of multiple MCT cell trapping was increased after escalating the inflow rate.

4.6.3 Effect of the height of main flow microchannel on microdevice capacity

The other critical factor which extremely governed the capability of microdevice was the height of the main flow microchannel. In this study, when the height was decreased from 160 to 70 mm, the capacity of entrapment was 5.24 fold soared but, as same as the other parameters, the possibility in multiple cell ensnaring was significantly increased.

4.7 Investigation of OCT4-dependent self-renewal in entrapped MCT cells

To clarify the function of OCT4 in a regulation of self-renewal, OCT4-immunocytofluorescense was employed in this study. Firstly, the accuracy of method was verified by reacting the antibodies with the positive control (canine keratinocyte cell line). Keratinocytes were clearly stained positive with the antibodies (Figure 4.28). Furthermore, some trypsinized MCT cells in the smear were also positive for OCT4-ICF (Figure 4.29). And a few of MCT cells in suspension were positively stained by the OCT4 antibodies (Figure 4.30).

Upon those study consequences; therefore, some trapped MCT cells would probably be positive for OCT4-ICF. Finally, the result substantially exhibited the positivity of OCT4-immunofluorescence in a few MCT cells trapped in the microwell. Their OCT4 were positively stained red intranuclearly. Meanwhile, the negative MCT cells were not tangible with OCT4-immunocytofluorescence and were stained by DAPI only as shown in Figure 4.31.

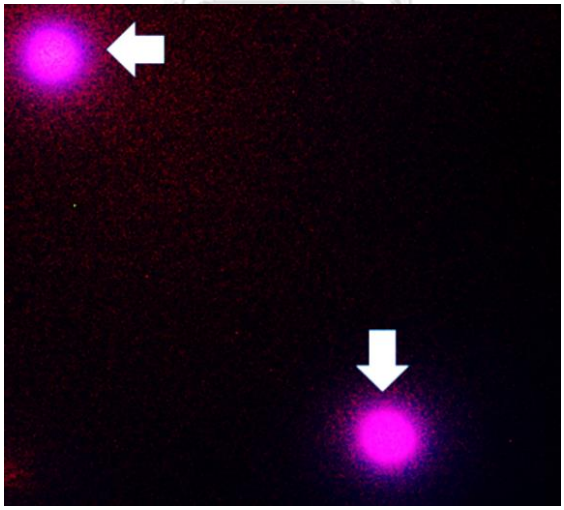

Figure 4. 28: The positive control (canine keratinocyte cell line) was positive to OCT4-immunocytofluosecence. The fluorescent signaling was illuminated pink or red under λ_{575} light source.

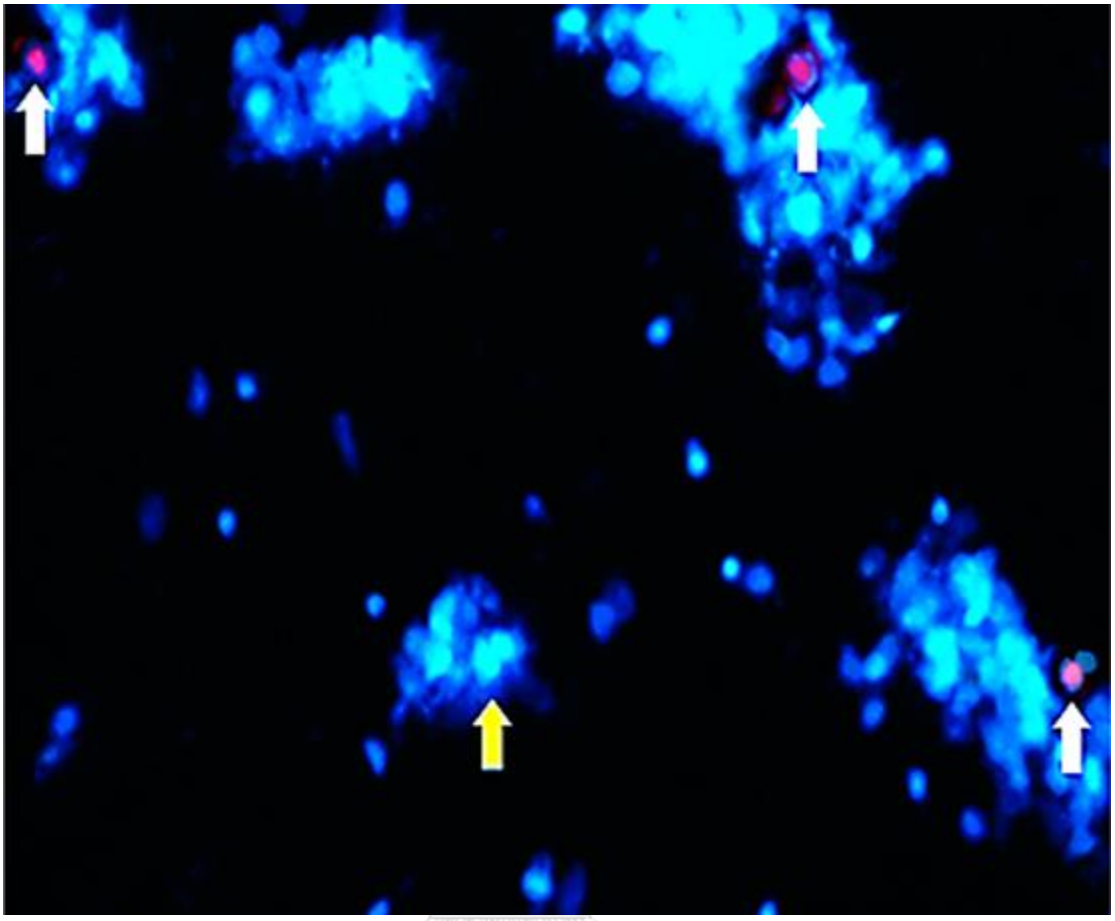

Figure 4. 29: The OCT4-ICF positivity of trypsinized MCT cells in a cell smear. Intuitively, only a few trypsinized MCT cells were positive for OCT4-immunocytofluorescence (white arrows). This suggests the existence of MCT cells which were undergoing self-renewal. Therefore, these cells would be proposed to be MCT-CICs compared to the other which were OCT4-ICF negative (yellow arrow).

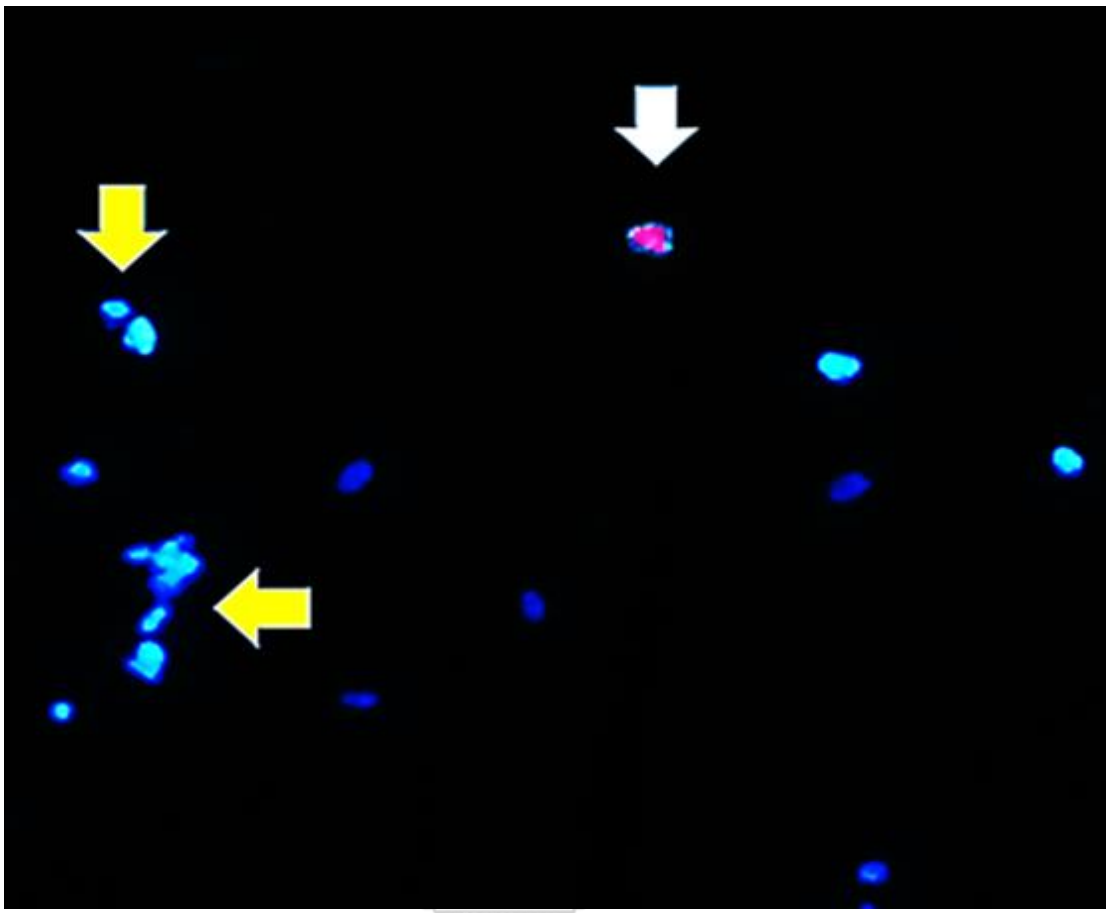

Figure 4. 30: This figure represents the presence of a putative MCT-cancer initiating cell (white arrow) in MCT cell suspension. Meanwhile, the OCT4-ICF negative were speculated to be terminally-differentiated MCT cells which have lost their self-renewal.

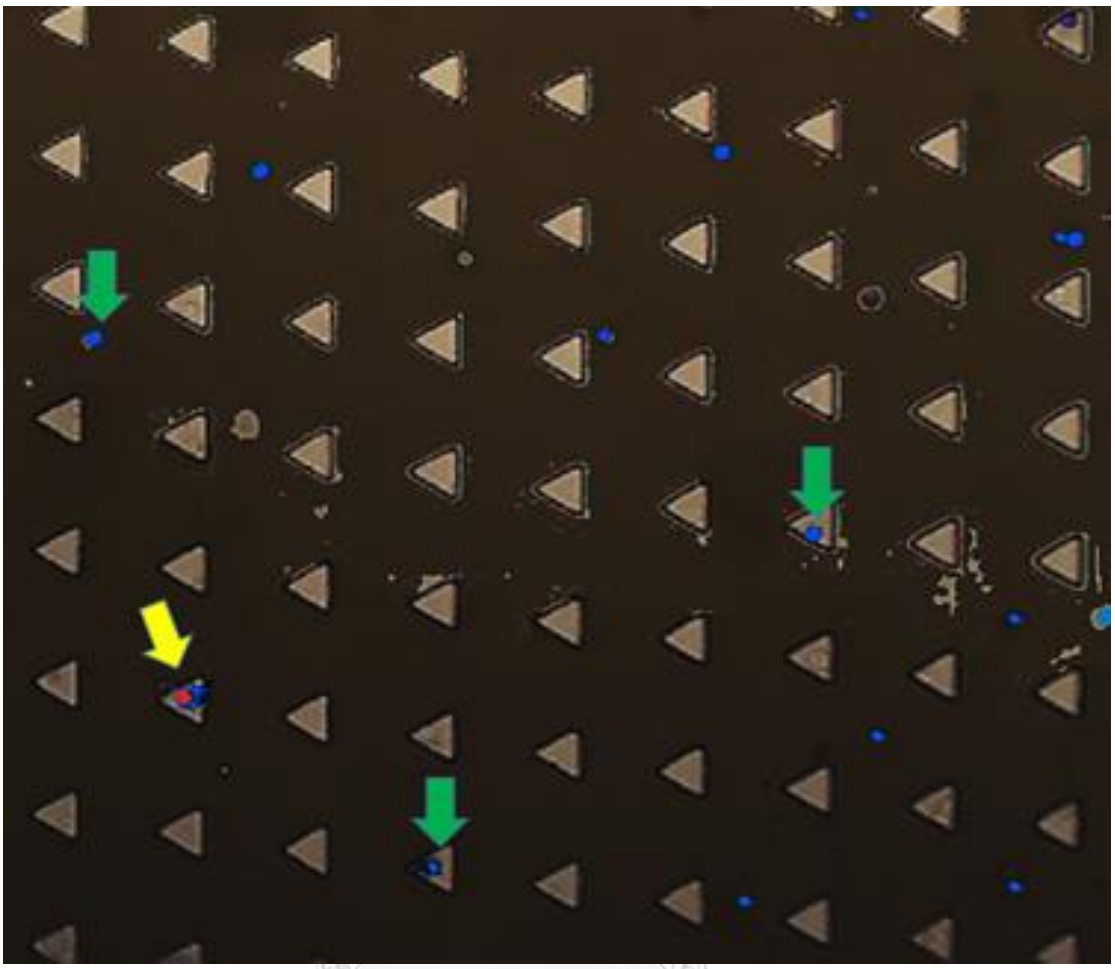

Figure 4. 31: The figure illustrates the positivity of OCT4-ICF in an ensnared single MCT cells (yellow arrow). Meanwhile, the others were negative (green arrows).

CHAPTER V
DISCUSSION AND CONCLUSION

5.1 Discussion

In this study, six cutaneous masses were histopathologically evaluated and the results confirmed the existence of MCT cells in those masses. Later, single MCT cells were separated by trypsinization from them. The conformational figures revealed almost MCT cells were round-to-oval MCT cells, although anaplastic MCT cells were also observed in such circumstances. The cells usually contained single nuclei except the anaplastic cells having bizarre nuclei. Their cytoplasm under Giemsa staining was basophilic filled with fine-metachromatic granules.

Under microfluidic-based single cell analysis, we achievably employed our predesignated Archimedean spiral microchannel (ASM) to passively enrich the MCT cells in the group III (15-19 μm) and IV (20-30 μm) out from their mixed subpopulations of terminally-differentiated counterparts, MCT group I (5-9 μm) and II (10-14 μm) according to their distinguished sizes at the high-throughput rate (> 500,000 cells/min). Because we hypothesized that the MCT cells in both groups should have the biological idiosyncrasy resemblance to putative MCT cancer initiating cells, at least their bigger sizes. We also investigated the dreadful effects of fluid shear stress (FSS) and extensional fluid stress (EFS) on the vitality of sorted MCT cells after microfluidic inertia focusing in our ASM system. Because they were never performed before.

Nevertheless, we had also fabricated the microfluidic chip which was used for passively-inertial single cells trapping. In this step, we studied some physical parameters which might dictate the potency of the trapping device as well, and the study outcome could be further used for improving its performance in the future. In the last phase, we investigated the expression of a key embryonal transcription factor; OCT4, which controls the self-renewal of stem cells, in singly entrapped MCT cells.

Pertaining to the study results, taken together, our ASM was the 500x130μm, five-turned curvilinear rectangle microchannel for size-based cell sorting, and the

microfluidic chips with 40μm-high x 15 μm-deep, triangular microwell array for single cell entrapment were successfully been fabricated by the standard photoresist-soft-lithography. It is overtly seen that our ASM was capable sorting out MCT cells group-III and -IV from their smaller counterparts (MCT group-I and -II). Instinctively, MCT cells group-III and -IV focused into their respective streamlines upon their individual sizes of which their focused streams were close to the inner wall of the microchannel. These sorted cells then mainly surged out at the outlet II.

On the other hand, the MCT group-II were streamed up toward the center of microchannel; while the cells in group-I were unfocused. Therefore, MCT group-II were principally collected at the outport III and IV. And MCT group-I undoubtedly could be obtained at all outlets.

Since the crux of the ASM sorting is something the resolution and the noxious effect on sorted cells. However, the combinatorial result from FACS size-based quantification and hemocytometry enumeration indicated that our spiral microchannel could not completely separate MCT cell group III from group II, and the device was also detrimental to the sorted cells.

For the sorting resolution, the efficacy of our ASM was counterintuitively lower than premised so that the resolution of our ASM was still remarkably questionable when compared to the other studies. Based on other previous studies, the separation efficiencies of various spiral microchannel were claimed to be higher than 80%, although the geometry configurations of them were different from one another (Di Carlo et al., 2007; Kuntaegowdanahalli et al., 2009; Nivedita and Papautsky, 2013; Tanaka et al., 2012).

To the best of our knowledge, the parameters that might govern the device resolution were prophesized to be; the geometry of microchannel in particular the exit channel and its outlets in this case, the initial concentration of single cells, intraluminal bubble formation, the cell wreckage, the biological properties of the cells themselves and the differential sizes of cells in suspension (Martel and Toner, 2014).

Geometrically, our spiral microchannel had the asymmetrical exit channel followed by ten unequally-long subsidiary outlets. Compare to the others in previous studies, almost spiral microchannel had symmetrical exit channels connecting to several outlets and their path lengths were usually equivalent. Accordingly, the intraluminal pressures at the exit channel might sharply reduce in our case because of the different pressure gradients across ten outlets. This might cause two adjacent focusing streamlines defocused, swayed and finally bounced together leading to the interference of neutrally focusing forces. As of the number and the uniformity of the outlets might get involve in a maintenance of particle focusing. Hence, it is indispensable to carefully design an exit channel and its outlets (Kuntaegowdanahalli et al., 2009).

Likewise, the incipient concentration of cell suspension might impact on the sorting resolution. Naturally, single MCT cell suspension is prepared in PBS. This fluid medium ideally is Newtonian fluid of which its viscosity is fixed. However, when the cells are added in the medium. It may increase the medium viscosity. And when the fluid medium becomes viscid, its property will shift to non-Newtonian fluid and the whole cell suspension will resist to the flow (Wu et al., 2010). One of the good example of natural, non-Newtonian fluid is the blood.

As in case of the blood, when the hematocrit (Hct) is increased, there is much more chance in which erythrocytes will aggregate together causing red corpuscle clumping. Therefore, in highly concentrated MCT suspension, the density of cells is extremely high and there is an increased opportunity in which adjacent MCT cells will interact or adhere altogether. Nonetheless, the high amount of MCT cells also results in an increment of media viscosity as well.

The cell-to-cell interaction in non-Newtonian fluids such as blood commonly impacts to the device efficacy. Even though, a couple of Dean Drag Forces still do strongly exert on the cells in the non-Newtonian fluid (Nivedita and Papautsky, 2013).

In 2012, Tanaka and his colleague had examined an influence of fluid viscosity on the sorting resolution of a barbell-shape microchannel. In that study, human breast

cancer cells (MDA-MB-231) were mixed with the whole bloods. The particle Reynold's number (Re_p) of the cells was fixed at 0.622 and the blood viscosity was directly variegated on the pack cell volume (PCV). The result indicated that the inertial migration of cells inversely proportionated to the viscosity owing to cell-to-cell interactions (Tanaka et al., 2012). In spiral microchannel, an overwhelming of cell aggregation at the focusing position also frequently intervenes the adjacent focusing streams resulting in the decrement of separation resolution. Anyhow, cell dilution can prevent this adverse effect and perhaps improves the device efficiency (Nivedita and Papautsky, 2013).

Although, our experiment setup in general would prevent a bubble formation. However, along the experiments, there were various factors which could generate the bubbles especially Taylor bubbles which always obstruct flow tracts completely and cause a fluid backflow. Basically, the bubble formation is a function of the microchannel geometry, size of microfluidic devices, gas, flow focusing and rate, fluid property, temperature change, the hydrophobic of PDMS, and configurations of connectors, adaptors, and valves (Fu et al., 2009; Wang et al., 2012). Unfortunately, when air bubbles have arisen in microfluidic systems, they barely coalesce with one another (Fu et al., 2009) and are extremely difficult to remove according to an increased volume-to-surface ratio of the bubbles (Fu et al., 2009; Geng et al., 2013). Thus, a bubble formation in a microchannel can reduce device resolution (Geng et al., 2013). Due to our microfluidic sorting system was the semi-opened system, the bubbles in the system were therefore generated by several causes. The first was the instrumentation of the device because of there were many connectors and feeding conduits connected to the device; thus, there was an increased occasion that the air in the ambient atmosphere would flow in the microchannel. And the second would be from the reduction of flow rate from 3-5 ml. min^{-1} used for bubble propelling in the preparatory step, to the experiment flow rate at 1 ml. min^{-1}. This might bring about the back pressures at the outlets which drove the bubble formation.

The physical properties of MCT cells themselves could also influence on the performance of the sorting device. In order to survive, all cells including MCT cells

dynamically change in their physiology over the time to cope with any intrinsic and extrinsic stimuli. This is the leading cause of the change in cell compositions resulting in the variations in sizes, shapes and viscoelastic rheological properties of cells, and probably affecting the inertial migration and vitality of sorted cells (Tanaka et al., 2012). The nuance in cell sizes may cause MCT cells in group III and II which their subscale sizes were minutely different from each other (i.e., 13.6 and 15.3 μm) to focus either at the same displacement or more close together in the curvilinear microchannel. Thus, this might lower the sorting efficiency in our experiment system.

Although, the device resolution was an important factor to determine the sorting efficacy. However, at the heart of our sorting process, the vitality of sorted MCT cells was the most crucial parameter. Hemocytometry enumeration confirmed the loss of sorted MCT cells in the system because the concentration of MCT cells after sorting was overtly lower than as foreseen. Approximately sixty percent of our isolated MCT cells were lost in the sorting system (e.g., in the cell delivery portion and the spiral microchannel itself). However, the harvested cells which had been sorted out, were not almost healthy or even damaged. Many were vulnerable, deformed, aggregated or dead after sorting based on light microscopy, scanning electron microscopy, vital dye staining and leakage DNA content assay.

In the recent decade, fluid shear stress (FSS) and extensional flow stress (EFS) have been speculated to get involve in hydrodynamic cell injuries. For example, the high fluid shear stress in a bioreactor can cause a sloughing of cultured cells from their base attachment and lead to cell deformation (Wu, 1999). In addition, RBCs which have flown through a stenotic cardiac valve may be experienced the surge of EFS in the blood which causes hemolysis. The other obvious example is the deformation of endothelial cells induced by the hemodynamic wall shear stress causing atherosclerosis (Cunningham and Gotlieb, 2005), atherothrombosis and myocardial infarction under turbulent hemodynamic (Heo et al., 2014). However, in microfluidic system, the information is still scanty.

Based on our CFD simulations, the results substantially suggested the high FSS at the upper and lower boundaries of the spiral microchannel; meanwhile, the high

EFS was observed at the lesser curvature of the microchannel. Antithetically, the FSS was not typically noticeable along the feeding system but the EFS was remarkably high at all the junctions. Although, the magnitude of the EFS in the feeding system might not strengthen enough to produce MCT damage as well as the cells had moved through the areas within an ephemeral interval. However, the EFS in the delivery portion might endow the vulnerability to the flown-through MCT cells. Therefore, this predisposing weakness would instigate fed MCT cells to be easily destroyed when they were continually received the combined effect of FSS and EFS in the spiral microchannel.

Basically, MCT as well as other mammalian cells are prone to be damaged under the highly hydrodynamic shear stresses according to the lack of cell walls (Kretzmer and Schugerl, 1991) and high cytoplasmic contents. Physiologically, mammalian cells are able to adapt themselves to cope with many mechanical injuries by changing their intracellular components such as cytoskeletal proteins, and/or altering an expression of metabolic and survival genes. But under pathologic-like conditions, the cells usually lose these adaptive abilities and then undergo cell degeneration or necrosis.

For example, intact erythrocytes are never mechanically damaged in the physiological circulations because of cellular adaptation on cell membrane compositions and cortical cytoskeletons. However, they easily break down when they have flown through a corporeal circulating device, such as a stenotic cardiac valve (20-50 Pa) or an artificial heart and valve (1-1000 Pa). Because of the high shear stress over physiological level; hence, the sudden onset of cell devastation usually takes place (Lee et al., 2004). This anticipation is hypothesized to occur in case of MCT cells under a high shear stress as well.

Albeit, the pathogenesis of hydrodynamic stress-induced cell damage is currently unclear; however, some associated factors, such as cell types, exposure time of stresses (Barnes et al., 2012) and sorting methodologies in use, have also been reported so far. Primarily, fluid shear stress and extensional flow stress are supposed to induce a reorganization of cytoskeletons bringing about the cell deformation

(Gossett et al., 2012). In general, cells which have undergone deformations, can be recovery as long as they never cross the point of no return in which it sentences the survival of death to the cells. Moreover, cell membrane integrity is an excellent indicator for membrane damage; while, cytoskeletal disarrangement is the best index for cell deformation. The reduction of cell deformity also suggests the irreversible cell injury (Lee et al., 2004).

In 2009, Park and his coworkers have reported that human prostate cancer cells (PC 3) which had adhered to the PDMS on the floor of their microfluidic culturing devices, would be dead after experiencing the FSS over than 0.5 Pa. but at the lower magnitude; 0.2 Pa, the cells just launched the deformation (Park and Jung, 2009). As same as in the baby hamster kidney cells (BHK 21 c13), they initiated cell necrosis when they had exposed the FSS at 1.5 Pa for 3 hours in an adherent bioreactor; however, these cells were not dead but changed in their biomembrane integrity evidenced by the leakage of internal cytoplasmic enzyme; lactate dehydrogenase (LDH) at the FSS of 0.16 Pa (Kretzmer and Schugerl, 1991). In one study with the colorectal adenocarcinoma cells (COLO 205), the cancerous cells which had been injected out of the syringe through the needle were almost died in the system in which FSS was tremendously high (75-650 Pa). Undoubtedly, at these FSS scales, the cells could not endure the shear stresses and then underwent cell necrosis (Barnes et al., 2012; Mitchell and King, 2013). Basically, the threshold of shear stress in normal cells is approximately 150-400 Pa in range (Lee et al., 2004) and cells do not deform unless the Young's modulus (E) of cells is over than 10^2 Pa (Tanaka et al., 2012).

Consistently to our preliminary study, the results indicated that canine leukocytes were more resistive to the effects of FSS and EFS than MCT cells (unpublished data). The deformation and survival rate of canine leukocytic cells was extremely lower when compared to MCT cells (20 and 40%, respectively). One of the probable explanation is the differences in extracellular and intracellular components of the structural macromolecules. Notwithstanding, there have been evidence showing that various circulating tumor cells (CTC) are more deformable than their normal counterparts (Byun et al., 2013).

The differentiation stage of cells also affect to the resistance of FSS and EFS. The evidence has shown that differentiated neuroblastoma SH-SY5Y cell lines have 3-fold larger elastic modulus than that of undifferentiated cells. Therefore, mature cells would endure the hydrodynamic stresses than undifferentiated cells (Zhao et al., 2015). In our sorted MCT cells, we also anticipated that terminally-differentiated MCT cells would resist to the FSS and EFS more than putative MCT-CICs.

According to the study result, the majority of our sorted MCT cells were dead from the high-grade FSS and EFS taking place in our experimental system. By these amplitude scales, the stresses could cause the sudden disintegration of their basic components of cell membranes in particular high-molecular-weight (HMW) integral proteins and lipid rafts resulting in increased membrane permeability and/or membrane rupture as observed by increased DNA content and cell debris.

When the cells had been wreckage, the cell debris in the sorting system could aggregate together and might adhere to the sidewall of microchannel. In addition, with the fabrication defect, we also observed some unidentified threads existing in our sorting system which might be a crucial cause of the reduction in ASM sorting resolution. These additional factors have been illustrated in Appendix K.

Intriguingly, the aggregation of cell debris would be narrowing the channel and would result in an increment of the shear stresses. Moreover, after cell rupture, the cytoplasmic contents such as proteins, enzymes and DNA contents would contaminate in the fluid medium resulting in an increase of fluid viscosity. Finally, it causes an interference in sorting resolution.

For single MCT cell entrapment, the result had suggested that our triangular microwell array had a capacity to ensnare the targeted single-MCT cells. Anyhow, there were a probability in which the microwell would capture multiple MCT cells, even though, in less frequency.

Furthermore, OCT4-immunocytofluorescence substantially suggested that, in mixed-populations of singly ensnared MCT cells, there were the potency in which a small subpopulation would has the self-renewal capacity. Hypothetically, this

biological property usually belongs to cancer stem cells. Therefore, our OCT4-ICF results might reflect an existence of the putative MCT cancer stem cell referred as MCT cancer initiating cell (MCT-CIC) in this study.

Since the working principles are dependent on the hydrodynamic recirculation in the microwell and the gravity; therefore, all MCT cells were stochastically entrapped. However, based on the study, we observed some physical parameters governing the increment of device efficiency, such as the initially experiment concentration, the geometry of the microdevice and the characteristic of the flow.

5.2 Conclusion

Conclusively, herein, we have demonstrated the accomplishment on microfabrication and application of the Archimedean spiral microchannel to enrich the larger MCT cells in group III and IV from the MCT cells group I and II in the naturally buoyant, multiple-sized MCT suspension. However, the critical problems of the sorting system, which need for an urgent amendment, are the resolution of the device and the dreadful effect caused by fluid shear and extensional flow stresses.

In term of cell biology, viable cells are essentially valuable by which they can be further used in a comprehensive study for their biology in particular diseasing cells. Therefore, the loss of viable cells may cause us wasting the targeted cells and an increased performance of separating devices is still the matter in so essence. For this aspect; cell vitality is the reminiscently critical parameter. Although, the viable MCT cells in this study was approximately 40%. However, it was acceptable because the percentage was higher than our speculation.

In addition, we have demonstrated the utilization of the triangular microwell array for single MCT cell entrapment. However, the efficiency of the chip also requires an improvement for increasing its trapping performance. However, in this study, we have preliminarily studied some physical parameters which influences on its efficacy. The information will be beneficial for a further experiment design, a companion experiment and device improvement in the future.

Ultimately, the pros and cons of this study will ignite another research groups to fully reestablish a new geometry design of curvilinear microchannel which is able to complete the size-based cell sorting. We are also looking forward that any caveats observed in our study will prevent any pernicious effect to the cells which have been passively sorted by a spiral microchannel in the future.

In the epilogue, this study was the pioneer work utilizing two microfluidic platforms; Archimedean spiral microchannel and triangular microwell array, for size-based single MCT cell sorting and trapping in the veterinary field, respectively. The achievement will enhance our outright savvy in any change in cell biology especially from neoplastic cells. Furthermore, this study was the first microfluidic laboratory which had sorted single cells under Dean-induced inertial cell focusing in the real neoplastic cells in which there was a natural nuance in their sizes and buoyancies. In addition, we have the propensity to combine these two microfluidic platforms together to completely form a lab-on-a-chip (LOC) microdevice which is able to isolate, entrap, culture and investigate the "omics" of various targeted cells in the future and its accomplishment will ultimately be beneficial for almost biomedical engineering researches in the upcoming future.

REFERENCES

Abaci HE, Shen YI, Tan S and Gerecht S 2014. Recapitulating physiological and pathological shear stress and oxygen to model vasculature in health and disease. Sci Rep. 4: 4951.

Aguado BA, Mulyasasmita W, Su J, Lampe KJ and Heilshorn SC 2012. Improving viability of stem cells during syringe needle flow through the design of hydrogel cell carriers. Tissue Eng Part A. 18(7-8): 806-815.

Akenhead ML and Shin HY 2015. The contribution of cell surface components to the neutrophil mechanosensitivity to shear stresses. Biophysics. 2(3): 318-335.

Almendro V, Marusyk A and Polyak K 2013. Cellular heterogeneity and molecular evolution in cancer. Annu Rev Pathol. 8: 277-302.

Altschuler SJ and Wu LF 2010. Cellular heterogeneity: when do differences make a difference? Cell. 141(4): 559-563.

Baracca A, Sgarbi G, Solaini G and Lenaz G 2003. Rhodamine 123 as a probe of mitochondrial membrane potential: evaluation of proton flux through F(0) during ATP synthesis. Biochim Biophys Acta. 1606(1-3): 137-146.

Barnes JM, Nauseef JT and Henry MD 2012. Resistance to fluid shear stress is a conserved biophysical property of malignant cells. PLoS One. 7(12): e50973.

Braasch D 1969. The relation between erythrocyte deformability, cell shape, and membrane surface tension. Pflugers Arch. 313(4): 316-320.

Burkhardt E 1979. Scanning electron microscopy of peripheral blood leukocytes of the chicken. Cell and Tissue Research. 204(1): 147-153.

Butler LM, Bonnett BN and Page RL 2013. Epidemiology and the Evidence-Based Medicine Approach. In: Withrow and MacEwen's Small Animal Clinical Oncology (Fifth Edition). Saint Louis: W.B. Saunders. 68-82.

Butler PJ, Norwich G, Weinbaum S and Shu C 1999. Shear stress increases endothelial cell-membrane fluidity. Proceedings of the First Joint BMES/EMBS Conference. 1999 IEEE Engineering in Medicine and Biology 21st Annual Conference and the 1999 Annual Fall Meeting of the Biomedical Engineering Society (Cat. N:6 vol.1.

Byun S, Son S, Amodei D, Cermak N, Shaw J, Kang JH, Hecht VC, Winslow MM, Jacks T, Mallick P and Manalis SR 2013. Characterizing deformability and surface friction of cancer cells. Proceedings of the National Academy of Sciences. 110(19): 7580-7585.

Castiello FR, Heileman K and Tabrizian M 2016. Microfluidic perfusion systems for secretion fingerprint analysis of pancreatic islets: applications, challenges and opportunities. Lab Chip. 16(3): 409-431.

Chen J, Chen D, Xie Y, Yuan T and Chen X 2013. Progress of Microfluidics for Biology and Medicine. Nano-Micro Letters. 5(1): 66-80.

Chen WEI 2006. Electroconformational Denaturation of Membrane Proteins. Annals of the New York Academy of Sciences. 1066(1): 92-105.

Chen YC, Ingram PN, Fouladdel S, McDermott SP, Azizi E, Wicha MS and Yoon E 2016. High-Throughput Single-Cell Derived Sphere Formation for Cancer Stem-Like Cell Identification and Analysis. Sci Rep. 6: 27301.

Cheng X, Irimia D, Dixon M, Sekine K, Demirci U, Zamir L, Tompkins RG, Rodriguez W and Toner M 2007. A microfluidic device for practical label-free CD4(+) T cell counting of HIV-infected subjects. Lab Chip. 7(2): 170-178.

Cheng YH, Chen YC, Brien R and Yoon E 2016. Scaling and automation of a high-throughput single-cell-derived tumor sphere assay chip. Lab Chip. 16(19): 3708-3717.

Cucina A, Sterpetti AV, Pupelis G, Fragale A, Lepidi S, Cavallaro A, Giustiniani Q and Santoro D'Angelo L 1995. Shear stress induces changes in the morphology and cytoskeleton organisation of arterial endothelial cells. Eur J Vasc Endovasc Surg. 9(1): 86-92.

Cucullo L, Hossain M, Puvenna V, Marchi N and Janigro D 2011. The role of shear stress in Blood-Brain Barrier endothelial physiology. BMC Neurosci. 12: 40.

Cunningham KS and Gotlieb AI 2005. The role of shear stress in the pathogenesis of atherosclerosis. Lab Invest. 85(1): 9-23.

de Mora F, Puigdemont A and Torres R 2006. The role of mast cells in atopy: what can we learn from canine models? A thorough review of the biology of mast cells in canine and human systems. Br J Dermatol. 155(6): 1109-1123.

Di Carlo D, Irimia D, Tompkins RG and Toner M 2007. Continuous inertial focusing, ordering, and separation of particles in microchannels. Proceedings of the National Academy of Sciences. 104(48): 18892-18897.

Dobson JM and Scase TJ 2007. Advances in the diagnosis and management of cutaneous mast cell tumours in dogs. J Small Anim Pract. 48(8): 424-431.

Down LA, Papavassiliou DV and O'Rear EA 2011. Significance of extensional stresses to red blood cell lysis in a shearing flow. Ann Biomed Eng. 39(6): 1632-1642.

Duncan JR and Prasse KW 1979. Cytology of Canine Cutaneous Round Cell Tumors. Veterinary Pathology. 16(6): 673-679.

Fiorini GS and Chiu DT 2005. Disposable microfluidic devices: fabrication, function, and application. Biotechniques. 38(3): 429-446.

Friedman N 2013. Studying gene expression at the level of the single cell. Brief Funct Genomics. 12(2): 73-74.

Fritzsch FS, Dusny C, Frick O and Schmid A 2012. Single-cell analysis in biotechnology, systems biology, and biocatalysis. Annu Rev Chem Biomol Eng. 3: 129-155.

Fu T, Ma Y, Funfschilling D and Li HZ 2009. Bubble formation and breakup mechanism in a microfluidic flow-focusing device. Chemical Engineering Science. 64(10): 2392-2400.

Galbraith CG, Skalak R and Chien S 1998. Shear stress induces spatial reorganization of the endothelial cell cytoskeleton. Cell Motil Cytoskeleton. 40(4): 317-330.

Geers AJ, Morales HG, Larrabide I, Butakoff C, Bijlenga P and Frangi AF 2017. Wall shear stress at the initiation site of cerebral aneurysms. Biomechanics and Modeling in Mechanobiology. 16(1): 97-115.

Geng Z, Ju Y, Wang W and Li Z 2013. Continuous blood separation utilizing spiral filtration microchannel with gradually varied width and micro-pillar array. Sensors and Actuators B: Chemical. 180: 122-129.

Gossett DR, Tse HT, Lee SA, Ying Y, Lindgren AG, Yang OO, Rao J, Clark AT and Di Carlo D 2012. Hydrodynamic stretching of single cells for large population mechanical phenotyping. Proc Natl Acad Sci U S A. 109(20): 7630-7635.

Gross A, Schoendube J, Zimmermann S, Steeb M, Zengerle R and Koltay P 2015. Technologies for Single-Cell Isolation. Int J Mol Sci. 16(8): 16897-16919.

Hanahan D and Weinberg RA 2000. The hallmarks of cancer. Cell. 100(1): 57-70.

Hanahan D and Weinberg Robert A 2011. Hallmarks of Cancer: The Next Generation. Cell. 144(5): 646-674.

Hasni AE, Göbbels K, Thiebes AL, Bräunig P, Mokwa W and Schnakenberg U 2011. Focusing and Sorting of Particles in Spiral Microfluidic Channels. Procedia Engineering. 25: 1197-1200.

He JL, Chen AT, Lee JH and Fan SK 2015. Digital Microfluidics for Manipulation and Analysis of a Single Cell. Int J Mol Sci. 16(9): 22319-22332.

Heo KS, Fujiwara K and Abe J 2014. Shear stress and atherosclerosis. Mol Cells. 37(6): 435-440.

Hill and Martin 1998. A review of mast cell biology. Veterinary Dermatology. 9(3): 145-166.

Hou HW, Warkiani ME, Khoo BL, Li ZR, Soo RA, Tan DS-W, Lim W-T, Han J, Bhagat AAS and Lim CT 2013. Isolation and retrieval of circulating tumor cells using centrifugal forces. Scientific Reports. 3: 1259.

Huntley JF 1992. Mast cells and basophils: A review of their heterogeneity and function. Journal of Comparative Pathology. 107(4): 349-372.

Joshi DC and Bakowska JC 2011. Determination of mitochondrial membrane potential and reactive oxygen species in live rat cortical neurons. J Vis Exp. (51).

Kent DG, Lin JC and Aubert G 2011. The First AACR special conference on stem cells, development, and cancer: some of these cells are not like the others. Cancer Res. 71(17): 5616-5620.

Ketpun D, Bhanpattanakul S, Sailasuta A, Tongmanee T, Suwannaphan T, Pimpin A, Srituravanich W, Jeamsaksiri W, Sripumkhai W and Piyaviriyakul P 2015. A microfluidic model for single microparticle and future single-cell trappings. The 40th International Conference on Veterinary Sciences, IMPACT Forum, Muang Thong Thani, Thailand.

Ketpun D, Sailasuta A, Piyaviriyakul P, Onlamoon N and Pattanapanyasat K 2013. Rapid Evaluation of Mutant Exon-11 in c-kit in a Recurrent MCT Case Using CD117 Immunocytofluorescence, FACS-Cell Sorting, and PCR. Case Reports in Veterinary Medicine. 2013: 4.

Kosovsky M 2012. "Subject: Culture and assay systems utilized for cancer stem cell research" (online). Available: http://www.flowcytometri.dk/literature/Kosovsky%202012%20BD%20ecm_cancer_stem_cell.pdf.

Kretzmer G and Schugerl K 1991. Response of mammalian cells to shear stress. Appl Microbiol Biotechnol. 34(5): 613-616.

Kumar V 2013. Neoplasia. In: Robbins basic pathology. 9th ed. Vinay Kumar, Abul K. Abbas, and Jon C. Aster. (eds). Philadelphia: Saunders, Elsevier. 161-214.

Kuntaegowdanahalli SS, Bhagat AA, Kumar G and Papautsky I 2009. Inertial microfluidics for continuous particle separation in spiral microchannels. Lab Chip. 9(20): 2973-2980.

Lecault V, White AK, Singhal A and Hansen CL 2012. Microfluidic single cell analysis: from promise to practice. Curr Opin Chem Biol. 16(3-4): 381-390.

Lee RC 2005. Cell injury by electric forces. Ann N Y Acad Sci. 1066: 85-91.

Lee SS, Ahn KH, Lee SJ, Sun K, Goedhart PT and Hardeman MR 2004. Shear induced damage of red blood cells monitored by the decrease of their deformability. Korea-Aust Rheol J. 16(2): 141-146.

London CA and Seguin B 2003. Mast cell tumors in the dog. Vet Clin North Am Small Anim Pract. 33(3): 473-489, v.

London CA and Thamm DH 2013. Mast Cell Tumors. In: Withrow and MacEwen's Small Animal Clinical Oncology. 5th ed. David M. Vail and Rodney L. Page (eds). Saint Louis: W.B. Saunders. 335-355.

Longo DL 2010. Approach to the patient with cancer. In: HARRISON'S Hematology and Oncology. 17th ed. Anthony S Fauci, Eugene Braunwald, Dennis L Kasper, Stephen L Hauser, Dan L Longo, J Larry Jameson, and Joseph Loscalzo (eds). New York: McGraw-Hill. 320-331.

Magee JA, Piskounova E and Morrison SJ 2012. Cancer stem cells: impact, heterogeneity, and uncertainty. Cancer Cell. 21(3): 283-296.

Marschel P and Schmid-Schönbein GW 2002. Control of Fluid Shear Response in Circulating Leukocytes by Integrins. Annals of Biomedical Engineering. 30(3): 333-343.

Martel JM and Toner M 2012. Inertial focusing dynamics in spiral microchannels. Phys Fluids (1994). 24(3): 32001.

Martel JM and Toner M 2014. Inertial focusing in microfluidics. Annu Rev Biomed Eng. 16: 371-396.

Marusyk A, Almendro V and Polyak K 2012. Intra-tumour heterogeneity: a looking glass for cancer? Nat Rev Cancer. 12(5): 323-334.

Marusyk A and Polyak K 2010. Tumor heterogeneity: causes and consequences. Biochim Biophys Acta. 1805(1): 105-117.

Merlo DF, Rossi L, Pellegrino C, Ceppi M, Cardellino U, Capurro C, Ratto A, Sambucco PL, Sestito V, Tanara G and Bocchini V 2008. Cancer incidence in pet dogs: findings of the Animal Tumor Registry of Genoa, Italy. J Vet Intern Med. 22(4): 976-984.

Michor F and Polyak K 2010. The origins and implications of intratumor heterogeneity. Cancer Prev Res (Phila). 3(11): 1361-1364.

Mitchell MJ and King MR 2013. Computational and experimental models of cancer cell response to fluid shear stress. Front Oncol. 3: 44.

Mohamed H 2012. Use of Microfluidic Technology for Cell Separation. In: Blood Cell - An Overview of Studies in Hematology. Terry E. Moschandreou (ed). Rijeka: InTech. Ch. 11.

Mu X, Zheng W, Sun J, Zhang W and Jiang X 2013. Microfluidics for manipulating cells. Small. 9(1): 9-21.

Nerem RM 1991. Shear force and its effect on cell structure and function. ASGSB Bull. 4(2): 87-94.

Nivedita N and Papautsky I 2013. Continuous separation of blood cells in spiral microfluidic devices. Biomicrofluidics. 7(5): 54101.

Ouellette J 2003. A New Wave of Microfluidic Devices. The Industrial Physicist. 9(4): 14-17.

Park JS and Jung HI 2009. Multiorifice flow fractionation: continuous size-based separation of microspheres using a series of contraction/expansion microchannels. Anal Chem. 81(20): 8280-8288.

Pinho D, Yaginuma T and Lima R 2013. A microfluidic device for partial cell separation and deformability assessment. BioChip Journal. 7(4): 367-374.

Prussin C and Metcalfe DD 2006. 5. IgE, mast cells, basophils, and eosinophils. J Allergy Clin Immunol. 117(2 Suppl Mini-Primer): S450-456.

Reif JS 2007. Chapter 4 - The Epidemiology and Incidence of Cancer A2 - Withrow, Stephen J. In: Withrow & MacEwen's Small Animal Clinical Oncology (Fourth Edition). David M. Vail (ed). Saint Louis: W.B. Saunders. 68-76.

Resnick N, Yahav H, Shay-Salit A, Shushy M, Schubert S, Zilberman LC and Wofovitz E 2003. Fluid shear stress and the vascular endothelium: for better and for worse. Prog Biophys Mol Biol. 81(3): 177-199.

Reya T, Morrison SJ, Clarke MF and Weissman IL 2001. Stem cells, cancer, and cancer stem cells. Nature. 414(6859): 105-111.

Romanelli E, Sorbara CD, Nikić I, Dagkalis A, Misgeld T and Kerschensteiner M 2013. Cellular, subcellular and functional in vivo labeling of the spinal cord using vital dyes. Nat Protocols. 8(3): 481-490.

Russom A, Gupta AK, Nagrath S, Di Carlo D, Edd JF and Toner M 2009. Differential inertial focusing of particles in curved low-aspect-ratio microchannels. New J Phys. 11: 75025.

Sackmann EK, Fulton AL and Beebe DJ 2014. The present and future role of microfluidics in biomedical research. Nature. 507(7491): 181-189.

Sailasuta A, Ketpun D, Piyaviriyakul P, Theerawatanasirikul S, Theewasutrakul P and Rungsipipat A 2014. The Relevance of CD117-Immunocytochemistry Staining Patterns to Mutational Exon-11 in c-kit Detected by PCR from Fine-Needle Aspirated Canine Mast Cell Tumor Cells. Vet Med Int. 2014: 787498.

Salieb-Beugelaar GB, Simone G, Arora A, Philippi A and Manz A 2010. Latest Developments in Microfluidic Cell Biology and Analysis Systems. Anal Chem. 82(12): 4848-4864.

Scaduto Jr RC and Grotyohann LW 1999. Measurement of Mitochondrial Membrane Potential Using Fluorescent Rhodamine Derivatives. Biophysical Journal. 76(1): 469-477.

Sengupta A and Cancelas JA 2010. Cancer stem cells: a stride towards cancer cure? J Cell Physiol. 225(1): 7-14.

Shipitsin M and Polyak K 2008. The cancer stem cell hypothesis: in search of definitions, markers, and relevance. Lab Invest. 88(5): 459-463.

Siegel RL, Miller KD and Jemal A 2017. Cancer statistics, 2017. CA: A Cancer Journal for Clinicians. 67(1): 7-30.

Strayer DS and Rubin E 2012. Neoplasia. In: Rubin's pathology : clinicopathologic foundations of medicine. 6th ed. David S Strayer Rubin Raphae, and Emanuel Rubin (ed). China: Lippincott Williams & Wilkins. 157-212.

Strayer DS and Rubin E 2014. Neoplasia. In: Essentials of Rubin's pathology. 6th ed. Emanuel Rubin and Howard M. Reisner (ed). China: Lippincott Williams & Wilkins. 93-122.

Tanaka T, Ishikawa T, Numayama-Tsuruta K, Imai Y, Ueno H, Yoshimoto T, Matsuki N and Yamaguchi T 2012. Inertial migration of cancer cells in blood flow in microchannels. Biomed Microdevices. 14(1): 25-33.

Tang DG 2012. Understanding cancer stem cell heterogeneity and plasticity. Cell Res. 22(3): 457-472.

Thamm DH and Vail DM 2007. Mast Cell Tumors. In: Withrow & MacEwen's Small Animal Clinical Oncology. 4th ed. Saint Louis: W.B. Saunders. 402-424.

Thanormsridetchai A, Ketpun D, Pimpin A, Srituravanich W, Piyaviriyakul P, Sailasuta A, W. Jeamsaksiri, Sripumkhai W, Jantawong J and Supadech J 2014. Sorting of Multiple-Size Cells Using Spiral Microchannels. 27th International Microprocesses and Nanotechnology Conference, Hilton Fukuoka Sea Hawk, Fukuoka, Japan.

Theoharides TC, Alysandratos K-D, Angelidou A, Delivanis D-A, Sismanopoulos N, Zhang B, Asadi S, Vasiadi M, Weng Z, Miniati A and Kalogeromitros D 2012. Mast cells and inflammation. Biochimica et Biophysica Acta (BBA) - Molecular Basis of Disease. 1822(1): 21-33.

Visvader JE and Lindeman GJ 2012. Cancer stem cells: current status and evolving complexities. Cell Stem Cell. 10(6): 717-728.

Wang X, Zandi M, Ho CC, Kaval N and Papautsky I 2015. Single stream inertial focusing in a straight microchannel. Lab Chip. 15(8): 1812-1821.

Wang Y, Lee D, Zhang L, Jeon H, Mendoza-Elias JE, Harvat TA, Hassan SZ, Zhou A, Eddington DT and Oberholzer J 2012. Systematic prevention of bubble formation and accumulation for long-term culture of pancreatic islet cells in microfluidic device. Biomed Microdevices. 14(2): 419-426.

Ward RJ and Dirks PB 2007. Cancer stem cells: at the headwaters of tumor development. Annu Rev Pathol. 2: 175-189.

Warkiani ME, Khoo BL, Wu L, Tay AK, Bhagat AA, Han J and Lim CT 2016. Ultra-fast, label-free isolation of circulating tumor cells from blood using spiral microfluidics. Nat Protoc. 11(1): 134-148.

Wheeler AR, Throndset WR, Whelan RJ, Leach AM, Zare RN, Liao YH, Farrell K, Manger ID and Daridon A 2003. Microfluidic device for single-cell analysis. Anal Chem. 75(14): 3581-3586.

Wu H-W, Lin C-C and Lee G-B 2011. Stem cells in microfluidics. Biomicrofluidics. 5(1): 013401.

Wu J, Day D and Gu M 2010. Shear stress mapping in microfluidic devices by optical tweezers. Opt Express. 18(8): 7611-7616.

Wu S-C 1999. Influence of hydrodynamic shear stress on microcarrier-attached cell growth: Cell line dependency and surfactant protection. Bioprocess Engineering. 21(3): 201-206.

Xiang N, Chen K, Dai Q, Jiang D, Sun D and Ni Z 2015. Inertia-induced focusing dynamics of microparticles throughout a curved microfluidic channel. Microfluidics Nanofluidics. 18(1): 29-39.

Yamada M, Kano K, Tsuda Y, Kobayashi J, Yamato M, Seki M and Okano T 2007. Microfluidic devices for size-dependent separation of liver cells. Biomed Microdevices. 9(5): 637-645.

Yin H and Marshall D 2012. Microfluidics for single cell analysis. Curr Opin Biotechnol. 23(1): 110-119.

Zellmer VR and Zhang S 2014. Evolving concepts of tumor heterogeneity. Cell Biosci. 4: 69.

Zhang C, Guan Y, Sun Y, Ai D and Guo Q 2016. Tumor heterogeneity and circulating tumor cells. Cancer Lett. 374(2): 216-223.

Zhang J, Yan S, Sluyter R, Li W, Alici G and Nguyen N-T 2014. Inertial particle separation by differential equilibrium positions in a symmetrical serpentine micro-channel. Sci Rep. 4: 4527.

Zhao S, Stamm A, Lee JS, Gruverman A, Lim JY and Gu L 2015. Elasticity of Differentiated and Undifferentiated human neuroblastoma cells characterized by atomic force microscopy. J Mech Med Biol. 15(05): 1550069.

Zhou J and Papautsky I 2013. Fundamentals of inertial focusing in microchannels. Lab Chip. 13(6): 1121-1132.

APPENDIX

APPENDIX A

MICROSTRTUCTURE OF COUNTING GRIDS

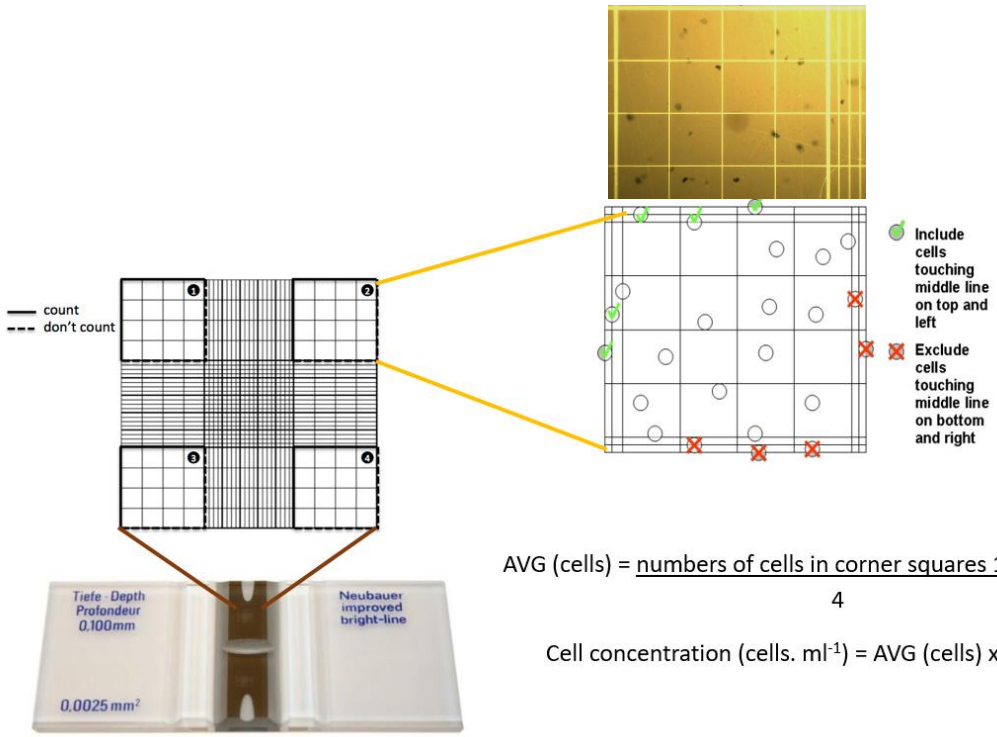

AVG (cells) = $\frac{\text{numbers of cells in corner squares 1+2+3+4}}{4}$

Cell concentration (cells. ml^{-1}) = AVG (cells) x 10^4

The microtructure of counting grids and the counting rule

APPENDIX B

INPUT PARAMETERS FOR COMPUTERIZED FLUID DYNAMIC SIMULATION OF THE CELL DELIVERY PORTION

Conduit portion	Length (mm)	Inner Diameter (mm)	Cross-sectional area (mm^2)
Syringe barrel	54.45	9.65	71.20
Syringe male luer taper at 1.72° FLL	3.50	-	-
Syringe luer tip	10.7	2.46	4.77
6% female luer hub of 20G3/4 IV catheter	10.67	-	-
Polymer tube of 23G3/4 IV catheter	15	0.91	0.65
Silicone tube	100	0.51	0.20
21G1 metal connector	25.4	0.82	0.53

APPENDIX C

FOCUSING POSITIONS

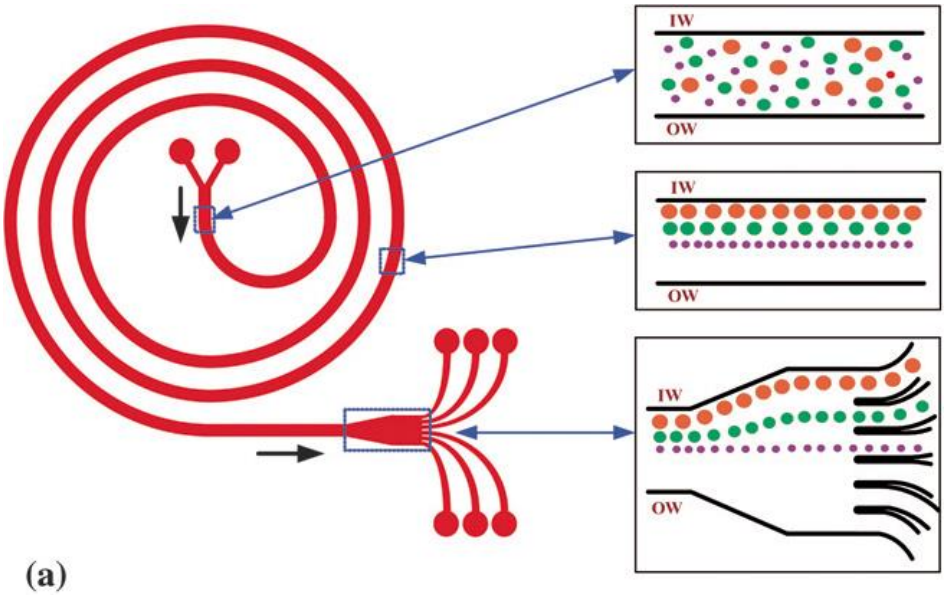

(a)

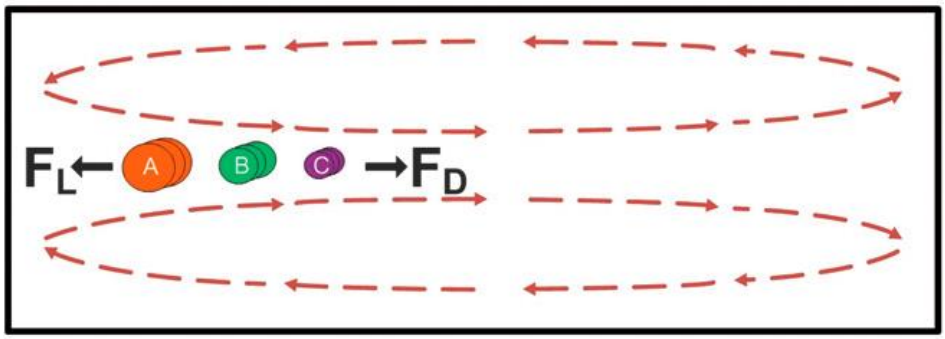

(b)

APPENDIX D

TWO KEY INERTIA FORCES FOR SINGLE CELL ENTRAPMENT

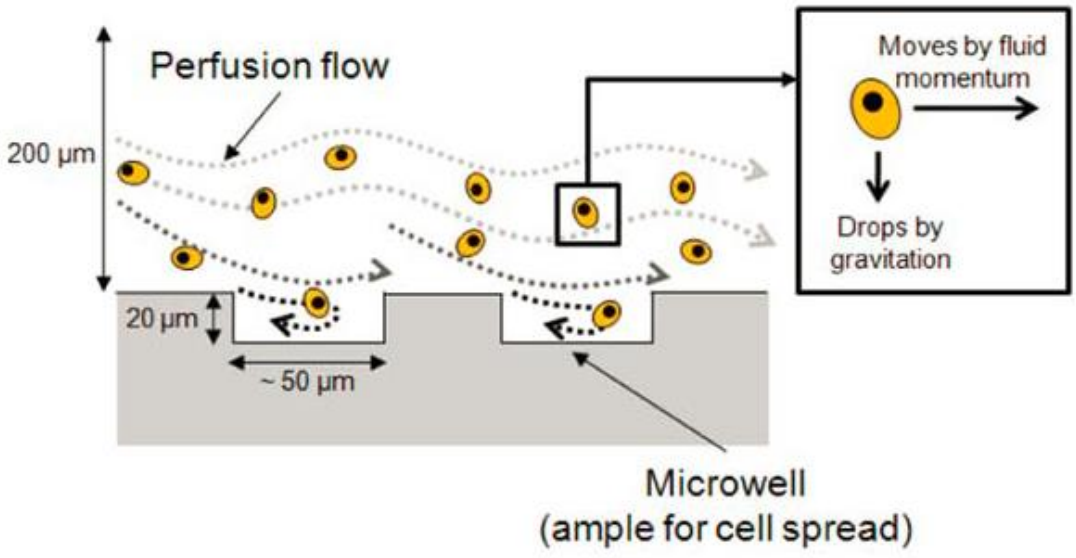

APPENDIX E

RECIRCULATION FORCES IN VARIOUS MICROWELL GEOMETRIES

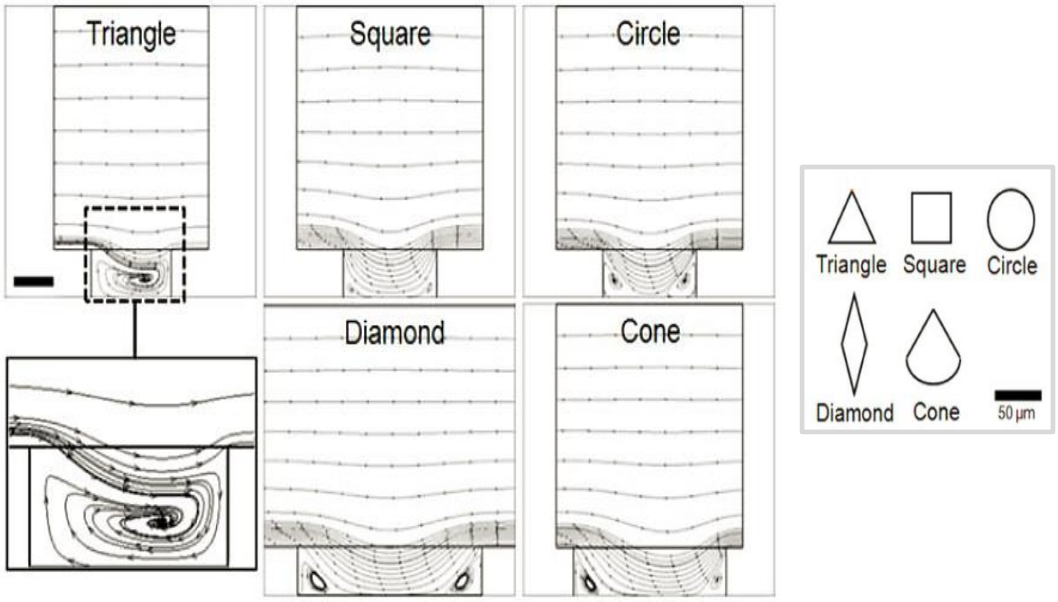

APPENDIX F

EFFICIENCY OF SINGLE CELL ENTRAPMENT IN EACH MICROWELL GEOMETRY

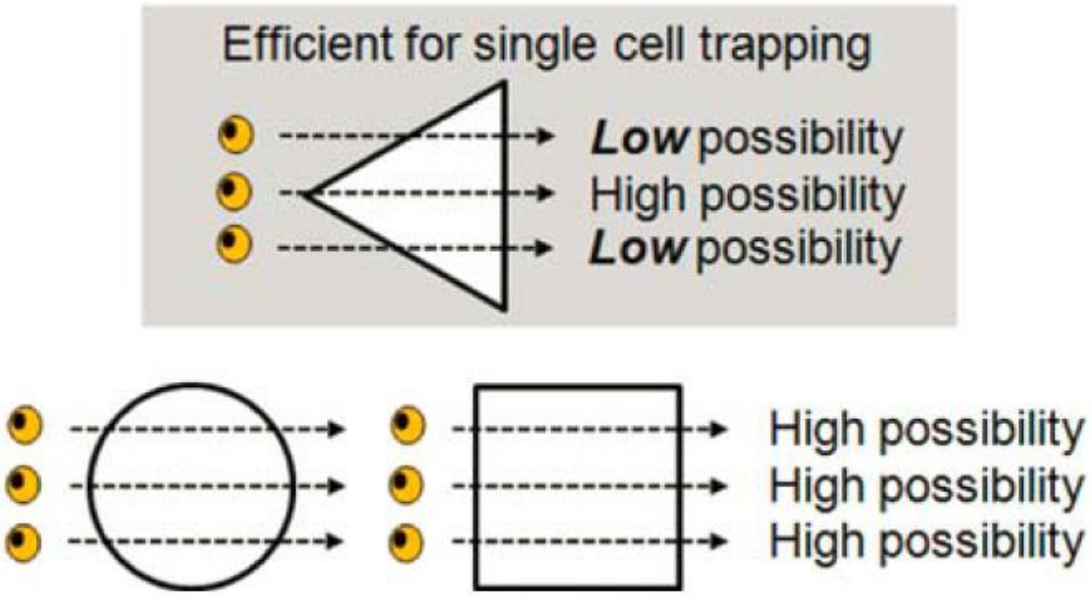

APPENDIX G

PHOTORESIST-SOFT-LITHOGRAPHY AND MICROFABRICATION

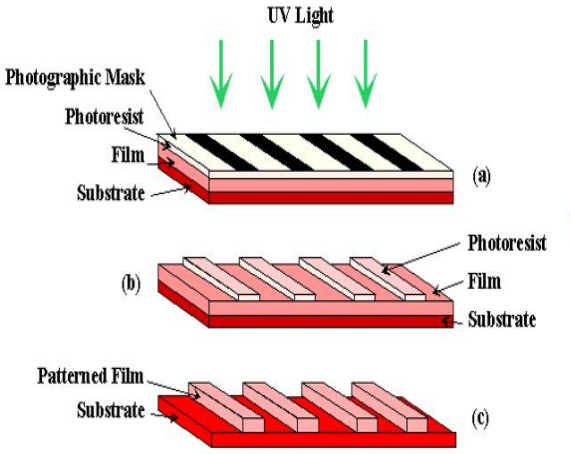

Photoresist-Soft-Lithography

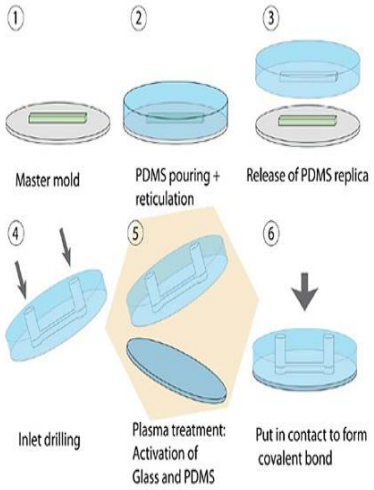

PDMS (POLYDIMETHYLSILOXANE) Fabrication

APPENDIX H

MICRODEVICE INSTRUMENTATION

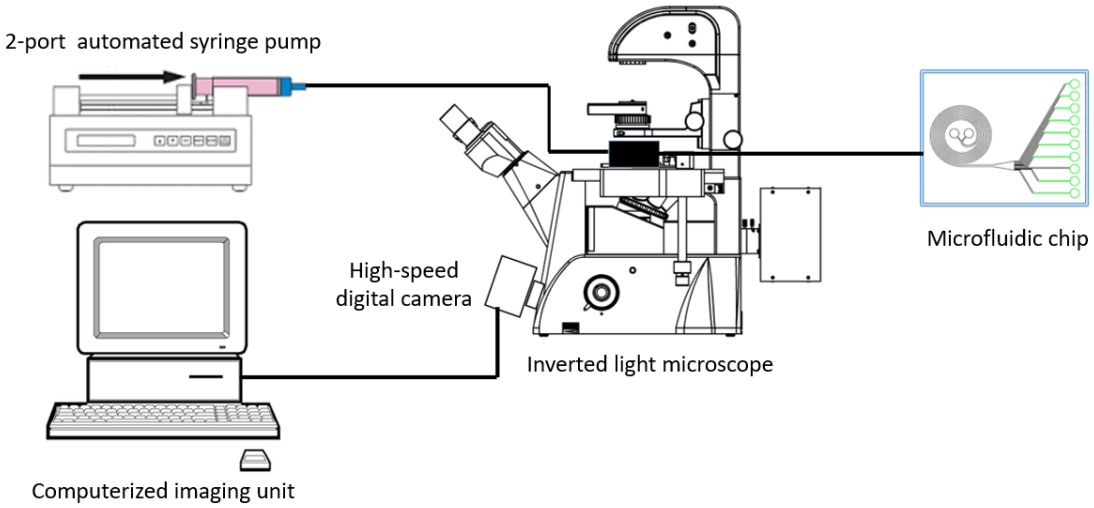

APPENDIX I

1mm GRID

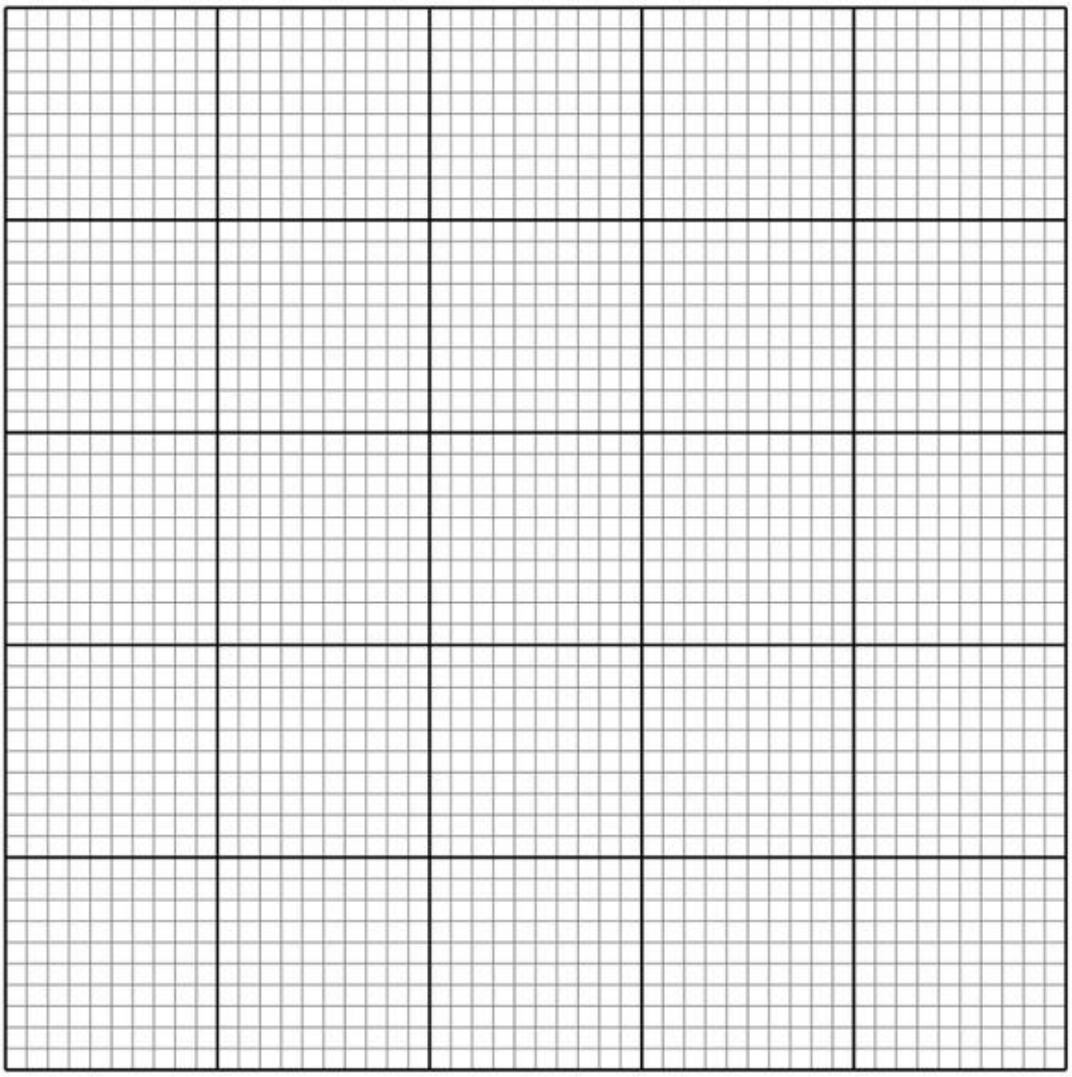

APPENDIX J

CU-Vet MPS® FOMULAR

In 6 ml, the formula of the membrane-piercing solution utilized in this study consists of;

I.	10% neutral formalin	2 ml
II.	Absolute methanol	2 ml
III.	Fetal calf serum	1 ml
IV.	PBS	1 ml

APPENDIX K

CELL DEBRIS AGGREGATION AND UNIDENTIFIED THREAD IN THE MICROCHANNEL

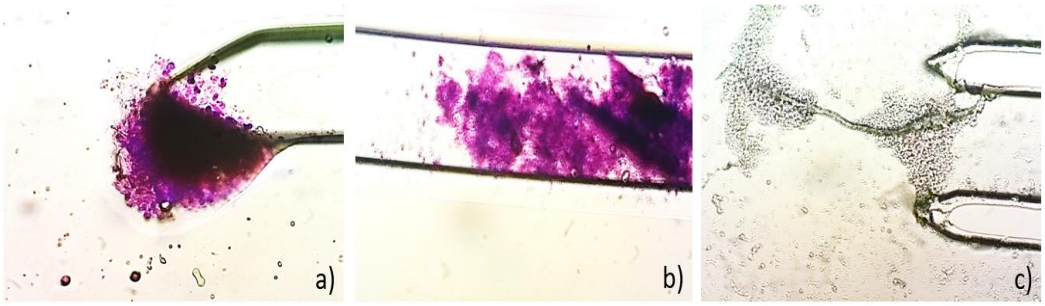

VITA

Dettachai Ketpun was born in Jan 6, 1971 at Rajvithi general hospital, Bangkok, Thailand. His father is a retired government officer at Department of Labour Skill Development, Ministry of Labour and Social Welfare. And his mother is the housewife.

He finished his high school from Suankularb Wittayalai, Bangkok, Thailand in 1988, and his bachelor degree of Doctor of Veterinary Medicine in 1995, from Faculty of Veterinary Medicine, Kasetsart University, Thailand. He won a position of Doctor of Medicine (MD) candidates from Faculty of Medicine, Chulalongkorn University for 2 successively academic years (1998 and 1999). He has completed his Master of Science in Veterinary Pathobiology since 2012. He was also a VIRS from the University of British Columbia, Okanagan campus, Kelowna, British Columbia, Canada. So far, he has just finished his Doctor of Philosophy in Veterinary Biosciences and is going further for his researches of interest consisting of biology of cancer stem cells, biology of stem cells, microfluidic-single cell analysis, microfluidic-single cell culture, 3D-bioprinting, cell signaling, veterinary and medical pathobiology, and veterinary and medical oncology.

Nevertheless, along his Ph.D. study, he was an invited speaker in microfluidic-based single cell analysis, the head of cancer stem cell research group as well as the head of Microfluidic-single cell analysis group of CAC-RU, Faculty of Veterinary Science and Faculty of Engineering, Chulalongkorn University, Bangkok, Thailand. And he is a mentor of those research groups, recently.

For an academic experience, he has been a lecturer in Veterinary Pathology and Parasitology at the Faculty of Veterinary Medicine, Western University, Kanchanaburi Campus, Thailand, so far.